

AN ABSTRACT OF THE THESIS OF

Sachin Laddha for the degree of Master of Science in Industrial Engineering
presented on November 21, 2008.

Title: The Effect of Feedstock Composition on Defect Evolution in Powder
Injection Molded Ceramic Microarrays using Simulations and Experiments

Abstract approved: _____

Sundar V. Atre

Micro Powder injection molding (μ PIM) is a cost-effective technique for producing small, complex, precision parts in high volumes from ceramic and metal nanoparticles. This study focuses on research conducted on fabrication of Micro Ceramic Arrays (MCAs) parts using μ PIM. MCAs are widely used as the major components and design features for many microsystems in various applications, such as micro fluidics, micro optics, micro heat exchangers, micro transducers, micro reactors, medical instruments and devices, IC packaging, etc. However, lots of defects are associated while molding these MCAs with micro features. These defects can be avoided by carefully studying the part geometry, feedstock properties and studying the effect of change in processing parameters on the fill of micro features. In this study we dealt with all the three methods to avoid defects with a concentration on effect of feedstock properties on defect occurrence. In order to have a good understanding of the μ PIM process and to provide the necessary data for simulation studies, characterization of the feedstock is essential. In this thesis, characterization of feedstock consisting of alumina nanopowder (average particle size of 400 nm) with ethylene-propylene/wax (Standard Mix) and polyacetal binder systems (Catamold AO-F,

BASF) for μ PIM is reported. It is found that the Standard Mix system has lower viscosity and heat capacity compared to the Catamold AO-F. However, it can be inferred from the results that Catamold AO-F fills the microcavities (50 μ m) in a more efficient way, despite having a higher viscosity at higher shear rates. These results from Moldflow Simulations were further varied using experimental platforms and scanning electron microscopy.

© Copyright by Sachin Laddha

November 21, 2008

All Rights Reserved

The Effect of Feedstock Composition on Defect Evolution in Powder Injection
Molded Ceramic Microarrays using Simulations and Experiments

by
Sachin Laddha

A THESIS

submitted to

Oregon State University

in partial fulfillment of
the requirements for the
degree of

Master of Science

Presented November 21, 2008
Commencement June 2009

Master of Science thesis of Sachin Laddha presented on November 21, 2008.

APPROVED:

Major Professor, representing Industrial Engineering

Head of the School of Mechanical, Industrial and Manufacturing Engineering

Dean of the Graduate School

I understand that my thesis will become part of the permanent collection of Oregon State University libraries. My signature below authorizes release of my thesis to any reader upon request.

Sachin Laddha, Author

ACKNOWLEDGEMENT

This material is primarily based on research sponsored by Hewlett-Packard. Additional funding was provided by Air Force Research Laboratory under agreement number FA8650-05-1-5041. The views and conclusions contained herein are those of the authors and should not be interpreted as necessarily representing the official policies or endorsements, either expressed or implied, of Air Force Research Laboratory or the U.S. Government.

I would like to thank,

- Dr. Sundar Atre for his kind guidance throughout the project.
- Dr. Shiwoo Lee for providing all the necessary resources to work with.
- Dr. Park and Carl Wu for their technical contributions.
- My parents, Ganeshchandra Laddha and Kirandevi Laddha for their love and support; and my family.

TABLE OF CONTENTS

	<u>Page</u>
Chapter 1: Introduction	1
1.1. Powder InjectionMolding	1
1.1.1. Background.....	1
1.1.2. Micro Powder Injection Molding	2
1.2. Micro fluidic devices and microchannels arrays (MCAs).....	7
1.2.1. Other PIM applications.....	9
1.3. The microPIM process.....	12
1.4. Problem Statement and mold filling stage	17
1.5. PIM Simulation.....	19
1.5.1. Numerical modeling and simulation.....	19
1.5.2. Modeling tools	20
1.5.3. Flow Model Development.....	21
1.6. Goals Of The Study.....	22
Chapter 2: Experimental Methods	24
2.1. Simulation Method	24
2.1.1. Injection Molding.....	24
2.1.1.1 Filling Phase.....	24
2.1.1.2 Packing Phase	25
2.1.1.3. Cooling Phase	27
2.1.2. Meshing.....	27
2.1.2.1 Midplane Meshing.....	28
2.1.2.2 Fusion Mesh.....	28
2.1.2.3 3D Mesh.....	29
2.1.3. Important Definitions	30
2.1.3.1 Design Rules	31
2.1.3.2 Part Volume	34

2.1.4. Selection of Materials	35
2.1.5. Moldflow Plastic Insight	38
2.1.5.1 Importing a model	39
2.1.5.2 Model Manipulation	40
2.1.5.3 Generating fusion mesh	41
2.1.5.4 Selecting a material.....	42
2.1.5.5 Designing a cooling circuit	43
2.2. Microchannel Arrays.....	46
2.3. Materials.....	50
2.3.1. Binders.....	50
2.3.2. Powder	51
2.3.3. Feedstock	54
2.4. Characterization and properties of the feedstocks.....	56
2.4.1. Rheological Studies	57
2.4.2. Thermal Conductivity.....	60
2.4.3. Specific Heat	60
2.4.4. Pressure-Volume-Temperature behavior.....	61
2.5. Processing.....	63
2.5.1. Powder Injection Molding Machine.....	63
2.5.2. Precision micro mold system	65
Chapter 3: Results And Discussion.....	70
3.1. Material Properties	70
3.1.1. Rheological Properties	70
3.1.2. PVT properties	73
3.1.3. Specific Heat	76
3.1.4. Thermal Conductivity.....	77
3.2. Processing Parameters.....	78
3.2.1. Injection Speed	78

3.2.2. Packing Pressure.....	79
3.2.3. Melt Temperature.....	80
3.3. Part Geometry	82
3.3.1. Bulk Thickness	82
3.3.2. Microchannel end	86
3.3.3. Multiple Gates.....	87
3.4. Summary of Sensitivity analysis.....	88
Chapter 4: Comparison of Feedstocks in MCA	91
4.1. Progressive filling of Microchannels.....	91
4.2. Through Simulations.....	95
4.3. Through Experimentation	96
Chapter 5: Conclusion and Future work	99

Bibliography

Appendix

LIST OF FIGURES

<u>Figure</u>	<u>Page</u>
1. Different application of microfluidic devices.....	7
2. Micro fluidic chambers in inkjet print head.....	8
3. Ink ejected from nozzle.....	9
4. Sample components produced using micro PIM technique.....	10
5. Schematic diagram of the PIM processing steps making part having micro features.....	12
6. Typical injection molding cycle.....	16
7. A typical schematic of the MCA part used in the study.....	17
8. Definition of the problem statement.....	18
9. Material inhomogeneity in micromolding nanoparticulate suspensions.....	19
10. An approach towards reaching the goals of the study.....	23
11. Fountain Flow while polymer melt fills the cavity.....	25
12. Difference between the end of the filling phase and end of packing phase.....	26
13. Cross-section of an image from midplane meshing.....	28
14. Cross-section of an image from fusion meshing.....	29
15. Cross-section of an image from 3D meshing.....	30
16. Meaning of colors in MPI.....	30
17. Gate locations.....	31
18. Best gate location.....	32

LIST OF FIGURES (Continued)

<u>Figure</u>	<u>Page</u>
19. Flow length.....	33
20. Multiple gate locations.....	35
21. Experiment part design.....	47
22. Typical image of the part from MPI.....	49
23. Asphy's plot of Maximum Service Temperature vs Price.....	52
24. Asphy's plot of Thermal Conductivity vs Price.....	53
25. Scanning Electron Micrograph (SEM) of the alumina (A16SG).....	54
26. Three possible situations in a powder-binder mixture:.....	55
27. TGA & DSC studies of Standard Mix.....	57
28. Relationship between viscosity (Pa-s) and shear rate (s^{-1}) for Catamold AO-F and Standard Mix at varying shear rates.....	58
29. Thermal conductivity of Catamold AO-F and Standard Mix as a function of temperature.....	60
30. Specific heat as a function of temperature for the Catamold AO-F and the Standard Mix.....	61
31. PVT relationships for the Catamold AO-F and the Standard Mix.....	62
32. Powder injection molding machine used in the study, ALLROUNDER 270C from Arburg.....	64
33. A and B plates of the test mold.....	65
34. Mold runners and Dutchman.....	65
35. Cavity vents, vacuum paths, and water channels.....	66
36. Ceramic injection molded alumina microchannel arrays (MCAs) used in this study.....	68
37. The 50 μ m channels on the MCA.....	69
38. Screen shot of the viscosity coefficients changed in MPI.....	71

LIST OF FIGURES (Continued)

<u>Figure</u>	<u>Page</u>
39. Change in viscosity constants influence the behavior of viscosity v/s shear rate.....	72
40. Effect of change in viscosity constants on flow in microchannels.....	73
41. The comparison of percentage fill in microchannels to bulk as a function of time with different values of specific heat for Catamold AO-F.....	77
42. The gradual increase of injection speed and its effect on the flow of feedstocks in the microchannels.....	79
43. The print screen of the MPI software while changing packing pressures.....	80
44. The effect of changing melt temperature on microchannels, bulk and complete fill of the part.....	81
45. The actual amount of the material flowing through the different sections of the part per unit area per unit time for Catamold AO-F...	81
46. Effect of melt temperature on microchannels to bulk fill for Catamold AO-F.....	82
47. Comparison of bulk thicknesses for Catamold AO-F and Standard Mix.....	83
48. 0.25 mm thick bulk from MPI.....	84
49. 0.5 mm thick bulk from MPI.....	85
50. 1.5 mm thick bulk from MPI.....	86
51. The effect of change in shapes of bulk on the flow of feedstocks in microchannels.....	87
52. The effect of multiple gates on the flow of feedstocks in microchannels.....	88

LIST OF FIGURES (Continued)

<u>Figure</u>	<u>Page</u>
53. Progressive filling of microchannels using Catamold AO-F at a melt temperature of 190°C from Moldflow simulations.....	92
54. Comparison of Catamold AO-F and Standard Mix in microchannels and bulk at melt temperature of 170°C & 190°C.....	95
55. Comparison of Catamold AO-F and Standard Mix in microchannels and bulk at melt temperature of 190°C.....	96
56. The cross-sections of the MCA molded using Catamold AO-F and Standard Mix respectively.....	97
57. The cross-sections of the microchannels ribs after ion milling for Catamold AO-F and Standard Mix respectively.....	98

LIST OF TABLES

<u>Table</u>	<u>Page</u>
1. Different binder systems for μ PIM feedstocks.....	5
2. Some of the debinding and sintering methods used for μ PIM feedstocks.....	6
3. The wide range of PIM applications separated by related industry.....	11
4. The process conditions used for simulation studies of the ceramic microchannel array part for Catamold AO-F and Standard Mix....	49
5. Composition of Standard Mix and Catamold AO-F.....	50
6. Properties of the Almatix alumina powder.....	54
7. Value and definition of different constants for Catamold AO-F and Standard Mix.....	59
8. PVT coefficients for Catamold AO-F and Standard Mix.....	62
9. Major technical data of Arburg injection molding machine (270/300).....	64
10. Processing conditions used to mold 50 μ m MCA.....	67
11. Cylinder Zone temperatures	68
12. Results of the sensitivity analysis.....	89
13. Recommendation to mold a MCA with minimum defects for both the feedstocks.....	101

CHAPTER 1: INTRODUCTION

1.1 Powder Injection Molding

1.1.1 Background

Powder injection molding (PIM) is a fast-developing powder-forming technique used to fabricate small and hard-to-manufacture parts with complex features. This hybrid technology has proven to be an attractive and viable option to economically mass-produce high-performance components with the shape-forming capability of plastic injection molding, the precision of die-casting and the material selection flexibility of powder metallurgy [1, 2, 3]. In the 1960's and 1970's, when powder injection molding (PIM) first entered the field of modern manufacturing, it was not meant to have any market success but was more of a proprietary and close-guarded secret of these early companies. The applications were more "in-house" rather than for commercial purposes [4, 5]. Later, in the late 1980's and early 1990's, with the standardization of the process, PIM underwent several evolutionary changes, which provided opportunities for fabricating more complex components and also became more attractive for mass-production. This increased potentiality was soon followed by the realization that PIM applications had to be carefully selected as they heavily depended on the availability of the raw materials and also on the ability to reliably design the process/part [6, 7].

The incumbent trial-and error based design approach is dependent on the designer's experience with the materials and the process rather than on fundamental engineering concepts. This has led to difficulties in timely deliverance of orders, within the available budget and with the required quality factors such as reliability, stability, and adaptability. It also lacks the adaptation of modern concurrent engineering concepts thus hindering further growth of this highly versatile technology [8, 9, 10]. To overcome the problem, extensive

researching is being undertaken to understand various fundamental aspects of PIM designing. It is evident that for any further development of PIM, the designing process should be modernized by implementing the concurrent engineering techniques and also by the use of advanced computer technology [11, 12].

Several attempts and approaches have been carried out during the last decade or so to understand and tackle the problems in PIM designing that directly or indirectly affect the quality and reliability of the final component [13]. These attempts have focused on many different fields, such as new and improved feedstocks, improved and innovative molding techniques, introduction of flow analysis and numerical simulations, etc. Notwithstanding the various attempts in development of several simulation softwares, its realization into the design process remains an unaccomplished and seemingly difficult task. PIMSolver® is one such design package which is tailor-made for PIM. Moldflow Plastic Insight (MPI) is also one of the softwares that can be used to simulate the PIM process very well. This study exhibits Moldflow's ability to accurately predict the flow behavior of the feedstock-melt into the mold cavity. Another aspect which this study is aimed at, is undertaking a systematic and detailed approach in achieving the design-solution which is very essential for the success of any engineering problem [14, 15].

1.1.2 Micro Powder Injection Molding

Micro-systems and related products will have increasing applications and potential huge markets in the new millennium. Micro-systems can be used in the fields of information and communication technology, medical and biotechnology, and micro-sensor and micro-actuator technology. Economic success of micro-systems technology requires cost-effective fabrication in large

series as well as a great diversity of materials-processing technologies. Techniques such as X-ray lithography, electro-forming, micro-molding and excimer laser ablation are used for the production of microcomponents out of silicon, polymer and a limited number of pure metals or binary alloys [16, 17]. However, the production cost is very high in most cases, and the materials available are also limited. To overcome these drawbacks, micropowder injection molding (μ PIM), a variant of powder injection molding (PIM), has been developed in recent years [18, 19]. μ PIM inherits the features of conventional PIM such as low production cost, shape complexity, applicability to many materials, good tolerance and good mechanical properties.

The μ PIM process enables the use of a wide range of materials such as those with high strength, hardness or other functional properties, which will broaden the applications of microcomponents. Currently, existing commercial feedstocks have some limitations in filling microstructures with high aspect ratio and hence, feedstock specifically for μ PIM is required [20, 21, 22]. Unlike PIM feedstock, more stringent requirements are required for μ PIM feedstock from the perspectives of powder, binder system and mixing. In the case of powder, small particle sizes are necessary as they: (a) contribute to smaller structural details, higher aspect ratio and better shape retention of microstructures [23, 24], (b) give fairly isotropic behaviour [25, 26] and (c) yield better surface finish [27, 28]. As for the binder system, firstly, sufficiently low viscosity is desired for complete filling of the microcavities during injection molding. Secondly, molded microstructures with high strength at the mold temperature are imperative to enable successful demolding [29, 30]. Thirdly, the binder system has to allow for pressure free, complete debinding and sintering without deformation in the submillimeter range [20, 26]. After the selection of appropriate powder and binder system, mixing of the powder and binder system are conducted to form the feedstock for injection molding. A suitable powder loading (powder-binder

ratio) has to be established. This is not only because the feedstock directly influences the subsequent processing steps but also due to the fact that fine spaces or interstices between small particles, where the binder must flow, make mixing more difficult [28, 31]. During mixing, insufficient binder will induce incomplete wetting of the powder surface that leads to molding difficulty. This is particularly important in μ PIM since smaller particle size generally demands a larger amount of binder to wet the free surface and the filling of the microcavities is more sensitive to viscosity change. In contrast, excessive binder will lower the viscosity of the feedstock, and this may cause powder-binder separation under high stress during molding [32]. On the other hand, molded microstructures with low strength may cause demolding problems as they may break or be distorted during demolding [31, 33]. Lower powder content will also cause the sintered microstructures as well as the overall dimensions to undergo higher shrinkage. The most important properties of the feedstock are its homogeneity and rheological behaviour [34]. Table 1 shows some related studies in the field of binders for μ PIM.

Table 1: Different binder systems for μ PIM feedstocks

Sr. No.	Binders used	Summary
1 [35]	Polyvinyl acetate (PVA) + Water, Ethylene vinyl acetate (EVA) + Paraffin Wax (PW) and Polyacrylonitrile (PAN) + EVA + High Density Polyethylene (HDPE)	A water-soluble binder system consisting of PVA was found to be unsuitable for μ PIM, as the viscosity was too high and the surface finish of the micro-components was poor. In the case of the PW + EVA binder system, thermal de-binding caused slumping problems. A binder system comprising PAN + EVA + HDPE proved to be suitable for use due to easy flowability in the micro cavities and easy de-binding of the binder at a later stage.
2 [36]	Cellulose acetate butyrate (CAB) and poly(ethylene glycol)(PEG)	This blend exhibited low enough viscosity to make homogeneous feedstock for μ PIM. Shape maintenance during the extraction of binder by water was excellent, and final sintered parts had excellent dimensional stability ($\pm 0.3\%$) and high sintered density over 98%. Also the injection cycle time was comparable to that of commonly used wax-based feedstock.
3 [37]	Paraffin wax (PW) + HDPE	The mold filling behavior was better than other binders used in previously mentioned studies; however, the shrinkage in the part was fairly high. It was also found out that less temperature of debinding increase the bending strength which is very important in the technological lines producing tools by μ PIM method.
4 [38, 39]	PW + PEG + Low Density Polyethylene (LDPE) + Polypropylene (PP)	Good flowability in micro cavities and good shape retention were found. However, the shrinkage in the final sintered part was high.

Table 2: Some of the debinding and sintering methods used for μ PIM feedstocks

Sr. No	Debinding process	Summary
1 [40]	Single-step thermal debinding at 800°C was carried out for 150 minutes.	The binders used were PEG and CAB. No residue of PEG was found at 420°C. Complete removal of CAB/PEG binders was observed at 800°C with lots of sink marks on the final part. This sink marks are due to the higher debinding temperatures and short time of exposures.
2 [41]	Multiple-step debinding was conducted at 650°C for 90 minutes.	In this study PVA, EVA, PW and PAN were the binder systems used. The binder removal was conducted in stages, such that after every stage the shape of the part is retained by other binder. It was observed that removal of PW shows the maximum amount of change in dimension of the part. This method was found to be expensive compared to single-step thermal debinding method.
3 [42]	Thermal debinding under inert atmosphere.	This study involved the use of PW as a binder. Inert atmosphere was helpful to increase the evaporation of PW at slower rates to maintain the dimensions of the final part. The final part was found to have fairly high density compared to other thermal debinding methods.
4 [43, 44]	Multiple-step debinding combined with inert atmosphere.	PAN and LDPE were the binders used in this study. Removal of LDPE was attainable at 320 °C while the temperature was raised to 450°C to remove PAN. Inert atmosphere helps the removal of binder slowly, maintaining the dimension of the final part. The final part was found to have highest density compared to other thermal debinding methods.

1.2 Micro Fluidic Devices and Microchannel Arrays (MCAs)

One of the major applications of the μ PIM is the micro fluidic devices. Figure 1 gives the different areas where μ Fluidic devices are used. MCAs fall in the Nano/MEMS and energy applications of the μ Fluidic device. These applications require higher temperature sustainability and hence, MCAs made up of alumina were studied in this thesis.

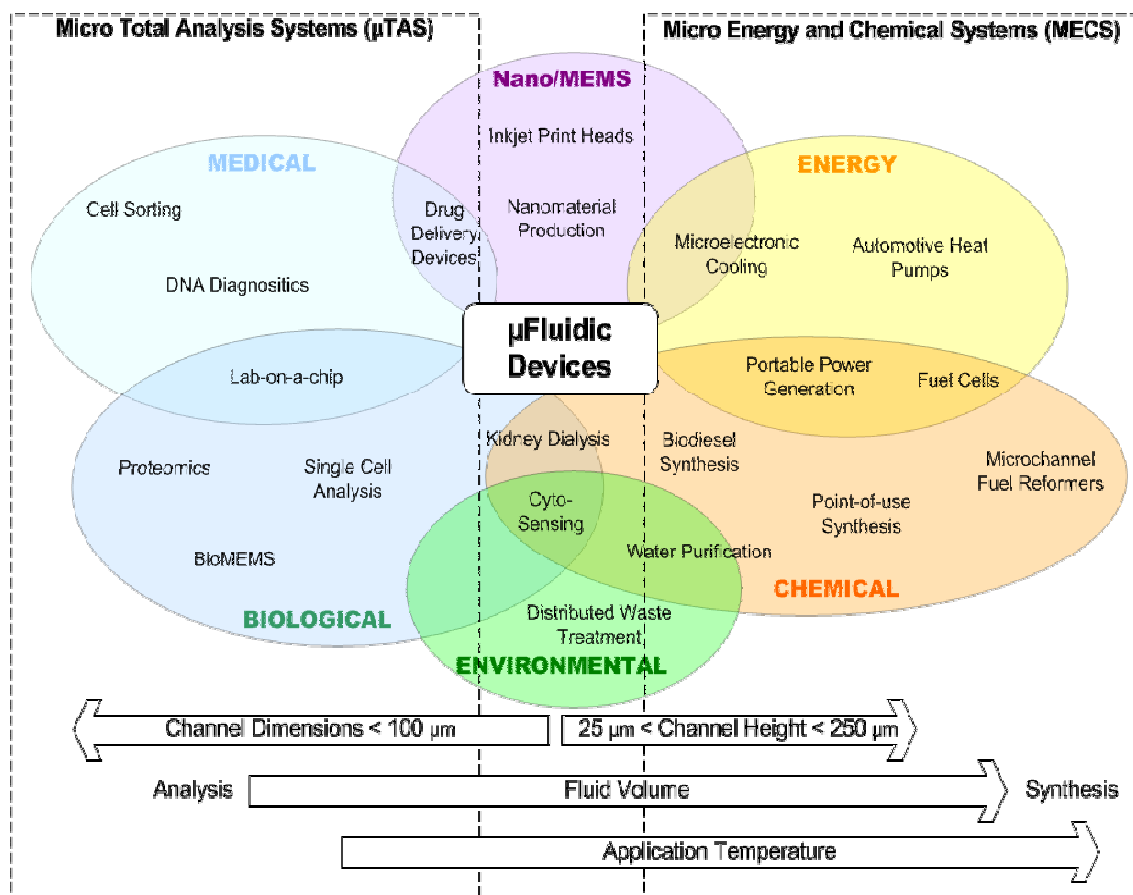


Figure 1: Different applications of μ Fluidic device

MCAs have been widely used as the major components and design features for many microsystems in various applications, such as micro fluidics,

micro optics, micro heat exchangers, micro transducers, micro reactors, medical instruments and devices, IC packaging, and so on.

The advantage of MCA is obvious. With its the microstructure, MCA has a large surface area to volume ratio, which can significantly improve the system performance in terms of greater material utilization, lower energy cost, more efficient and precise thermal management. One of most important applications of MCAs is micro fluidic devices, which have been considered for many products of today and the future. An example of this type of application can be found in inkjet products, the thermal or Piezo print heads, which are made of many micro fluidic channels, chambers and nozzles, (Figure 2 and Figure 3). Today's print heads are able to delivery the ink droplets with the weight of a few nano grams to the paper in the on-demand printing process.

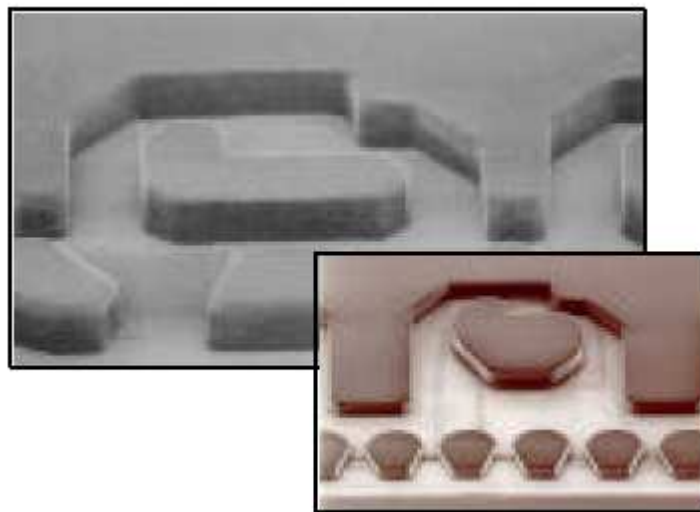


Figure 2: Micro fluidic chambers in inkjet print head



Figure 3: Ink ejected from nozzle

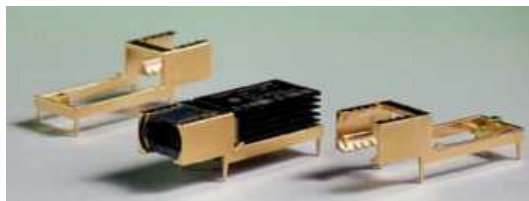
1.2.1 Other μ PIM Applications

The other applications of μ PIM (which are not studied in this thesis) range from low-priced components produced in bulk (50,000 to a million/yr) to highly complex custom-designed components produced in small and limited quantities (10,000/yr). μ PIM has its applications in the electronics industry, mechanical parts, armaments industry, household products, medical appliances, automotive parts, tooling, sporting goods and many more. Figure 4 shows some of the complex parts that have been manufactured using μ PIM. Table 3 gives some examples of the applications of μ PIM in the present-day industry [45, 46].

With the capability of utilizing a wide range of materials and also its ability to form complex shapes, μ PIM has the potential of providing mass-fabrication solution to several innovative multi-scale technologies.



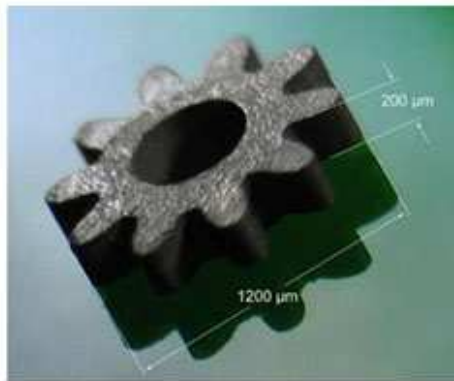
(1)



(3)



(2)



(4)

Figure 4: Sample components produced using micro PIM technique. **(1)** Stainless steel blades and miniature helical gears for surgical application (picture courtesy: MPIF); **(2)** Gear, rack and latch door for printer (picture courtesy: MPIF); **(3 & 4)** Kovar electronic gear.

Table 3: The wide range of μ PIM applications separated by related industry.

Industry	Applications
Electronics	<ul style="list-style-type: none"> • printer components • printed circuits • digital cameras • disk drive components • heat sinks
Mechanical	<ul style="list-style-type: none"> • weaving machine components • welding nozzles • heat-engine components • small transmission parts • lock mechanism
Armaments	<ul style="list-style-type: none"> • rifle sights • magazine catch • trigger and trigger guard • rocket guidance components • projectile stabilizer fin
Tools	<ul style="list-style-type: none"> • investment casting core • drill bits • wood cutting bit • machining tools
Medical	<ul style="list-style-type: none"> • orthodontic bracket • orthopedic implants • forceps • surgical equipment
Automotive	<ul style="list-style-type: none"> • valves • injection nozzles • transmission parts • airbag components • seat worm gear
Consumer	<ul style="list-style-type: none"> • electrical tooth-brush micro-gears • watch components • hair-cutting shears
Sports	<ul style="list-style-type: none"> • spikes/cleats • bicycle parts • ski-bindings

1.3 The μ PIM Process

As depicted in Figure 5, the steps involved in fabricating a part using μ PIM are:

1. Powder selection and characterization
2. Mixing the powder with a suitable binder
3. Pelletizing the mixed feedstock
4. Injection molding to give the 'green' part
5. Binder removal from the 'green' part by debinding resulting in the 'brown' part
6. Densification of the 'brown' compact by high-temperature sintering.
7. Finishing operations if necessary.

The part thus made from this process has features of micron meter measurements. Hence it differs from PIM process of making parts with larger dimensions (in centimeters).

The selected powder (metallic or ceramic) and the multi-component binder system are first characterized for the process and then mixed to give a homogenized mixture called 'feedstock'. Typically the binder system amounts to about 40 volume % of the feedstock volume. The binder system also has some additives that are added to modify/enhance certain attributes of the feedstock. Processing aids, mold release agents, coupling agents, plasticizers, solvents, lubricants, wetting agents and strengtheners are some of the common types of additives used in the PIM feedstock formulations. [47]

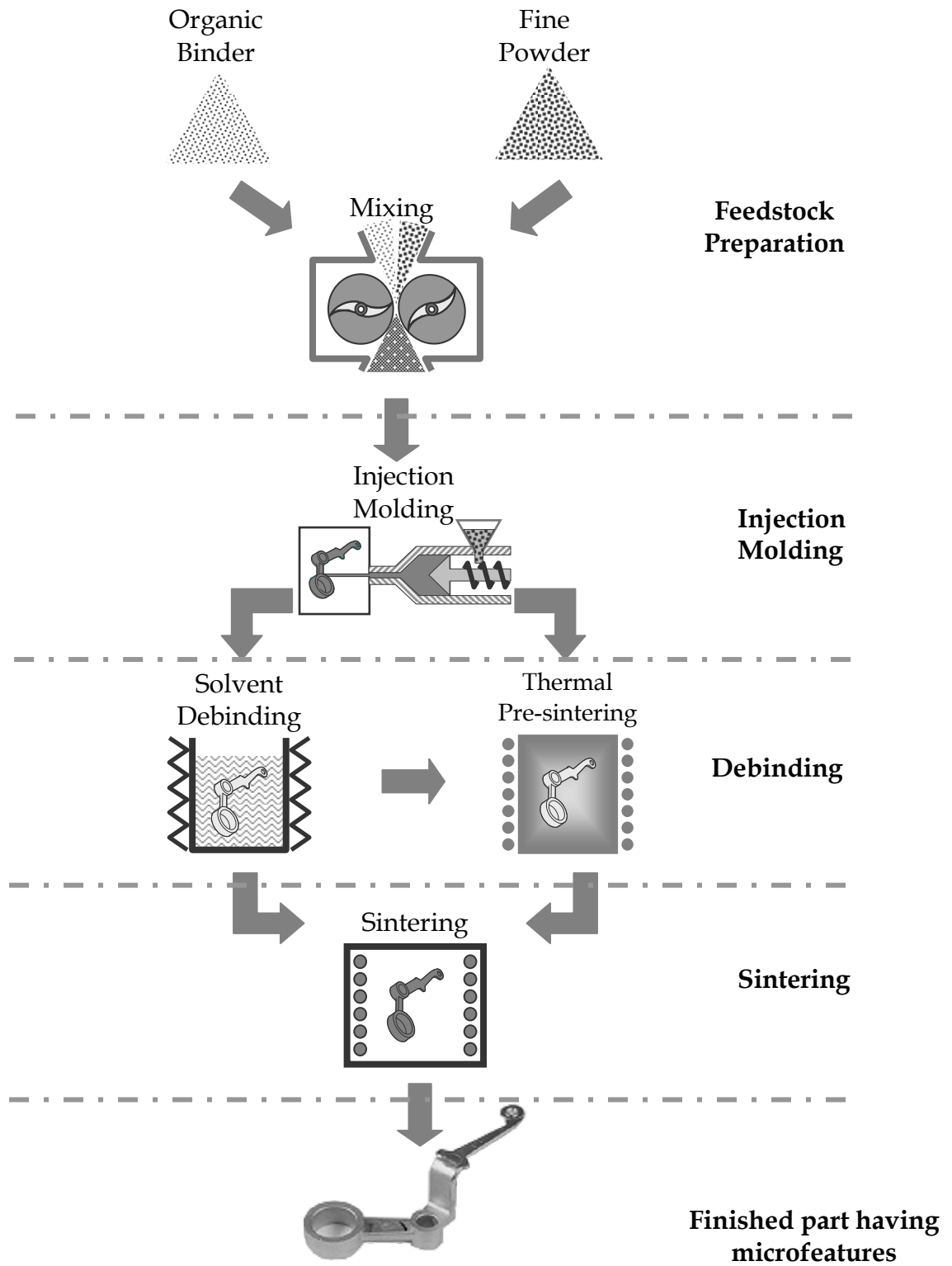


Figure 5: Schematic diagram of the μ PIM processing steps making part having micro features.

The feedstock properties are dictated by the choice of powder and binders selected. The rheological properties of the feedstock are mainly affected by this choice. The feedstock exhibits viscoelastic properties [48, 49]. During mixing and molding, the feedstock acts as a viscous material and once cooled it becomes elastic. The thermal conductivity, thermal expansion coefficient, heat capacity and thermal diffusivity are the thermal properties that need to be looked into while characterizing the feedstock. The viscosity of binder is mainly governed by the type of binder used, along with the powder loading and powder geometry. It is optimal to have tightly-packed particles with the binder completely filling the inter-particle places.

The feedstock is pelletized to facilitate easy handling and also to maintain its homogeneity once the mixing is done. The pelletizing step also recycles the scrap material back into the molding process. The scrap material comes from sprues, runners and defective molded components. The pelletized feedstock is then fed into the injection molding machine where it is molded into the desired shape by applying concurrent heat and pressure [50, 51].

The injection molding cycle takes place in five steps. Figure 2 shows the different steps of the PIM molding cycle. The feedstock (in granulated form) is first fed into the barrel of the injection molding machine via a feed hopper. In the barrel the feedstock is melted by the action of the reciprocating screw and external heating provided by the barrel heaters. The mold is first closed and then the molten feedstock is injected into the die cavity via the nozzle, sprue, runner and gates by the thrust (injection pressure) provided by forward motion of the reciprocating screw.

Once the cavity is about 98% filled, the transfer or switch-over occurs from filling to packing/ holding pressure. Here the reciprocating screw continues to push more material, at constant pressure, into the mold till hydrostatic equilibrium is reached. This is to compensate for the shrinkage due the cooling of the feedstock in the cavity [52]. This post-filling carries on until the gate freezes after which no more material can be injected into the die cavity. Now the pressure is released and the cooling phase begins. Once the part is cooled, the mold opens and the part is ejected by means of the ejector pins. The freshly molded 'green compact' is very brittle and prone to deformation. So care should be taken while handling such parts immediately after ejection. A typical injection molding cycle is depicted in Figure 6.

After molding, binder is slowly removed from the molded 'green' compact by either or a combination of thermal, solvent and/or capillary debinding techniques. The resulting in the 'brown' compact is porous and very brittle as the particles are weakly held together by the backbone binder. In the sintering step, the particles bond together, leading to densification of the brown part. During this stage the molded part undergoes volumetric shrinkages ranging from about 12 to 18%. The final step in the PIM process is the finishing operation which may include coining, machining, plating, and/or heat treatment. The finished component has excellent strength and microstructural homogeneity, which are superior to those resulting from other processing techniques [53, 54]

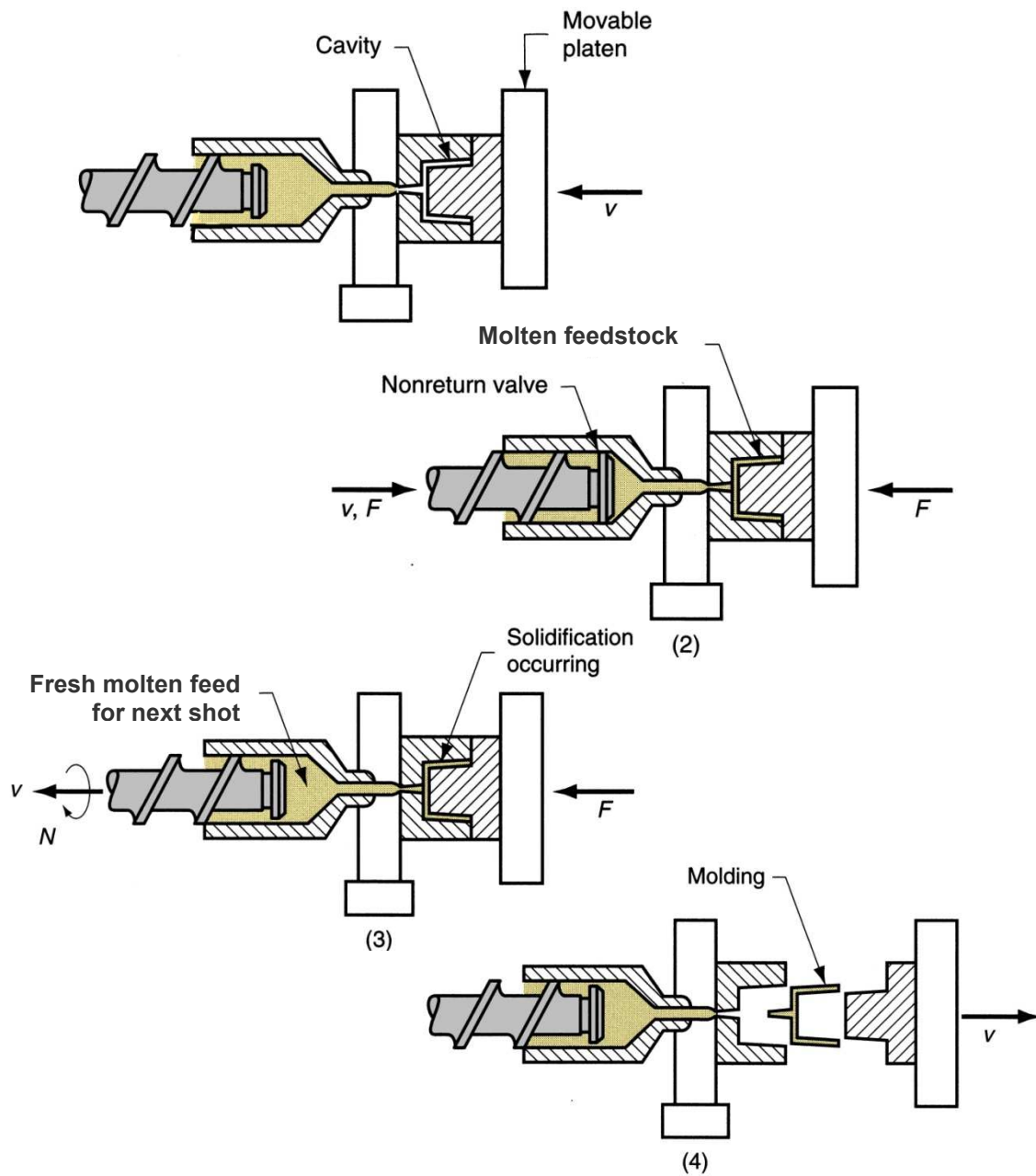


Figure 6: Typical injection molding cycle: (1) Mold is closed; (2) Melt is injected into the cavity and packed; (3) Screw is retracted and (4) Mold opens and part is ejected

1.4 Problem statement & Mold-filling stage:

The mold-filling stage is when the molten feedstock in the barrel is injected into the mold cavity via the sprue, runners and gates. This stage is one of the most vital stages in the injection molding process and controlling this stage is very critical to successfully mold a part [55, 56].

The problem specifically associated with this study (ceramic MCA) is the uneven filling of the cavity. The part shown in Figure 7 is the part used in this study. The details of the part dimensions will follow in Chapter 2. However, to define the problem statement to the readers, Figure 7 and 8 are added here. The part has microchannels of $50\mu\text{m}$ and a bulk substrate in millimeters.

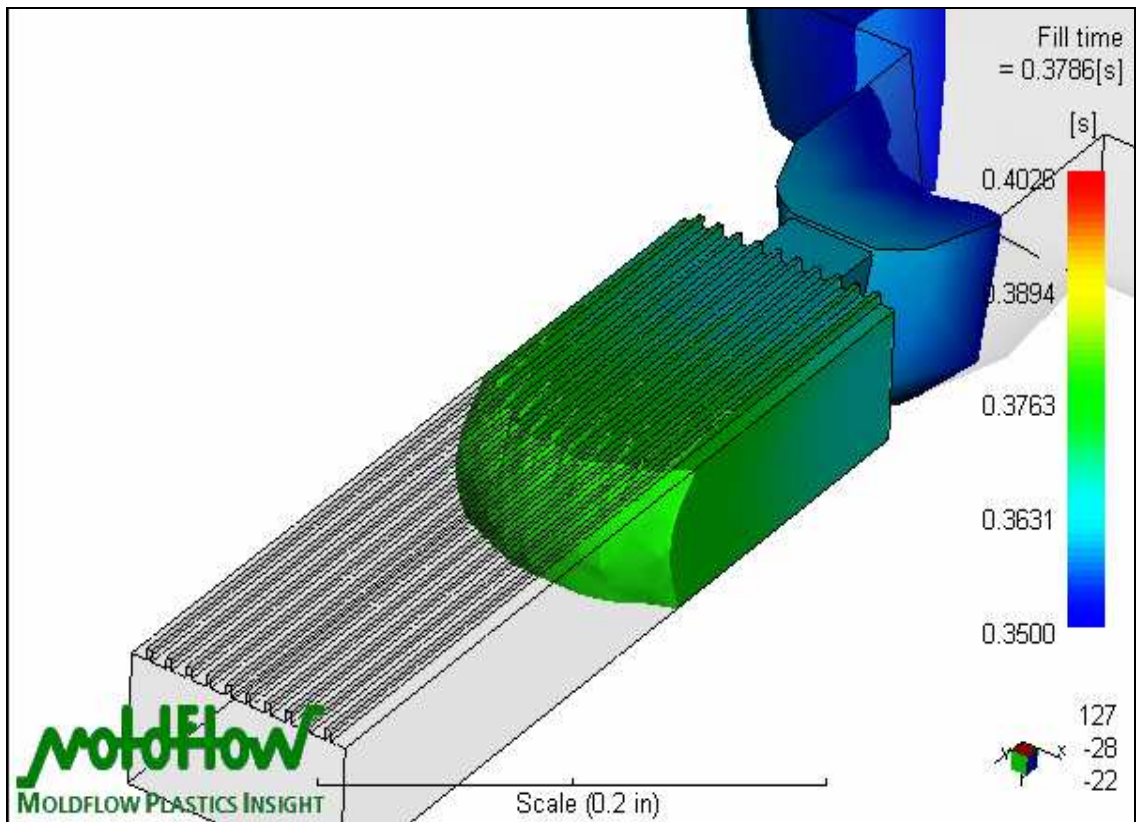


Figure 7: A typical schematic of the MCA part used in the study

Figure 8 is a self explanatory diagram. It shows the filling behavior of the feedstock into the cavity. It shows that the bulk substrate of the MCA fills much faster than the microchannels of the MCA. This particular flow pattern causes uneven filling and cooling in the part leading the various different defects shown in Figure 9.

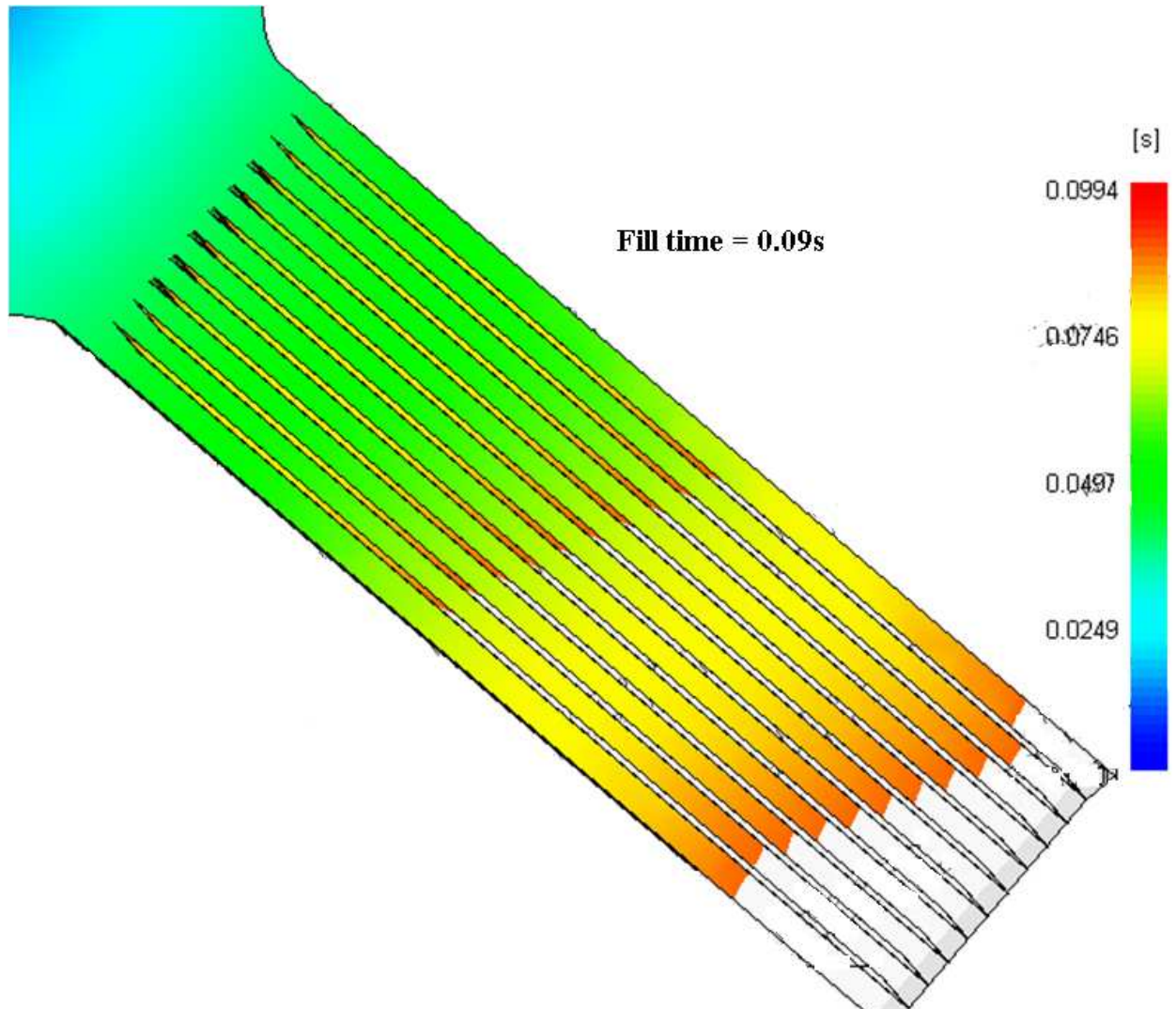


Figure 8: Definition of the problem statement

Figure 9 shows some of the defects that may occur if the process parameters are not defined correctly.

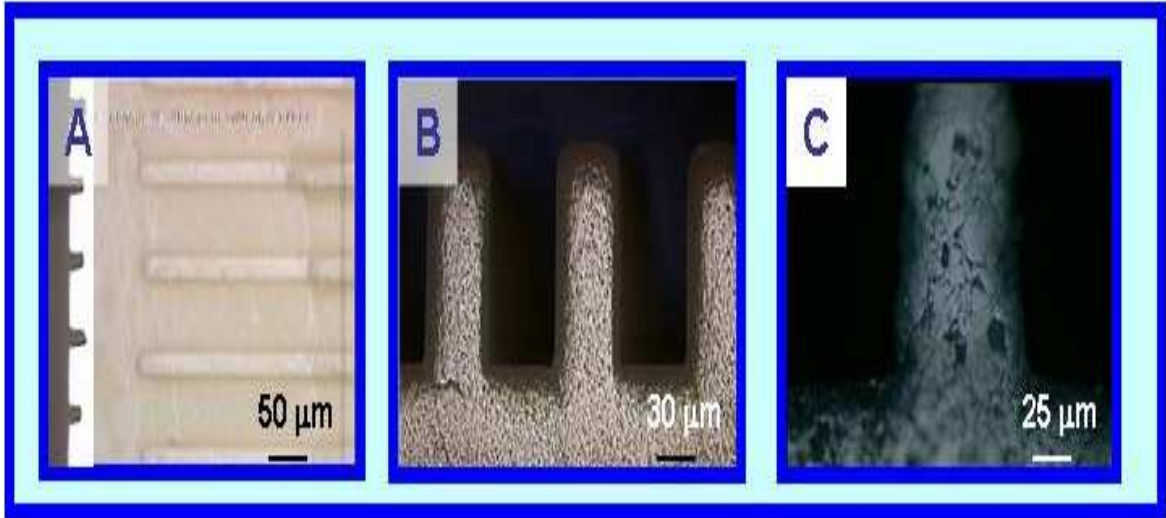


Figure 9: Material inhomogeneity in micromolding nanoparticulate suspensions: [A] incomplete mold fill, [B] ejection crack, [C] porosity distribution.

The study conducted in this thesis is to avoid such defects occurring in ceramic MCAs via simulations and experimentation.

1.5 PIM Simulation

1.5.1 Numerical Modeling and Simulation

CAE (computer-Aided Engineering) has been widely adopted and proved to be an important tool for industry and academic researches. By using CAE tools for PIM study, the part and mold designs can be effectively evaluated in design phase. The process variables can be developed and refined according to the simulation results even before the parts are made. The advanced CAT tool makes researches conducted in a more cost-efficient way. Two objectives for modeling and simulation developed have been set for this research. The first objective is to study flow behaviors of the suspension melt in mold cavities to

assist the powder injection molding process development for ceramic Microchannel Arrays (MCAs). The second propose is to study the process conditions that may contribute the macro scale material homogeneity issue such as short shots; and also to study the special melt flow effects that may be directly associated with the particle migration behaviors in microchannels such as the frozen and slip layers [57].

1.5.2 Modeling tools

Two modeling tools have been used for this research, Moldflow Plastic Insight (MPI) and PIM Solver. The former is a well known and a true solid modeling CAE tool broadly used by industry for plastic processing, especially the plastic injection molding. By using MPI, the injection molding process simulations can be carried out on the single solid model, in which the bulk and micro cavities are meshed with solid elements of the different resolution to achieve required precession and simulation efficiency. The tool is able to predict melt flow behaviors and potential defect under simulated process conditions. While MCI has strong ability in 3-D cavity melt flow simulation, it falls short in dealing with suspension materials (powdered metal and ceramic feedstock) and post PIM processes such as debindind and sintering. On the other hand, PIM Solver is a CAE tool, which is specifically designed for Powder Injection Molding (PIM). Like MPI, PIM Solver can accurately predict molding pressure, material velocity, and temperature profiles throughout the flow region. It can also track defects such as short shots, weld lines, air traps, and incomplete mold fills. The software composes two operation modules: PIM Solver Post and PIM Solver Pre. The former is used to construct the model and run the filling analysis. The latter is used to display the results of the analysis. The short fall for current version of PIM Solver is that the simulation analysis is based on 2.5-D modeling, which

limits the application in some complex cavity designs. Neither is these two CAE tool able to simulate the particle migration suspension in melt flow under high pressure, temperature and shear rate. Nor can they predict the material homogeneity of molded parts at green or sintered state.

1.5.3 Flow Model Development

The injection molding process can be divided into several stages including filling, packing and cooling. Each of these stages may affect material homogeneity and the dimensions of the modeled parts after ejection. In the filling stage, the hot suspension melt is injected into the cavity by the applied pressure. After the cavity is completely filled, additional melts is pushed into the cavity at the hold pressure to compensate the volume shrinkage of the melt during solidification. Ideally, once the gated is frozen, the packing phase stops and the cooling phase begin. In the cooling phase, the melt solidifies further until the preset ejected temperature is reached, and then the part is separated from the mold and ejected [57, 58]. There are set of non-Newtonian flow mechanic equations used in simulation of each of these process stages.

1.6 Goal of the Study

To understand the process of μ PIM (mold filling) with the help of computer simulations (Moldflow Plastic Insight) for ceramic microchannel arrays by investigating materials, processing and part designing issues.

Steps required to reach the goal were,

1. Prepare an alumina feedstock based on paraffin wax and polypropylene as binders for comparison with polyacetal based commercially available feedstock.
2. Characterize the rheological and thermal properties of the two alumina feedstocks.
3. Use the measured properties of the alumina feedstocks to analyze the mold-filling behavior in microchannel arrays using computer simulation.
4. Study the effect of processing parameters and part geometry on mold-filling behavior in microchannel arrays.
5. Conduct molding trials with the two alumina feedstocks on microchannel array.
6. Experimentally compare the differences in the molded microchannel array parts to understand the implications of the computer simulations.

Figure 10 gives the schematic view of the steps taken to reach the goal.

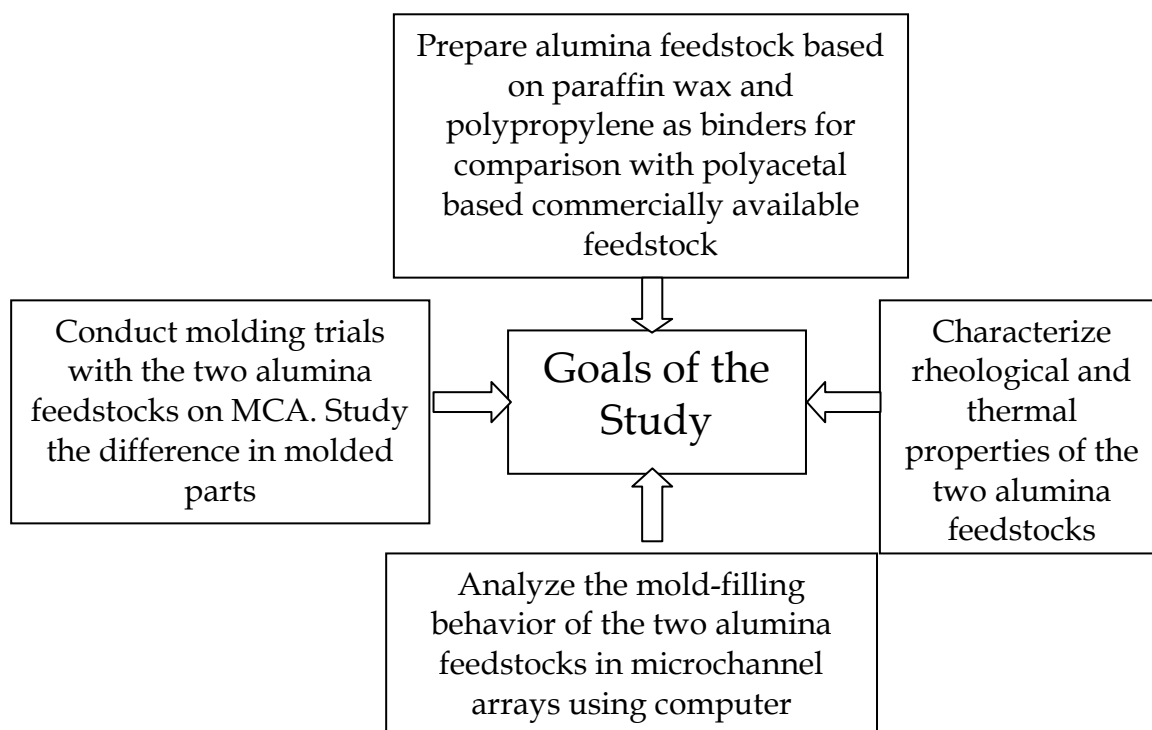


Figure 10: An approach towards reaching the goals of the study

CHAPTER 2: SIMULATION STUDIES & EXPERIMENTAL

METHODS

This section describes the simulation technique and the experimental method used for micro powder injection molding in this thesis.

2.1 Simulation method

For over two decades, Moldflow's software solutions have brought the promise of "better, faster, cheaper" plastic products to major companies in various industries around the world. Designs for molds and products ranging from toys to automotive and aerospace components to medical parts and many others have been simulated and optimized prior to production, saving manufacturers hundreds of thousands of dollars every year.

2.1.1 Injection Molding

The injection molding process can be broken into three phases:

- Filling phase.
- Packing phase.
- Cooling phase.

2.1.1.1 Filling phase

During the filling phase, plastic is pushed into the cavity until the cavity is just filled. As plastic flows into the cavity, the plastic in contact with the mold wall quickly freezes. This creates a frozen layer of plastic between the mold and the molten plastic. At the interface between the static frozen layer and the

flowing melt, the polymer molecules are stretched out in the direction of flow. This alignment and stretching is called orientation. Figure 11 show how the flow front expands as material from behind is pushed forward. This outward flow is known as fountain flow. The edges of the flowing layer come into contact with the mold wall in a near perpendicular direction and freeze. The molecules in the initial frozen layer are therefore not highly orientated, and once frozen, the orientation will not change.

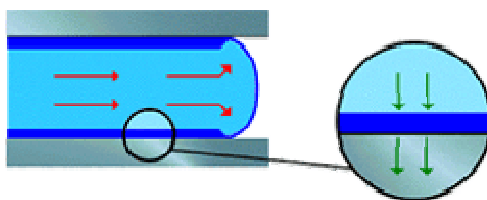


Figure 11: Fountain flow while feedstock melt fills the cavity

The red arrows show the flow direction of the molten plastic. The dark blue layers against the mold walls show the layers of frozen plastic. The green arrows indicate the direction of heat flow from the polymer melt into the mold walls.

The frozen layer gains heat as more molten plastic flows through the cavity, and loses heat to the mold. When the frozen layer reaches a certain thickness, equilibrium is reached. This normally happens early in the injection molding process, after a few tenths of a second.

2.1.1.2 Packing phase

The packing phase begins after the cavity has just filled. This involves further application of pressure to the material in an attempt to pack more material into the cavity, in order to produce uniform shrinkage at reduced levels and consequently, reduce component warpage.

Once the material has filled the mold cavity and the packing phase has begun, material flow is driven by the variation of density across the part. If one region of a part is less densely packed than an adjacent region, then polymer will flow into the less dense region until equilibrium is reached. This flow will be affected by the compressibility and thermal expansion of the melt in a similar way to which the flow is affected by these factors in the filling phase.

The material's PVT characteristics provide the necessary information (density variations with pressure and temperature, compressibility and thermal expansion data) so that when combined with the material viscosity data accurate simulation of the material flow during the packing phase is possible.

Figure 12 shows the difference between the end of the filling phase (left image) and the end of the packing phase (right image).



Figure 12: Difference between the end of the filling phase and end of packing phase

In practice, due to limitations of pressure and available unfrozen flow channel, it is not possible to pack enough material into the mold to fully compensate for shrinkage. The uncompensated shrinkage must be allowed for by making the cavity bigger than the desired part size.

2.1.1.3 Cooling phase

The cooling phase occurs after the end of packing. The cooling phase is the period of time from the end of packing to the instant that the mold clamp opens. Cooling of the plastic occurs from the commencement of the filling phase, so that this phase can be considered as the extra time required, after the packing time, to cool the part sufficiently for ejection. This does not necessarily mean that all sections of the part or runner system need be 100% frozen. The material at the center section of the part wall reaches its transition temperature and becomes solid during cooling time.

The rate and uniformity at which the part is cooled affects the finished molding quality and production costs. Mold cooling accounts for more than two-thirds of the total cycle time in the production of injection molded thermoplastic parts.

2.1.2 Meshing

Analyzing a model is a complex operation. Modeling the way molten plastic (a non Newtonian fluid) flows, especially through complex model geometry, is difficult.

To overcome these issues, a part is divided into smaller elements that are joined together. The result is a mesh. Temperature, pressure and velocity of flow are then calculated for each element within the mesh. The cumulative effect is a representation of the whole model.

There are three different types of mesh used in MPI: Midplane, Fusion and 3D.

2.1.2.1 Midplane mesh

Historically, a part was meshed by determining the thickness of the part and then assigning a surface plane through the middle of the thickness. This surface was then meshed with triangular elements (Figure 13) that are joined along their edges and corners (called nodes).

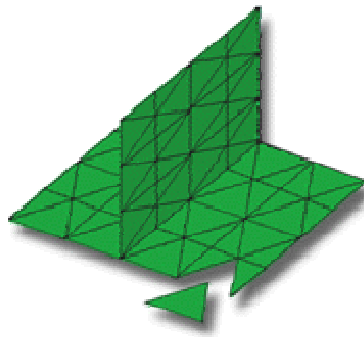


Figure 13: Cross-section of an image from midplane meshing

At each node, the thickness of the part at that point is recorded. Analysis then incorporates this measurement by dividing the thickness of the part into thin layers called laminae. This gives a defined part volume for calculations to be performed on.

2.1.2.2 Fusion mesh

A fusion mesh represents a solid CAD model by covering the surface of the model with triangular elements. The locations where the corners of adjacent triangles meet are called nodes (Figure 14). The model could be visualized as a hollow body covered with a surface shell.

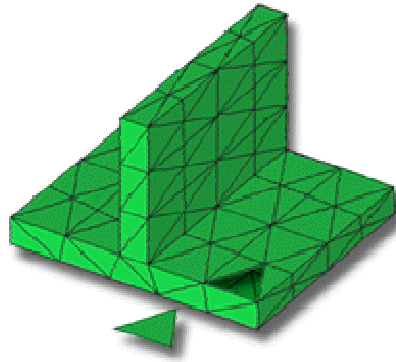


Figure 14: Cross-section of an image from fusion meshing

When analyzing a part, the volume of the model is represented by layers or laminae through the thickness of the part (typically 10 or more laminae through a thickness). To build these laminae, it is important that there are matching elements on the opposite face of the part. These matched elements ensure the alignment of element laminae (a stack of triangular wedges) through the thickness. These laminae permit an accurate representation of thin cross sectioned parts, where there is a rapidly changing characteristic profile (for example, temperature, and flow front velocity).

2.1.2.3 3D mesh

A 3D mesh represents the CAD model by filling the volume of the model with four-node, tetrahedral elements (Figure 15).

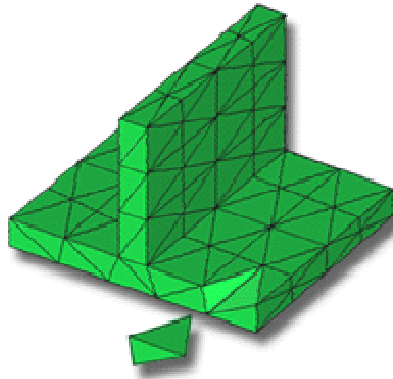


Figure 15: Cross-section of an image from 3D meshing

3D meshes work well for parts that are "thick and chunky" because tetra give a true 3D representation of the model. Analysis of a 3D mesh uses mathematical equations without the assumptions used for midplane or fusion mesh. The additional computational time this requires necessitates a less refined mesh. This makes 3D mesh more appropriate for thick, complicated shaped models, while midplane and Fusion mesh are more applicable for thin-walled, shell like parts.

2.1.3 Important Definition:

Fill Time: The time required for the polymer melt to completely fill the cavity.

Time to Freeze: The time required to completely freeze the polymer melt inside the cavity.

Meaning of colors here:



Figure 16: Meaning of colors in MPI

Gate: The location(s) where polymer is injected into the mold cavity (Figure 17). Each polymer injection location will inject plastic at the same pressure. This pressure increase is generally linear during the injection period, unless an end-of-fill spike occurs.

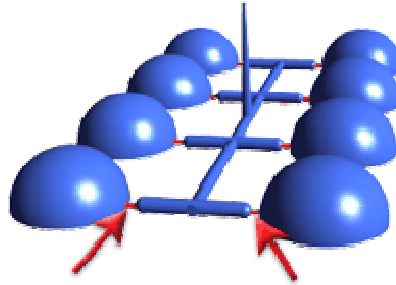


Figure 17: Gate locations

Why injection locations are important

The positioning of injection locations plays an important role in the effects of material orientation on part warpage. In some cases, changing the gate position is the only way of controlling orientation effects to produce a satisfactory design. The essence of proper gating is to avoid problems associated with overpacking, such as variation in shrinkage and product sticking in the cavity.

2.1.3.1 Design Rules

Gate centrally to provide equal flow length

Centralized gates provide equal flow lengths to all extremities of the part. This results in more even packing in all directions and a lower shrinkage difference, which lead to a higher quality part and lower rejection rate.

Gate symmetrically to avoid warpage

Symmetrical parts should be gated symmetrically to achieve balanced flow and avoid differential shrinkage and subsequent warpage of the part.

Gate into thicker sections for better filling and packing

Place polymer injection locations in thicker regions of the part, preferably at a spot where the function and appearance of the part are not impaired. This leads the material to flow from the thickest areas to the thinnest areas, and helps maintain the flow and packing paths. Gating into thinner sections can result in hesitation or sink marks and voids

Gate long, narrow parts from an end for uniform flow

When a long narrow part is centrally gated, packing near the gate and variable molecular or fiber orientation throughout the part will cause differential shrinkage, which will warp the part. Gating a long part at one end will provide a uniform molecular and fiber orientation in the length direction. Although the end with the gate will be packed more than the opposite end, the resulting difference in shrinkage will not cause warpage (Figure 18).

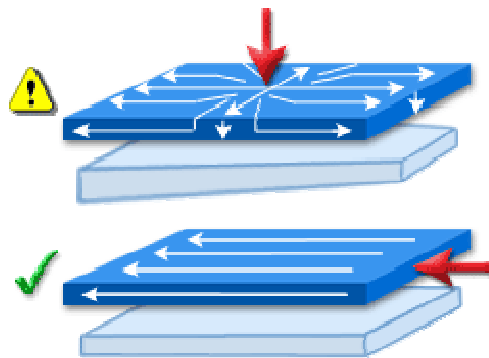


Figure 18: Best gate location

Position the gate away from load-bearing areas

The high melt pressure and high velocity of flowing material at a gate causes that area to be highly stressed. For this reason, you should locate the gate away from load-bearing areas.

Where to put polymer injection locations

One of the goals in selecting polymer injection locations is to ensure that all flow paths in the cavity fill at the same time (balanced flow paths). This prevents overpacking along the flow paths which might otherwise fill first. Altering the polymer injection location can also be used to change the position of weld lines and air traps, and reduce hesitation and other molding problems. In some cases it may be better to have more than one polymer injection location.

Number of injection locations

There are no exact rules for determining the number of polymer injection locations, as each part is different. However, there are some general factors to consider helping make this decision.

Flow length refers to how far the polymer must flow from the polymer injection location (Figure 19).

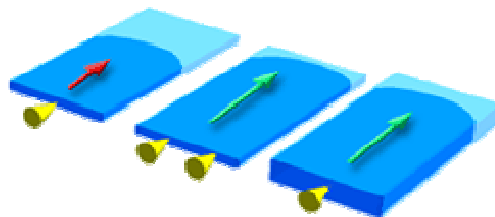


Figure 19: Flow length

Generally, parts with thicker walls can have longer flow paths than thin-walled parts as the material will flow more easily in the thicker regions. The flow characteristics of the plastic material affect how far material will flow for a given thickness and the shorter the flow length, the more gates required to fill a part. Each material has its own flow length. The materials datasheets from material suppliers contain information on flow lengths which can be achieved for each specific material at a range of thicknesses.

Very large parts, thinner walled parts and higher viscosity materials will typically require more gates to fill a part.

2.1.3.2 Part volume

Generally, parts with larger volumes require more polymer injection locations to fill properly.

What you should do

First, try a single gate in the flow centroid of the mold, and check that all flow paths fill at nearly the same instant in time.

If this criterion cannot be met with a single gate, then try using multiple gates (Figure 20). Mentally, divide the part mold into sub-moldings, with a gate positioned at the flow centroid of each sub-molding or in the middle of one side. The runner system dimensions should be set up so that each sub-molding is filled at nearly the same instant in time.

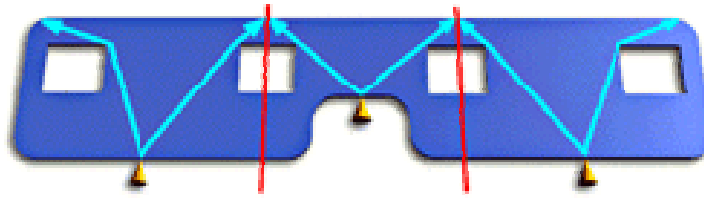


Figure 20: Multiple gate locations

The positions of the gates should achieve both uniform and acceptable values of shrinkage across the part. In some cases where thick and thin sections are present, it is good practice to position the gate nearer thicker sections, in order to avoid insufficient packing caused by premature freezing of the material between the gate and the thicker regions.

2.1.4 Selecting the material

This topic describes some important material characteristics to consider before selecting a thermoplastic material grade. The material that you select will depend on the characteristics that you require.

Crystallinity

The crystallinity of a material identifies the state of the polymer at processing temperatures, and can range from amorphous to crystalline states. Amorphous polymers are devoid of any stratification, and retain this state at ambient conditions. Crystalline polymers have an ordered arrangement of plastic molecules, allowing the molecules to fit closer together. Therefore, they are more dense than amorphous polymers. The rate of crystallinity is a function of temperature and time. Rapid cooling rates are associated with lower levels of crystalline content and vice versa. In injected molded parts, thick regions cool

slowly relative to thinner regions, and therefore have a higher crystalline content and volumetric contraction.

Mold and melt temperature

The mold temperature is the temperature of the mold where the plastic touches the mold. Mold temperature affects the cooling rate of the plastic, and cannot be higher than the ejection temperature for a particular material. The temperature of the molten plastic is the melt temperature. Increasing the melt temperature reduces the viscosity of a material, which also reduces shear stress. This results in less material orientation during flow. Additionally, the material is hotter which decreases the frozen layer thickness. Decreasing the frozen layer means that shear is less since the constriction to flow is less.

Thermal properties

The **specific heat (Cp)** of a material is the amount of heat required to raise the temperature of a unit mass of material by one degree Centigrade. It is essentially a measure of a material's ability to convert heat input to an actual temperature increase. It is measured at zero pressure and a range of temperatures, or averaged across the temperature range of 50°C to the material's maximum processing temperature.

The **thermal conductivity (k)** of a material is the rate of heat transfer by conduction per unit length per degrees Celsius. It is essentially a measure of the rate at which a material can dissipate heat. It is measured under pressure and at a range of temperatures, or averaged across the material's melt temperature range. The unit of measure is W/m-C, Watts per meter Celsius.

Viscosity

The viscosity of a material is a measure of its ability to flow under an applied pressure. Polymer viscosity is dependent on temperature and shear rate. In general, as the temperature and shear rate of the polymer increases, the viscosity will decrease, indicating a greater ability to flow under an applied pressure. The material database provides a viscosity index for materials, in order to compare ease of flow. It assumes a shear rate of 1000 1/s and indicates the viscosity at the temperature specified in brackets.

PVT data

To account for material compressibility during a flow analysis, Moldflow provides PVT models. A PVT model is a mathematical model using different coefficients for different materials, giving a curve of viscosity against pressure against temperature. An analysis based on PVT data is more accurate but computationally intensive - through iterations for temperature and pressure per node. However, this makes it particularly suited to complex models that have sudden and large changes in thickness.

Shrinkage

As plastics cool, there is a significant change in their dimension, due to volumetric shrinkage. The main factors that affect shrinkage are cool orientation, crystallinity, and heat concentrations.

Optical

Transparent plastic under stress can exhibit stress birefringence, where the speed of light through the part depends on the polarization of the light. Birefringence

can result in the transmission of unevenly-polarized light and in double images. Some materials are more prone to stress birefringence than others.

Composite materials

Composite materials contain fillers that are added for injection molding. Adding filler to a polymer can increase the strength of the polymer and ensure that good quality parts are produced. Most commercial composites contain 10-50% fibers by weight, which are regarded as being concentrated suspensions, where both mechanical and hydrodynamic fiber interactions apply. In injection-molded composites, the fiber orientation distributions show a layered nature and are affected by the filling speed, the processing conditions and material behavior.

2.1.5 Moldflow Plastics Insight (MPI)

Moldflow Plastics Insight (MPI) helps you determine the ideal combination of part geometry, material, mold design and processing conditions that will produce quality finished parts.

The main tasks that you will perform when you use MPI are:

- 1) Importing a model into MPI.
- 2) Creating a mesh to represent the model geometry (also known as meshing the model).
- 3) Repairing the mesh if it contains errors (we are not going to do this in our lab)
- 4) Modeling the mold (cavity layout, feed system and cooling).
- 5) Analyzing the study.

- 6) Viewing and interpreting the results of the analyses
- 7) Adjusting the molding parameters based on the analysis results.

2.1.5.1 Importing a model

MPI needs a model to analyze.

A model of the part needs to be imported into MPI for analysis. This model is saved into a **Project**. A project is used to store **studies**. Each study is a version of the original imported model and can be analyzed with different combinations of features such as injection locations, processing parameters, runner/cooling configurations, material, analysis sequences etc. Analysis results for a study are stored in separate files from the study and are linked to the study in the project. You can generate a new study at any time by using **File ➔Save Study As**.

For file management reasons, most users create a new project for each mold analyzed. Method to create a new project and import a study into it is as follows:

Creating a new Project

1. Click **File ➔New Project**. The **Create New Project** dialog appears.
2. Enter **Getting Started** in the **Project name** text box.

Note that the **Create in** text box outlines the pathway to where the project will be stored, and that the new Project name you have entered is included in this description. MPI has created a subfolder called "Getting_Started" for the new project.


3. Click **OK**.

A new project called Getting Started is created and opened in MPI.

Ensure the **Tasks** tab is selected. This is located at the top of the white Project Study Pane on the left hand side of the window. The **Getting Started** project you have just created is now listed in this section.

You will now import a study into the project you have just created.

Importing a study


1. Click  (**File ➔ Import**).
2. Select the file you got it in iges format.

The model is read in, and a new study is automatically created in the "Getting Started" project. This is illustrated in the Project View pane.

2.1.5.2 Model manipulation

In this task we will look at the tools that are available to rotate and zoom in and out of sections of the model you open in the previous task.

Ensure the model from the previous task is open.

1. Click the **Rotate**  icon which is located on the Viewer toolbar. (**View ➔ Toolbars ➔ Viewer**). Click anywhere on the model and, with the left mouse

button held down, move the mouse. The model will pivot around a central point. This is useful when investigating the geometry of the part.

2.1.5.3 Generating Fusion mesh

You will now generate a fusion mesh for this part.

1. In the **Study task** pane, double click **Create Mesh..**

This has the effect of opening the **Tools** tab **Generate Mesh** pane.

2. Click **Mesh Now**. The generation of the mesh will take a short time.
3. Rotate and zoom in on the part to investigate the mesh, especially at rounded corners and thin edges.
4. In the **Study Tasks pane**, note that the third line down now identifies the mesh as **Fusion** and the model is made up of approximately 14,500 elements

Notice in the Project View pane that there is a “F” symbol next to the study name. This shows you that you have selected a Fill analysis for that study. When the analysis has been run and results are available, the inside of the symbol is colored in.

When analyzing a part from an imported CAD model, it is recommended to always start with a basic filling ("Fill") analysis to checking the filling pattern, injection pressure, the location of air traps or weld lines, etc. Once you are

satisfied with the filling parameters for the part, you can run a full Flow analysis (filling + packing phase), and then further analyses such as cooling or warpage.

2.1.5.4 Selecting a Material

In this task, you will select a molding material based on:

- Supplier name.
- Trade name.
- Family of polymer.
- Filler material requirements.
- Comparison of similar material properties.

1. Ensure the model from the previous task is open.

Note that in the **Study Task** pane, the default material **Generic PP: Generic Default** is selected.

This part has a specified material, **Tenite LDPE 1870** from **Eastman Chemical Products** that needs to be used for analysis.

2. Double click on **Generic PP: Generic Default** and the **Select Material** dialog appears.
3. Click the **Manufacturer** drop-down list.
4. Either scroll up or down the list until you find **Eastman Chemical Products** or type **east** in the list box and the supplier will be selected.
5. Type **ten** in the **Trade name** drop-down box.

There are several Tenite materials available.

6. Either click the drop-down arrow and select the required material, or press the up and down keys on your keyboard until the desired material **Tenite LDPE 1870** is shown in the box.
7. Click **Details** and the material properties are displayed.
8. Click the **Recommended Processing** tab and note the recommended mold surface temperature of 40° Celsius and a Melt temperature of 220° Celsius.
9. Click **OK**. Twice.

The selected material is displayed in the **Study Tasks** pane.

10. Double click on **(Process Settings)** and note how the recommended process settings for the selected material are now listed at the top of the **Process Setting Wizard - Fill Settings** dialog.
11. Click **Cancel** to remove the dialog.

2.1.5.5 Designing a cooling circuit

In this task, you will design a simple cooling circuit layout using the Cooling System Wizard. The Wizard cannot create all possible features of a cooling system, but it is excellent for creating a quick initial layout that can serve as the basis for a more complex cooling system, for example, including bubblers, baffles and other cooling aids.

1. Ensure the project you created in task 1 is open.

Note: The Cooling Circuit Wizard requires that the part lies in the XY plane.

2. Click **(Front View)**.
3. From the **Tools** pane, click **(Move/Copy)** and select **(Rotate)**
4. **Select All** from the **Selection** toolbar (**View Toolbars Selection**).
(Alternatively **Edit Select All**).
5. Select **Z Axis** from the dropdown list and enter **90** in the **Angle** box.
6. Click **Apply**.
7. Rotate the model 90° around the X axis using the previous two steps as reference.

The XY plane is now parallel with the top surface of the model. Click **Close** on the **Tools** pane.

8. Click **Cooling Circuit Wizard** from the **Modeling** toolbar (**View Toolbars Modeling**).

The first page of the **Cooling Circuit Wizard** appears. This is used to specify the layout of the cooling circuits, in particular the channel diameters, the distance from the part surface to the cooling circuits and the alignment of the circuits relative to the part.

9. Enter the following values on the first page of the Cooling Circuit Wizard:
 - Channel diameter: **6 mm**
 - How far above and below: **15 mm**
 - Ensure that the **Y** alignment option is selected.
10. Click **Next** to move on to the next Wizard page.

The second page of the Wizard is used to specify the number of channels, and their spacing relative to one another and the part.

11. Enter the following values:

- Number of channels: **4**
- Distance between channel centers: **40**
- Distance to extend beyond part: **20**.

12. Click **Preview**.

The bottom of the Wizard has two additional options. **Delete existing circuits first**, which is **active** by default, and will remove any existing cooling circuits from the model before creating the new circuits. **Connect channels with hoses** allows the Wizard to apply the optional Hose attribute to the connecting end segments of the cooling channel; for this exercise, leave the check box deselected. Cooling circuit segments with the Hose attribute will have a heat transfer effectiveness of zero and therefore not contribute to the cooling of the part.

13. Click **Finish**.

Rotate the model to visually inspect the cooling system. Your model should now look as shown in the image below.

Tip: If you did not obtain the required results, click **(Undo)** to remove the cooling system, click **(Modeling Cooling Circuit Wizard)** to restart the Wizard. The Wizard remembers all the settings you last used so simply step through the Wizard pages and make adjustments as required.

It appears that the distance between cooling channels might to large.

14. Alter the distance between cooling channels to **30mm** using the above

instructions.

You will now inspect the coolant inlet parameters automatically applied by the Wizard and the change the coolant inlet temperature in both circuits to 30°C.

15. **Select** and then click one of the light blue coolant inlet symbols to select it. They are situated at the start of the cooling circuits.
16. Right-click and select **Properties**.

You will see the coolant is water and a default coolant temperature has been applied.

17. Change the coolant inlet temperature to 30°C, enter **Water - 30 degrees** in the Name box, and click **OK**.
18. Click on the other coolant inlet symbol (**Edit Assign Property**). From the list of properties in the Assign Properties dialog list, select the entry **Water - 30 degrees**, and click **OK**.

2.2 Microchannel Arrays design

Ceramic microchannel arrays (MCAs) were designed as the experiment samples for conducting the research. To make MCA study samples, an advanced experiment platform of the μ PIM was developed, which included Arburg powder injection molding machine, the precision micro cavity mold, a built-in sensor system and the fast data acquisition module. The μ PIM process was developed such that the selected critical process parameters would have effects on material heterogeneity of the molded MCA parts. The numerical simulation tool, Moldflow, was studied and used for assistance in the mold design, process

development, and study of the physical condition for binder and powder separation. As the most important contribution of this research, different analytical test methods were investigated and developed for material homogeneity characterization using green and sintered MCA components.

To carry out the research, experiment samples must be carefully designed with specific geometry and dimensions. The following criteria were used for selection of the sample designs.

1. Microfeatures with geometrical dimensions less than 0.5 mm
2. Enough suspension melts flow distance with a large flow path ration (L/T)
3. Multi-scale structure design to explore the volume depended share rate effects.
4. Significant contributions for science and techno development from the research conducted with designs.

Based on the sample design criteria, the ceramic microchannel arrays (MCAs) were selected for conducting the material homogeneity research (Figure 21).

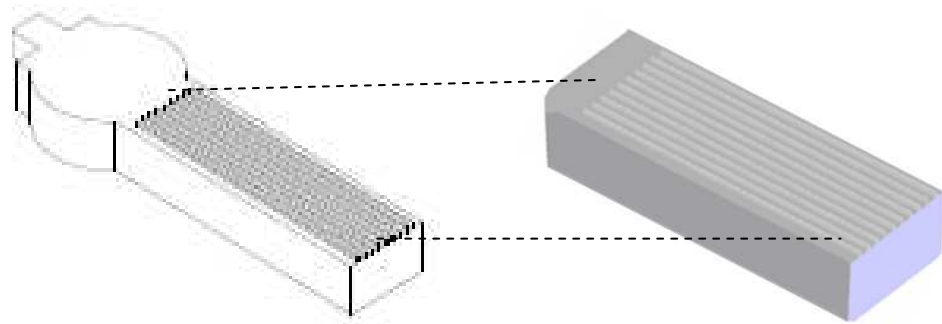


Figure: 21: Experiment part design

The study sample, designed for investigating the green material homogeneity of micro and macro scale from ceramic PIM, has the shape of a rectangular block, which comprises two structures, the bulk substrate and the micro channel arrays. Both macro and microscale material homogeneity studies were conducted on MCA micro features with macro scale study focusing on channel filling defects such as the short shot and microscale study on the particle and binder separation. MCA as the main study features was carefully designed with specific geometry and dimensions in terms of different channel wall width, thickness, channel width, and channel length. The flat pad (circular shape) at the end of the part was designed for landing the thermal sensor tip in the model cavity for process monitoring. The bulk size of the small parts with 50 μ m ribs was about 2.5 x 8 x 1.5 mm (width x length x thickness), with an approximate volume of 48 mm³ and the weight of 0.12g. The small part was also designed with the aspect ratio of 2:1 for the microchannel walls and the large flow path ratio of $L/T = 80$ (length/thickness).

Table 4 gives the process conditions used for simulation studies of the ceramic microchannel array part.

Table 4: The process conditions used for simulation studies of the ceramic microchannel array part for Catamold AO-F and Standard Mix

Processing Conditions /model design	Catamold AO-F & Standard Mix
Dosage Rate	$10 \text{ cm}^3 / \text{s}$
Injection Pressure	60 MPa
Holding Pressure	120 MPa
Mold Temperature	150°C
Melt Temperature	190°C
Number of Gates	1
Bulk Thickness	1.5mm

A typical image from the MPI is shown in Figure 22.

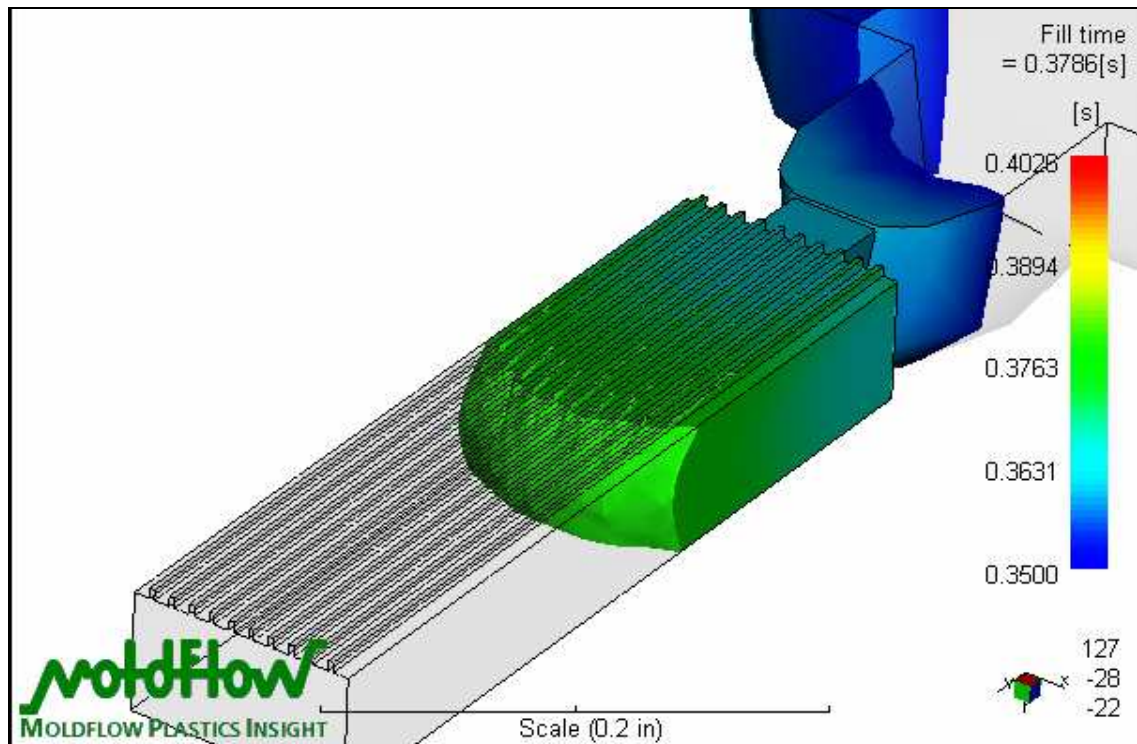


Figure 22: Typical image of the part from MPI

2.3 Materials

Although there is a relatively wide range of materials available for μ PIM, it is necessary to focus on powders of small particle size. The starting powder requirements for μ PIM are much more stringent than that used for conventional PIM. For example, the particle size should be at least about one order of magnitude smaller than the minimum internal dimension of the microscale part.

2.3.1 Binders

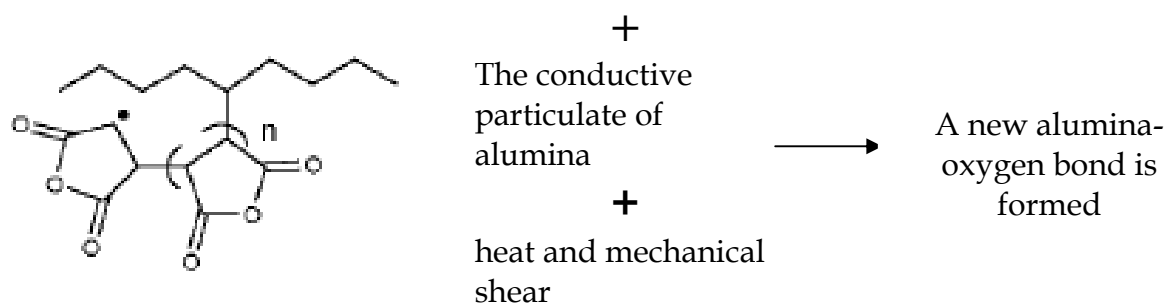
There have been studies on different binder systems in the past. [59, 60] studied the effect of different binder mixtures on the rheological properties of the feedstock using Polyvinyl acetate and Cellulose acetate butyrate as the binder systems. The feedstocks used in this research are the commercially available alumina-polyacetal feedstock (Catamold AO-F, BASF) and an in-house product, Standard Mix, comprising of alumina-propylene/paraffin wax (Composition is given in Table 5), both containing about 56 vol.% solids loading. The binder used in the Standard Mix is a blend of Proflo 3000 by Polyvisions, Fusabond-E MB 226D by Dupont, Paraffin Wax MP 130°C by Stevenson-Cooper, and Stearic Acid by Fisher Scientific.

Table 5: Composition of Standard Mix and Catamold AO-F

Composition	Standard Mix	Catamold AO-F
	(Vol %)	Supplied by BASF contains Polyacetal as a binder
Alumina	56.1	
Proflo 3000	15.4	
stearic Acid	2.2	
Fusabond-E MB 226D	4.4	
Paraffin Wax	22.0	

For preparing the standard mix, the binder components were added in progressively, starting with the binder component with the highest melting point. According to the thermal properties of the binder components, the mixing temperature was set higher than the highest melting point, but lower than the lowest degradation temperature of the binder components. The A16SG nanopowder and the binder system were mixed in *Haake Rheocord* mixer for 30 minutes at 150 °C. Mixing speed was kept at 50 rpm. The purpose of the components in Standard Mix's composition is as follows:

- Proflow 3000 is a polypropylene copolymer having a melt index of 2600 g/10 min when measured in accordance with ASTM D1238 at 230 °C and 2.16 kg.
- Stearic Acid is used as a processing aid.
- Paraffin Wax is the major binder composition in Standard Mix's formula.
- Fusabond-E MB 226D is a modified polyolefin comprising of high density polyethylene grafted with maleic anhydride.



The Fusabond E-MB226D bond thus formed prevents the powder and binder segregation in these kinds of feedstocks.

2.3.2. Powder

Although there is a relatively wide range of materials available for μ PIM, it is necessary to focus on powders of small particle size [61]. The starting powder requirements for μ PIM are much more stringent than that used for

conventional PIM. For example, the particle size should be at least about one order of magnitude smaller than the minimum internal dimension of the micro part [62]. Both of these feedstocks (Standard Mix and Catamold AO-F) contain alumina powder A16 SG, supplied by Almatiss, with an average diameter of 400 nm. The published density of the alumina powder is 3.9 g/cm^3 . The density and particle size were determined by a pycnometer and the particle size was measured using a particle size analyzer. Alumina powder was selected because of its higher service temperature and thermal conductivity at lower costs. Figure 23 and 24 give the Ashby's plots for Alumina showing the comparison of properties with other available materials.

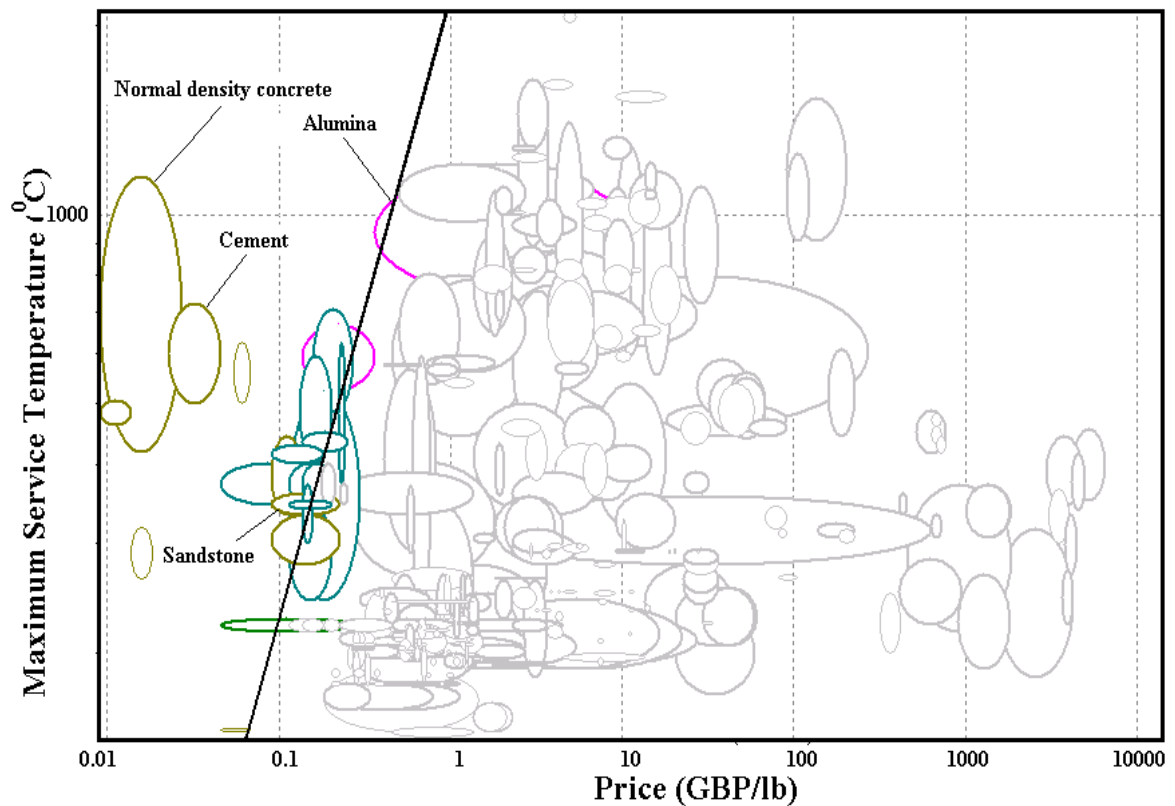


Figure 23: Ashby's plot of maximum service temperature vs price.

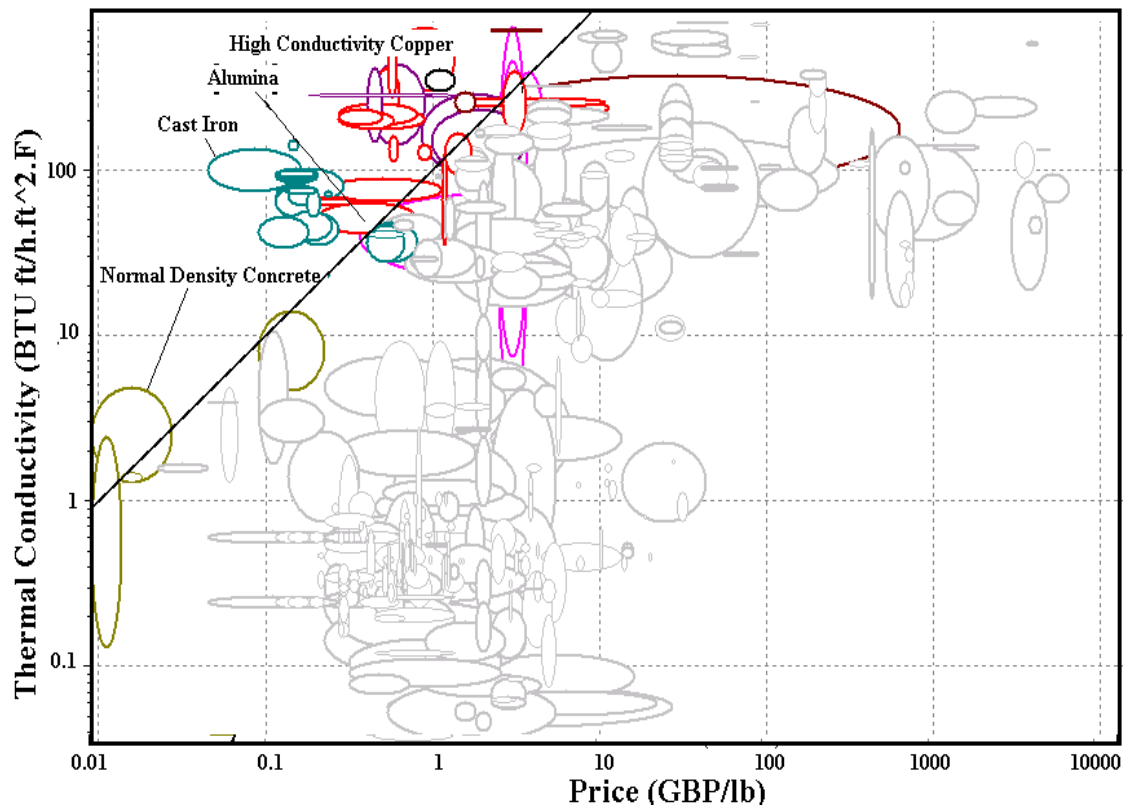


Figure 24: Ashby's plot of thermal conductivity vs price.

This powder is dry milled in alumina lined batch ball mills using alumina media. The grinding process eliminates the porous agglomerates formed during the calcination process resulting in optimal products for achieving the targeted alumina application properties. The calcination process used to produce the grinding feedstocks is carefully monitored and controlled to achieve the chemical purity and crystal structure required to consistently achieve the desired end product properties. The properties of the Almatix alumina powder used in this study are given in Table 6 and Figure 25 shows the SEM image of the Alumina used.

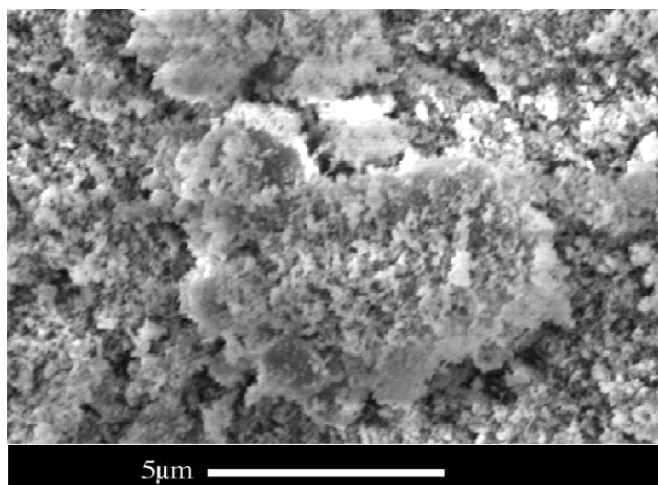


Figure 25: Scanning electron micrograph (SEM) of the alumina (A16SG)

Table 6: Properties of the Almatris alumina powder

Properties	Value
% Composition of Al_2O_3	99.8
Surface Area BET (m^2/g)	8.9
Wet - 325 Mesh Sieve (%)	99.6
Sedigraph d90 (μm)	1.5
Green Density (g/cc)	2.17
Shrinkage (%)	17.7
Firing Temperature ($^{\circ}\text{C}$)	1540

The feedstocks used in this research included a commercially available alumina-polyacetal feedstock (Catamold AO-F, BASF) and an in-house product Standard Mix of alumina-propylene/paraffin wax, both containing about 56 vol.% solids loading. Both of these feedstocks contain alumina powder, (A16SG supplied by Almatris for Standard Mix), with the median particle size of ~ 400 nm.

2.3.3. Feedstock

Feedstock preparation for Powder Injection Molding is a very crucial step since deficiencies in quality of the feedstock cannot be corrected by subsequent

processing adjustments. Hence, it is important that the feedstock is homogeneous and free of powder–binder separation or particle segregation. The quality of the feedstock in the mixing process depends on numerous parameters such as mixing time, mixing temperature, sequence of material addition, powder size and shape, formulation of binder, shear rate, and powder loading.

The μ PIM feedstock represents a balanced mixture of powder and binder. The amount of binder depends on the powder particle packing, since filling all of the void space among the powder particles is necessary to maintain a low viscosity. There are three possible situations for a given powder–binder mixture, as sketched in Figure 26. When the powder loading is higher than the critical loading, there is no sufficient binder to fill into the space among powder particles [63, 64]. Therefore, there are voids formed in the feedstock (Figure 26(a)). The feedstock has a high viscosity and is thus difficult to be molded. There is a critical powder loading at which the binder is just sufficient to form a strong, absorbed layer on the powder particles and to completely fill the inter-particulate voids (Figure 26(b)). It represents the densest packing of powder particles. When the powder loading is lower than the critical loading, there is too much binder in the feedstock (Figure 26(c)).

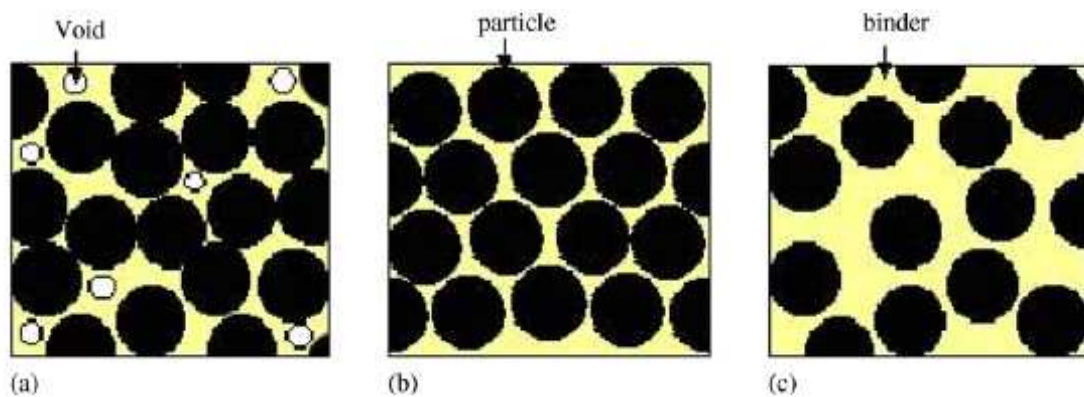


Figure 26: Three possible situations in a powder–binder mixture: (a) excess of powder, (b) critical and (c) excess of binder [65].

Before mixing, the alumina powder will be dried in a vacuum oven at a temperature of 80°C for 12 h to remove moisture.

Mixing experiments were conducted in a Haake rheocord 90 torque rheometer. A pair of roller rotor blades were used and the powder loading were carried out at 10 grams/ min to facilitate homogeneous mixing of the powder and binder components. Mixing speeds to be used are 30 and 50 rpm, and the mixing temperature used was 110°C. The mixing bowl was heated up to the required temperature of 110°C, while the mixing speed was set to the required value of 50 rpm. When the required mixing temperature was reached, all the binder components were loaded into the bowl and mixed until temperature equilibrium is achieved. The alumina powder is then loaded into mixing bowl and mixed at the required mixing temperature.

The given composition of the Standard Mix was selected keeping in mind to get a shear thinning behavior. The learnings from the literature review showed that shear thinning behavior of the feedstock might fill the micro-cavities in a more efficient manner.

2.4 Characterization & Properties of the feedstocks

After several trial runs, the basic injection molding process for alumina MCAs was set. All the material characterization was carried at DatapointLabs at Ithaca, NY.

The details of all the testing carried out at DatapointLabs is given in Appendix I and Appendix II.

Several test techniques were explored through this research for green ceramic material homogeneity and mold filling study. They included rheological and thermal properties.

The mix (Standard Mix) thus prepared was characterized using Differential Scanning Colorimeter (DSC) and Thermogravimetric Analysis (TGA). The runs were conducted at a rate of 10°C/min raise in temperature. It can be seen in Figure 27 that % weight loss is around 16% which corresponds to around 84 weight % (~56.1 volume %) alumina in the mix. Also, according to DSC, the binder melts at around 55°C and the four different components of the binder degrade at above 250°C. It is important to note that Standard Mix was prepared as the same powder-binder composition as of Catamold AO-F for one-to-one comparison of the two feedstocks.

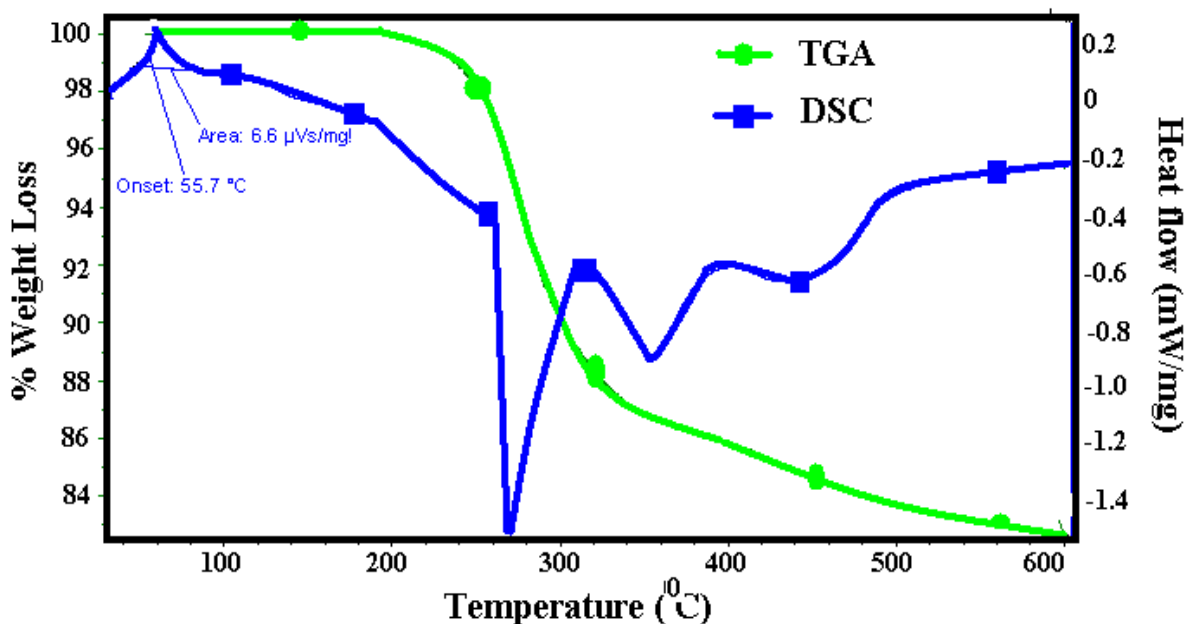


Figure 27: TGA and DSC studies of the Standard Mix

2.4.1 Rheological Studies

The rheological characteristics of the feedstock were examined on a Gottfert rheograph 2003 capillary rheometer at different shear rates and temperatures. The testing was carried out in accordance with ASTM D 3835. The temperatures were between the highest melting temperature and the lowest

degradation temperature of the binder system. The barrel of inner diameter of 1 mm and die length of 20 mm was used. The preheating time was kept at 6 minutes.

The viscosity of feedstock decreases with increasing shear rate. Normally, feedstock which exhibit shear thinning flow behavior during molding eases mold filling and minimizes jetting. Figure 28 shows the relation of viscosity against shear rate and temperature.

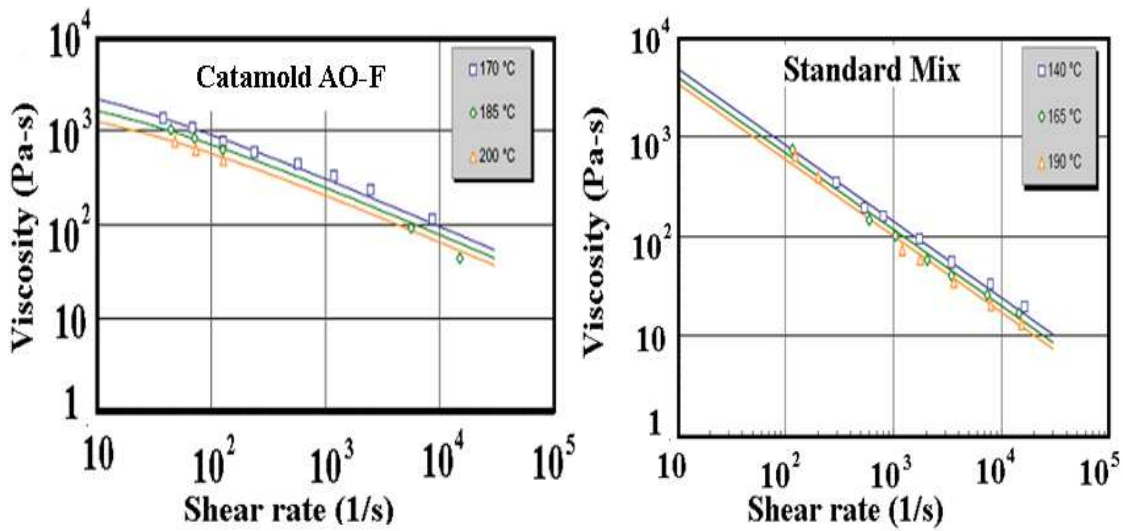


Figure 28: Relationship between viscosity (Pa-s) and shear rate (s^{-1}) for Catamold AO-F and Standard Mix at varying shear rates.

The rheological data was fitted to a modified Cross-WLF equation (equation 1) and was used for further analysis in a Moldflow package.

$$\left. \begin{aligned} \eta(T, \gamma, P) &= \frac{\eta_0(T, P)}{1 + \left[\frac{\eta_0(T) \times \gamma}{\tau^*} \right]^{(1-n)}} \\ T \geq T^*, \eta_0(T, P) &= D1 \times e^{\left\{ \frac{-[A1(T - T^*)]}{[A2 + (T - T^*)]} \right\}} \\ T < T^*, \eta_0(T, P) &= \infty \\ \text{where, } A_2 &= A_2 + D_3 \times P \\ T &= D_2 + D_3 \times P \end{aligned} \right\} \dots \dots (1)$$

η_0 is the zero-shear rate viscosity, $\dot{\gamma}$ is the shear rate, T is the temperature, p is the pressure, n , τ^* , D_1 , D_2 , D_3 , A_1 and A_2 are model constants. Most feedstocks exhibit two regimes of flow behavior: Newtonian and shear thinning. Newtonian behavior occurs at low shear rates, when the shear-stress-to-shear-rate relationship is linear. At higher shear rates, the viscosity decreases as the shear rate increases; this behavior is called shear thinning. In the Cross-WLF equation, the transition between the Newtonian and shear thinning regimes is characterized by the parameter, τ^* . τ^* represents the shear stress at which the onset of shear thinning behavior occurs. The value of $(1 - n)$, where n is a power-law coefficient in this model, represents the slope of the shear thinning curve. The remaining constants are used to model the zero-shear rate viscosity, η_0 . The parameter, T_b , characterizes the temperature sensitivity of η_0 . This tends to depend on temperature, especially near T_g . Table 7 gives the value and definition of these constants for both the feedstocks used.

Table 7: Value and definition of different constants for Catamold AO-F and Standard Mix

Coefficients	Definition	Catamold AO-F (SI units)	Standard Mix (SI units)
n	Power law index	0.48	0.23
τ^* (Pa)	Constant with Weissenberg-Rabinowitsch correction at user's specification during data fit; this value is used for material database.	24820	9400
D_1 (Pa-s)	Scale factor for viscosity	1.27E+14	1.67E+15
D_2 (K)	Glass transition temperature at zero gage pressure	263	263
A_1	WLF temperature shift factor	30.72	28.40
A_2 (K)	WLF temperature shift factor	51.6	51.6

2.4.2 Thermal Conductivity

A K-System II Thermal Conductivity System was used to evaluate the thermal conductivity of the feedstocks. The testing was carried out in accordance with ASTM D 5930. The initial temperature was 190 °C and final temperature was 30 °C. The probe voltage was kept at 4 V and acquisition time of 45 s.

Figure 29 shows the comparison of the thermal conductivity of the two feedstocks. The Catamold AO-F has a higher thermal conductivity than the Standard Mix.

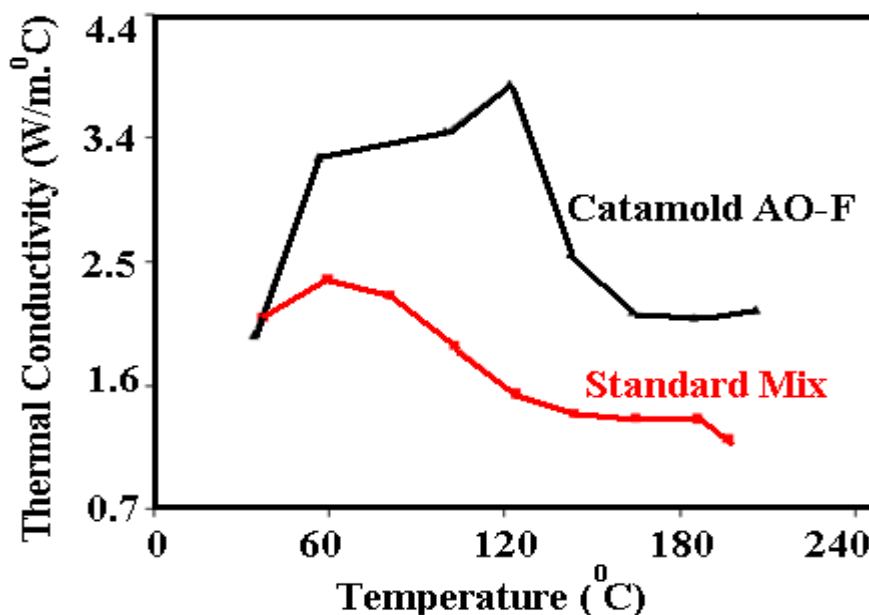


Figure 29: Thermal conductivity of Catamold AO-F and Standard Mix as a function of temperature.

2.4.3 Specific Heat

Specific heat measurements were carried out on Perkin Elmer DSC7 equipment in accordance with ASTM E 1269. The testing was done on a 11.85 g sample with the initial temperature of 190 °C and final temperature of 20 °C. The cooling rate was kept constant of 20 °C/minute.

The Catamold AO-F feedstock containing polyacetal has a higher specific heat value compared to the Standard Mix. Figure 30 shows the comparison of the specific heat for the two feedstocks.

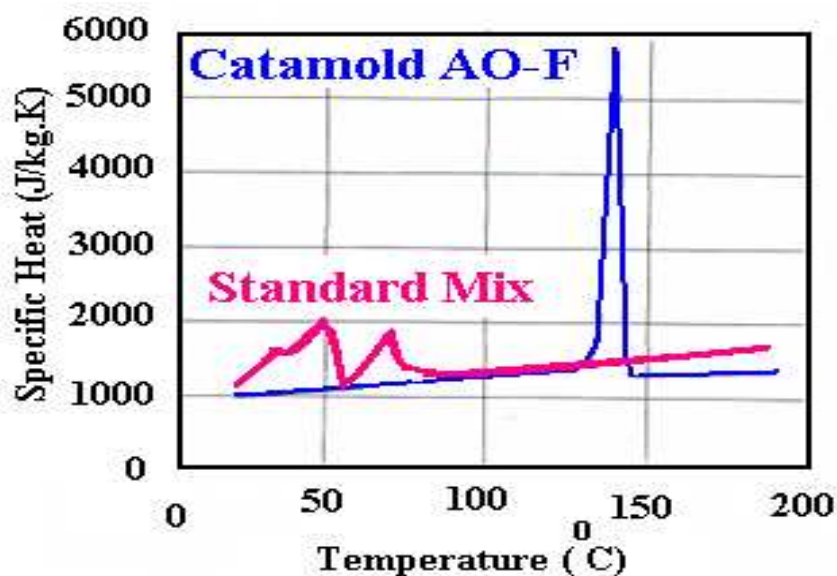


Figure 30: Specific heat as a function of temperature for the Catamold AO-F and the Standard Mix.

2.4.4 Pressure-volume-temperature behavior

A Gnomix PVT apparatus was used to find the PVT relationships of the feedstock materials. The test was carried out in accordance with ASTM D 792. The pellets were dried for 4 hours at 70 °C under vacuum. The measurement type used was isothermal heating scan with a heating rate of approximately 3°C/minute.

The pressure-volume-temperature (PVT) behavior of Catamold AO-F and Standard Mix (Figure 31), gives the specific volume changes of the melt in cavity as the function of cavity pressure and temperature.

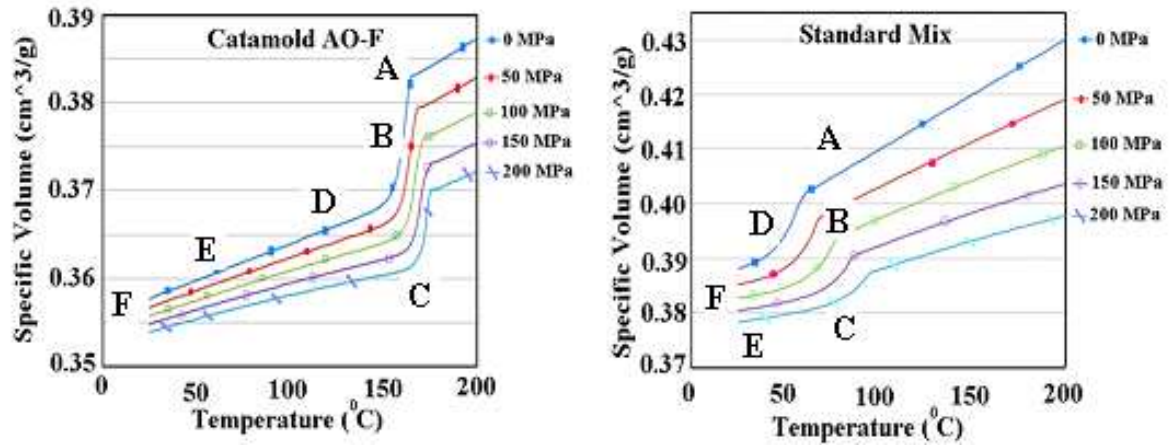


Figure 31: PVT relationships for the Catamold AO-F and the Standard Mix
Table 8 gives the values and definition of different PVT coefficients for the Catamold AO-F and the Standard Mix.

Table 8: PVT coefficients for Catamold AO-F and Standard Mix.

Coefficients	Definition	Catamold AO-F	Standard Mix
b5 (K)	Crystallization temperature	4.360E+02	3.322E+02
b6 (K/Pa)	Pressure sensitivity of b5	6.000E-08	1.800E-07
b1m (m³/kg)	Tait constants for melt	3.827E-04	4.015E-04
b2m (m³/kg-K)	Tait constants for melt	1.258E-07	2.027E-07
b3m (Pa)	Tait constants for melt	3.970E+08	2.953E+08
b4m (1/K)	Tait constants for melt	2.174E-03	4.709E-03
b1s (m³/kg)	Tait constants for solid	3.692E-04	3.893E-04
b2s (m³/kg-K)	Tait constants for solid	8.316E-08	5.312E-08
b3s (Pa)	Tait constants for solid	7.000E+08	6.574E+08
b4s (1/K)	Tait constants for solid	5.947E-03	3.868E-06
b7 (m³/kg)	Transition of specific volume from solid to melt	1.347E-05	1.223E-05
b8 (1/K)	Transition of specific volume from solid to melt	2.702E-01	9.116E-02
b9 (1/Pa)	Transition of specific volume to melt	1.926E-08	2.052E-08

2.5 Processing

The experiment platform used for micro powder injection molding study consisted of powder injection molding machine, which was able to mold microfeatures at the dimension scale of less than 100 micron meters; a precision micro mold system, which was designed with multiple cavities for different MCAs with the channel width of 50, 100, and 500 μm ; the build-in sensor system to monitor the micro cavity temperature and pressure in process and the fast data acquisition module to record and display the process condition at the real time

2.5.1 Powder Injection Molding Machine

ALLROUNDER 270C is a fully hydraulic injection molding machine from Arburg Co, Germany (Figure 32). The machine has the clamping force up to 800 kN, and its specifications are given in Table 9. In order to mold powdered ceramic or metal feedstock, the injection cylinder was made from special abrasive-resistant material titanium diboride (TiB_2). With the screw of 20 mm or smaller size the machine is capable for the minimal shot weights required by micro cavity injection. There is also a built-in vacuum system with the machine to help venting air tapped in the micro mold cavities.

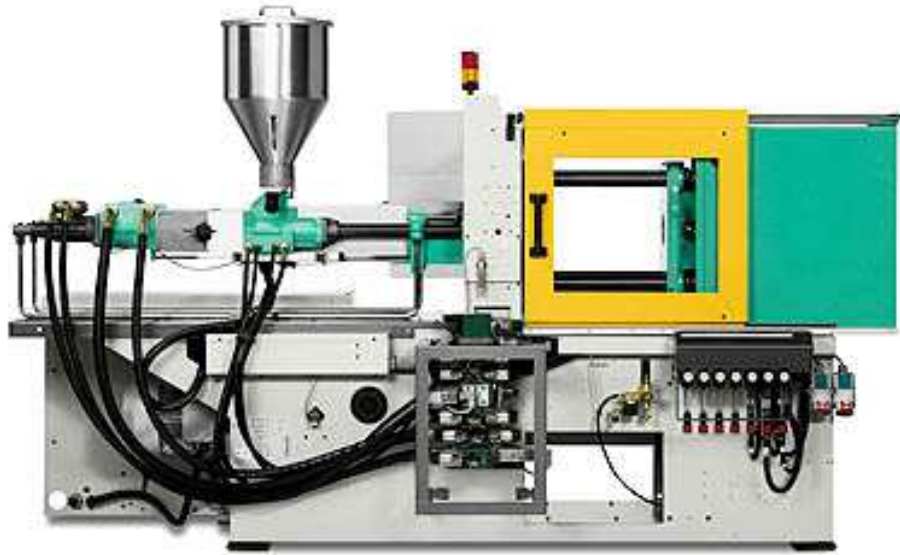


Figure 32: Powder injection molding machine used in the study, ALLROUNDER 270C from Arburg

Table 9: Major technical data of Arburg injection molding machine (270/300)

Technical Data	(Max)	Technical Data	(Max)	Technical Data	(Max)
Clamping force, kN	300	Screw dia, mm	20	Back pressure, bar	350
Closing force, kN	35	Effective Length, L/D	25	Nozzle force, kN	40
Open stroke, mm	350	Screw Stroke, mm	100	Nozzle retraction, mm	180
Ejector force, kN	30	Injection Pressure, bar	2500	Nozzle heating, W	600
Ejector stroke, mm	125	Injection flow, cm ³ /s	56		

2.5.2 Precision micro mold system

The stand-alone mold (OMNI 8"x8" 2 plates system) has an insert with three cavities for micro arrays in different size (Figure 33). A Dutchman mechanism was constructed in mold and used to determine which cavity would be active and to be filled in the molding process (Figure 34). The test component design was of multi-scale

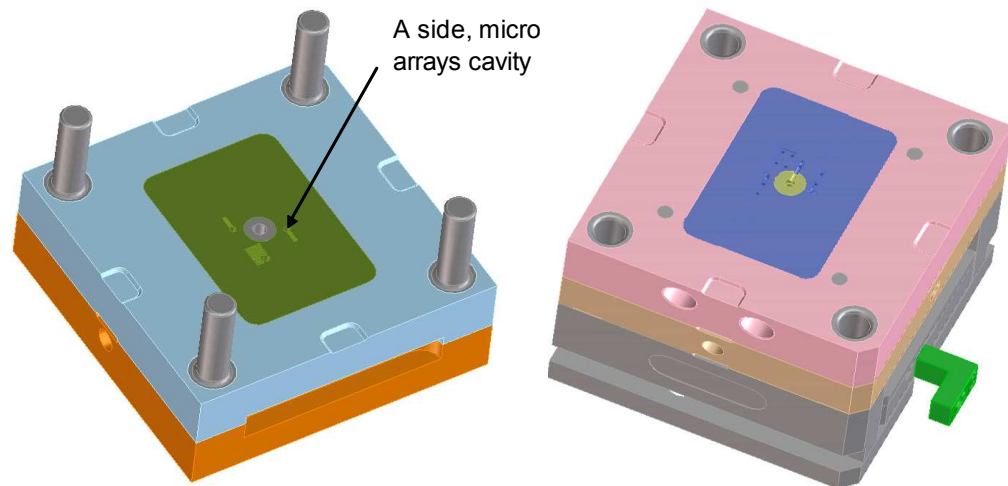


Figure 33: A and B plates of the test mold

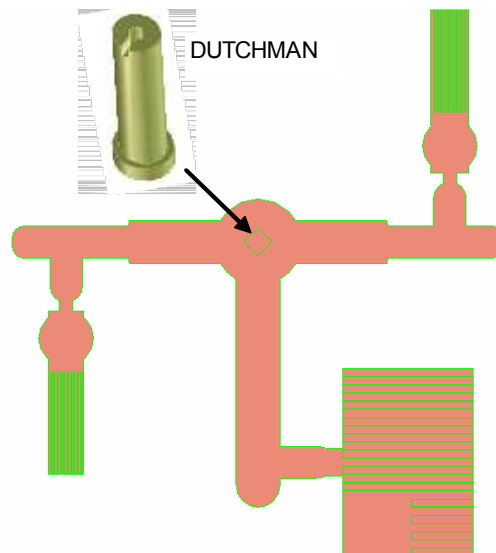


Figure 34: Mold runners and Dutchman

structure. The cavity for the bulk substrate (body) was on the B side (plate), the cavity of the MCA configuration was located on the A side (plate) to help the melt flow to the microchannels. The cavities were designed with gas vents and vacuum paths to improve degassing for fast melt fill, which are critical in the μ PIM process to reduce voids and microfeature short shot (Figure 35).

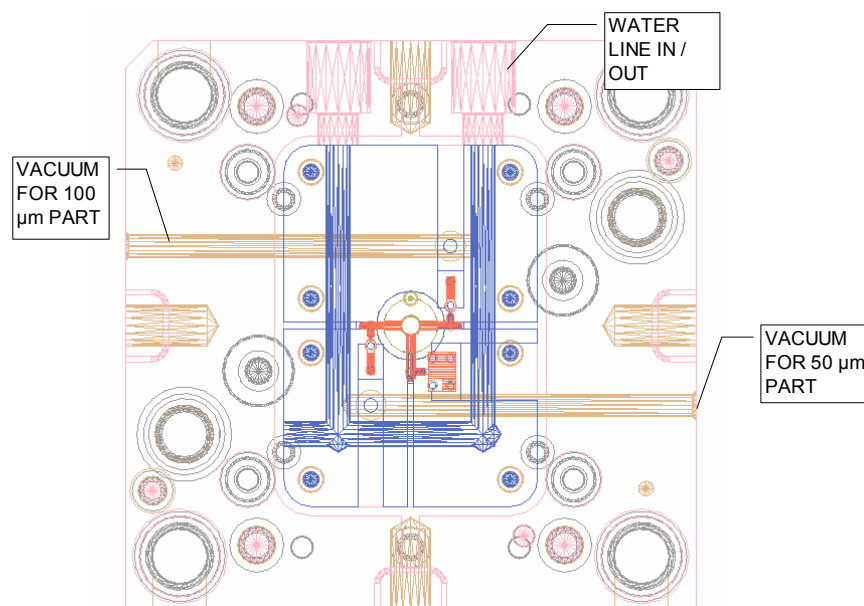


Figure 35: Cavity vents, vacuum paths, and water channels

The mold was fabricated at the tooling division of Hewlett-Packard (Corvallis, OR). The water lines of the mold were designed for two different applications, cooling water or heating path depending on injection molding materials and process conditions. The water cooling can be used for plastic injection molding with relative low mold temperature required for process. In the case of μ PIM, higher mold temperature was often required to reduce the frozen layer effect (mold temperature of 150°C for BASF Catamold AO-F feedstock for example). To heat up the mold, four cartridge heaters, two in each plate, were placed in the water lines for μ PIM. The water paths are located

beneath the outside surface and close to cavities, represented as blue lines in Figure 35, which will help the localized heat transfer, minimum core temperature, and fast heating. When the mold is closed, the mold cavity temperature may rise up to 150°C in 15 minutes at full power heating. The AC powered cartridge heaters used a voltage transformer and temperature controller to maintain the required temperature level and to prevent over heating. The mold assembly also used two ceramic plates, one for each side of the mold, for providing thermal insulation to the mold bases.

To investigate the feasibility of the feedstock for μ PIM, subsequent processing steps were conducted. MCA of 50 μ m microchannels were successfully injection molded. The experimental level values were chosen mainly based on the moldflow simulation. Table 10 and Table 11 gives the processing conditions used for Catamold AO-F and Standard Mix.

Table 10: Processing conditions used to mold 50 μ m MCA

Processing Conditions	Catamold AO-F & Standard Mix
Screw Speed	40 RPM
Back Pressure	1 MPa
Circumferential Speed	2.5 m/min (20 mm screw)
Injection Filling Time	0.4 second
Dosage Rate	10 cm^3 / s
Injection Pressure	60 MPa
Holding Pressure	120 MPa
Mold Temperature	150 °C
Cooling Time	3 second (air cooling)

Table 11: Cylinder Zone temperatures

Temperature (°C)					
Zones	Zone 1	Zone 2	Zone 3	Zone 4	Zone 5
Catamold AO-F & Standard Mix	175	175	180	180	185

The part geometry and processing conditions were kept similar for both the feedstocks to study the effect of material property on filling of microchannels. The MCA thus made is shown in Figure 36. Figure 37 shows the 50µm channels on the MCA.

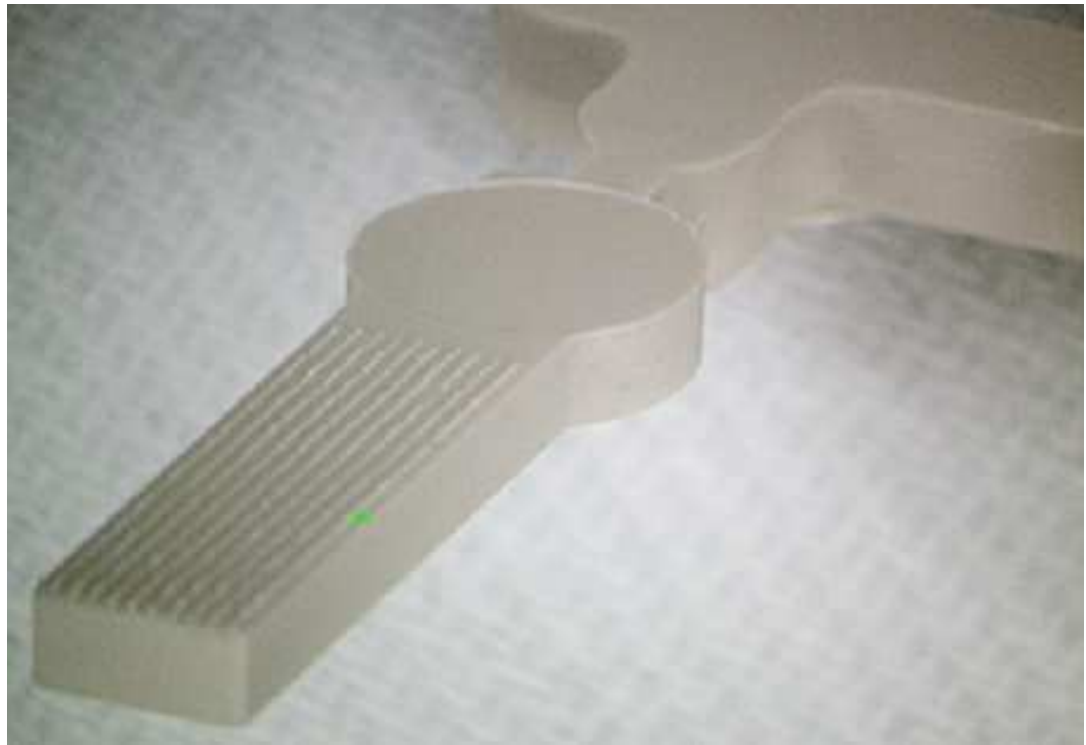


Figure 36: Ceramic injection molded alumina microchannel arrays (MCAs) used in this study



Figure 37: The 50 μ m channels on the MCA

CHAPTER 3: RESULTS & DISCUSSION

The aim of this section of the thesis is to identify the significant parameters affecting the mold filling of the MCA.

3.1 Material Properties

The objective in injection molding is to achieve complete cavity filling without short shots while avoiding the molding defects such as flash, sink mark, warpage, and demolding damage. To meet the objective, the material properties of feedstock melt (Section 2.4) are critical in addition to the appropriate machine setting and process parameters selection. The properties included thermal conductivity, coefficient of thermal expansion, transition temperature, specific heat, material flow behavior, viscosity at high shear, and PVT (pressure, volume and temperature) thermodynamic property.

3.1.1 Rheological properties:

For experimental purposes, the values of the rheological property's constants were varied in Moldflow software to see the effect of individual parameters/constants on microchannels fill. The variation in the property of Catamold AO-F is reported here. The Standard Mix also followed the similar behavior as Catamold AO-F.

Figure 38 shows the screen shot of the viscosity coefficients changed in MPI. Figure 39 shows the change in viscosity as a function of shear rate by changing the value of n , τ^* and D_1 individually for Catamold AO-F. n was changed from 0.4766 to 0.8766, τ^* was changed from 24820 to 248 and D_1 was changed from $1.27e+14$ to $1.27e+10$ for Catamold AO-F. It was observed that increasing the value of n and τ^* increases the Newtonian behavior of the

feedstock. However, increasing the value of D_1 , decreased the Newtonian behavior of the feedstock.

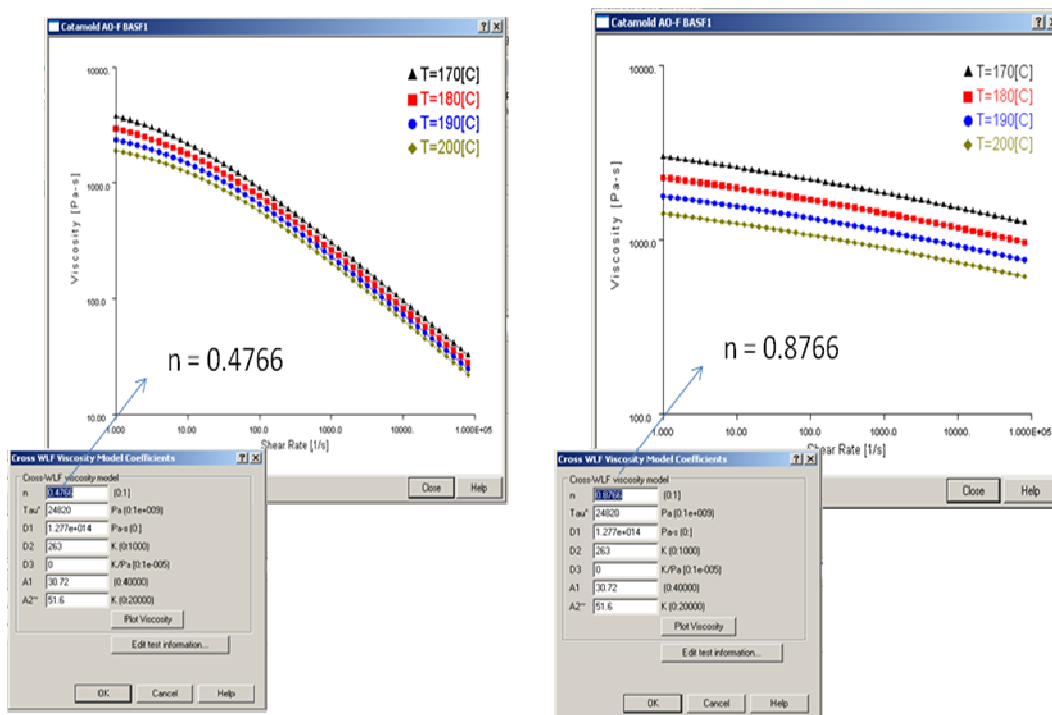


Figure 38: Screen shot of the viscosity coefficients changed in MPI

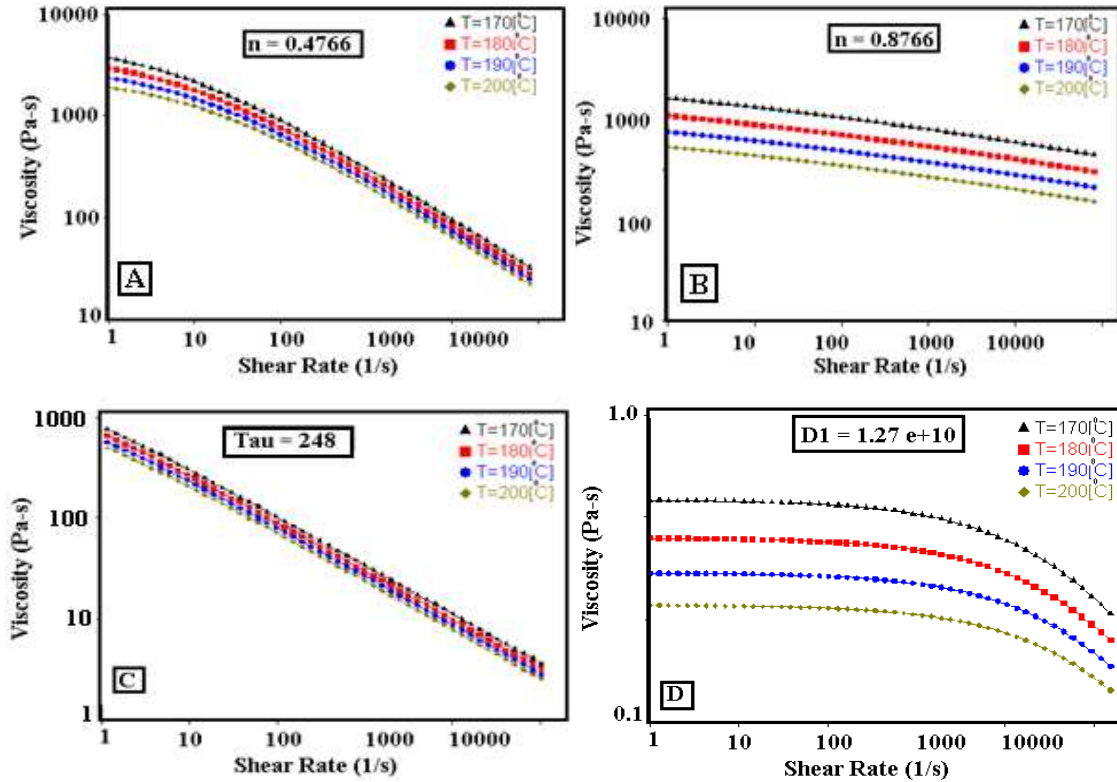


Figure 39: Change in viscosity constants influence the behavior of viscosity η vs shear rate. A: represents the data for the Catamold AO-F generated experimentally, B, C, & D represents change in n , τ^* & D_1 respectively.

Moreover the Standard Mix is also expected to show the same trends with change in n , τ^* & D_1 . Hence, the mold filling studies were carried out on Catamold AO-F to see the effect of change in these parameters to the flow in microchannels. Figure 40 shows the effect of change in n and τ^* on the filling behavior in microchannels. It was found that increasing the values of n and τ^* increased the flow of feedstock into the microchannels.

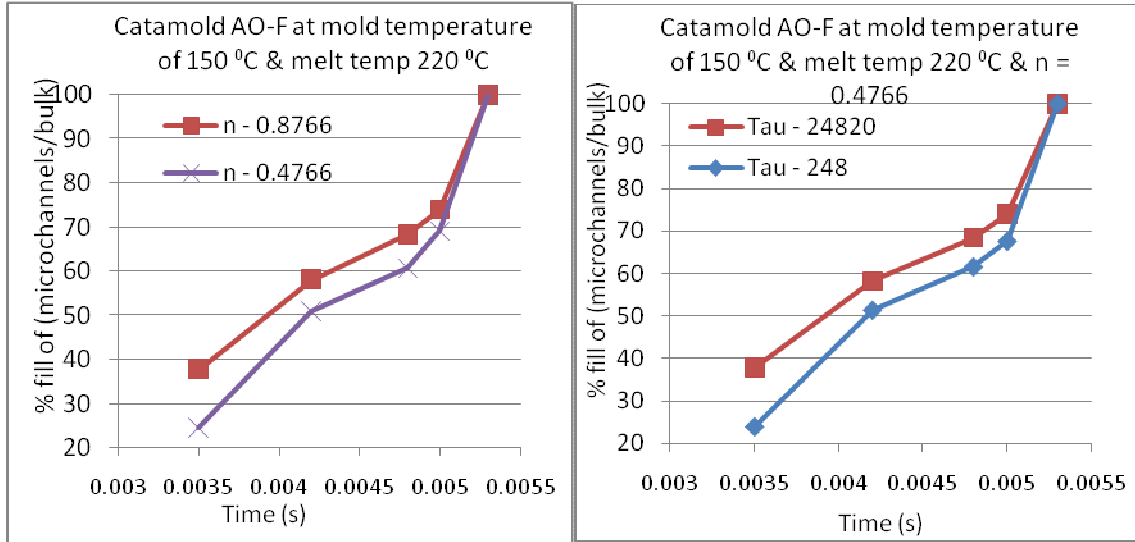


Figure 40: Effect of change in viscosity constants on flow in microchannels.

In other words, the feedstock showing Newtonian behavior shows a higher flow in the microchannels than a feedstock having non-newtonian behavior. A possible reason may be the build up in cavity pressure which forces the feedstock to flow into the thin microchannels.

3.1.2 PVT properties:

PVT helps to understand the compression and temperature effects during a typical injection molding cycle. The hold pressure should be chosen appropriately referring to the PVT-diagram so that the residual cavity pressure is near atmospheric pressure before demolding.

The diagram shown in Section 2.4.4 was made based on a modified Tait model, which is a two-domain empirical model, which defines two different domains, above and below a transition temperature T_i . The model parameters were determined by testing for the selected feedstock. A typical molding cycle

with Catamold AO-F and Standard Mix can be described using PVT-diagram as follows:

1. The melt is injected at a processing temperature at 175°C up to 185°C. The pressure is built up when the injection forces the melt through the runner system to begin filling the cavity (A)
2. The bulk cavity is filled. The melt in the cavity is compressed until the maximum pressure (hold pressure of 120 MPa) is reached. There is no noticeable cooling in this process stage (A-B).
3. Switchover from injection to holding stage after the hold pressure is attained. The melt begins to cool off and passes through the crystallization under constant hold pressure. In this stage, the specific volume drops (shrinkage) and more melt material flows in from barrel (B→C).
4. After the crystallization ending point C, the pressure starts to drop from cooling while volume is maintained. The gate is frozen and the cavity is sealed (D).
5. The pressure continues to drop and the material keeps cooling while volume remains constant (D→E). When atmospheric pressure is reached at point E the part separates from cavity wall and ready for ejection.
6. The ejected green part continues to cool and shrink to room temperature (E→F).

If the hold pressure is too high, the part will still be under pressure when the mold temperature has been reached, which may cause part ejection and stress relaxation problems. The higher slope in the PVT plot for the Standard Mix (Figure 42) implies higher possibility for shrinkage in the final part.

The famous Tait equations have been used widely in representing the volumetric behaviors of feedstocks as a function of temperature and pressure, but not for cooling rate. The Tait equation can be expressed as shown in equation 2:

$$v(T, P) = \left[v_0(T) \times \left(1 - C \times \ln \left(1 + \frac{P}{B(T)} \right) \right) + v_f(T, P) \right]^{-1} \dots\dots (2)$$

Where v is the specific volume in cm^3/g , T is the temperature in $^{\circ}\text{C}$, P is the pressure in MPa, C is a dimensionless constant, $B(T)$ is a temperature dependent parameter with the same dimension as pressure, v_0 and v_f are the specific volumes at room temperature and at temperatures above the transition temperature respectively. Specific volume at temperatures higher than the transition temperature is given by equation 3.

$$T \geq T_f, v_0(T) = b1_m + b2_m \times T^* \dots\dots (3)$$

Where T^* is any specific temperature above the transition temperature.

$B(T)$ can be expressed as shown in equation 4.

$$B(T) = b3_m \times e(-b4_m \times T^*) \dots\dots (4)$$

However, the specific volume at transition temperature is considered to be zero while heating the feedstock. It is represented with equation 5.

$$v_f(T, P) = 0 \dots\dots (5)$$

The specific volume at temperatures lower than the transition temperature is given by equation 6, where the feedstock is in solid and semi-solid state.

$$T < T_f, v_0(T) = b1_s + b2_s \times T^* \dots\dots (6)$$

Here, $B(T)$ can be expressed as shown in equation 7.

$$B(T) = b3_s \times e(-b4_s \times T^*) \dots\dots (7)$$

Here, T^* is any specific temperature below the transition temperature. The specific volume while cooling is given as shown in equation 8.

$$v_f(T, P) = b7 \times e(b8 \times T^* - b9 \times P) \dots\dots (8)$$

The subscripts, m and s , refer to the melt and solid states.

Following were some common observations from the PVT diagrams:

- Both Melt and Solid compressibility is very high for Standard Mix feedstock.
- Standard Mix might have high shrinkage after cooling.
- However, it is possible to compress the Standard Mix hard in the melt stage with higher holding pressures
- In general, when the pressure is increased, more thermal energy is required to get the chains moving, hence a higher T_g is found at higher pressures.
- This effect becomes significant when a polymer melt is cooled under pressure.
- When cooling under pressure, the polymer melt will solidify at a higher temperature than it would if being cooled at a lower pressure.

However, there was hardly any change in the microchannel fill was observed by changing these constants by 10% from the experimental values for both the feedstocks.

3.1.3 Specific Heat:

The effect of change in specific heat was studied in the mold filling behavior of Catamold AO-F and Standard Mix. Figure 41 shows the comparison of the percentage fill in microchannels to bulk as a function of time with different values of specific heat for Catamold AO-F. The Standard Mix also showed the similar trend (data not shown here).

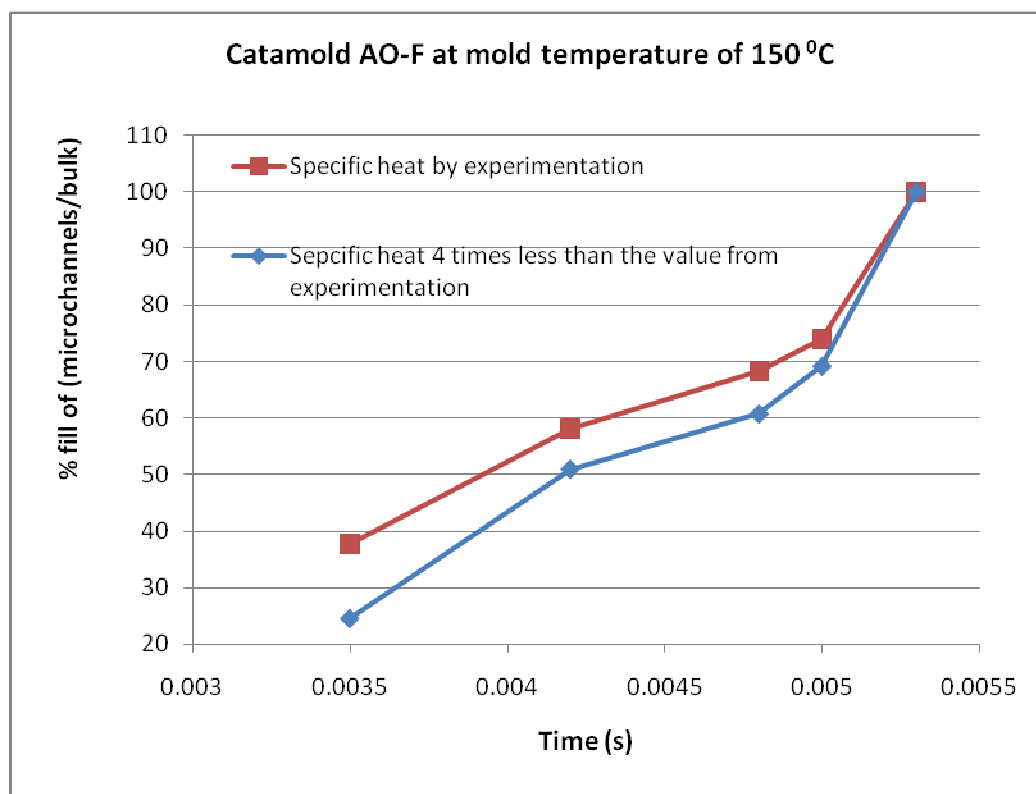


Figure 41: The comparison of percentage fill in microchannels to bulk as a function of time with different values of specific heat for Catamold AO-F.

It was found that decrease in specific heat of catamold by approximately 4 times decreases the flow in microchannels as shown in Figure 41.

3.1.4 Thermal Conductivity:

Catamold AO-F is found to have higher melt thermal conductivity than Standard Mix. The thing to be noted here is that, even though the alumina concentration in both the feedstocks is the same, the thermal conductivity of Catamold AO-F is higher than Standard Mix. This is due to the higher melt thermal conductivity of Polyacetal (binder used in Catamold AO-F) than Paraffin Wax (binder used in Standard Mix). This leads to slower removal of heat from the Catamold AO-F than the Standard Mix during the molding cycle, when the melt and mold temperature were kept constant for both the feedstocks. This led

to faster and more uniform filling of microchannels for the Catamold AO-F compared to the Standard Mix.

3.2 PROCESSING PARAMETERS

3.2.1 Injection Speed

An increase in the injection speed increases the amount of the feedstock flowing into the microchannels. Figure 42 shows the gradual increase of injection speed and its effect on the flow of feedstocks in the microchannels.

However, it is recommended to process these feedstocks at less injection speeds to avoid powder and binder segregation. In this experiment, the Moldflow simulations were carried out keeping the injection speed of 10 cm³/s.

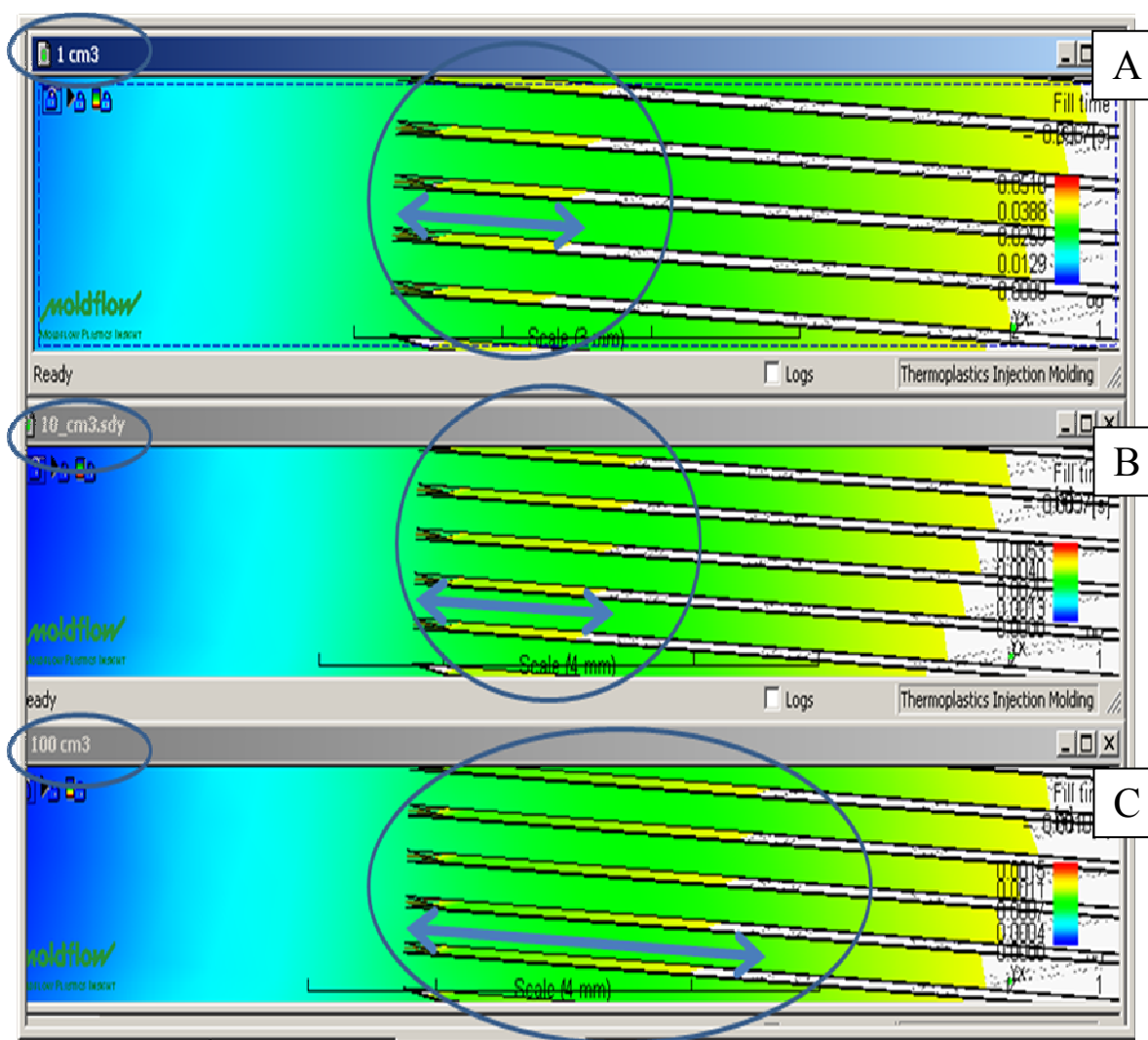


Figure 42: A - injection speed of 1cm³; B - injection speed of 10cm³; injection speed of 100cm³.

3.2.2 Packing Pressures

Different packing pressures profiles were tried using MPI to see the effect on flow of feedstocks in microchannels. However, the pressure profiles did not seem to affect the flow in microchannels. Figure 43 shows the print screen of the MPI software while changing packing pressures.

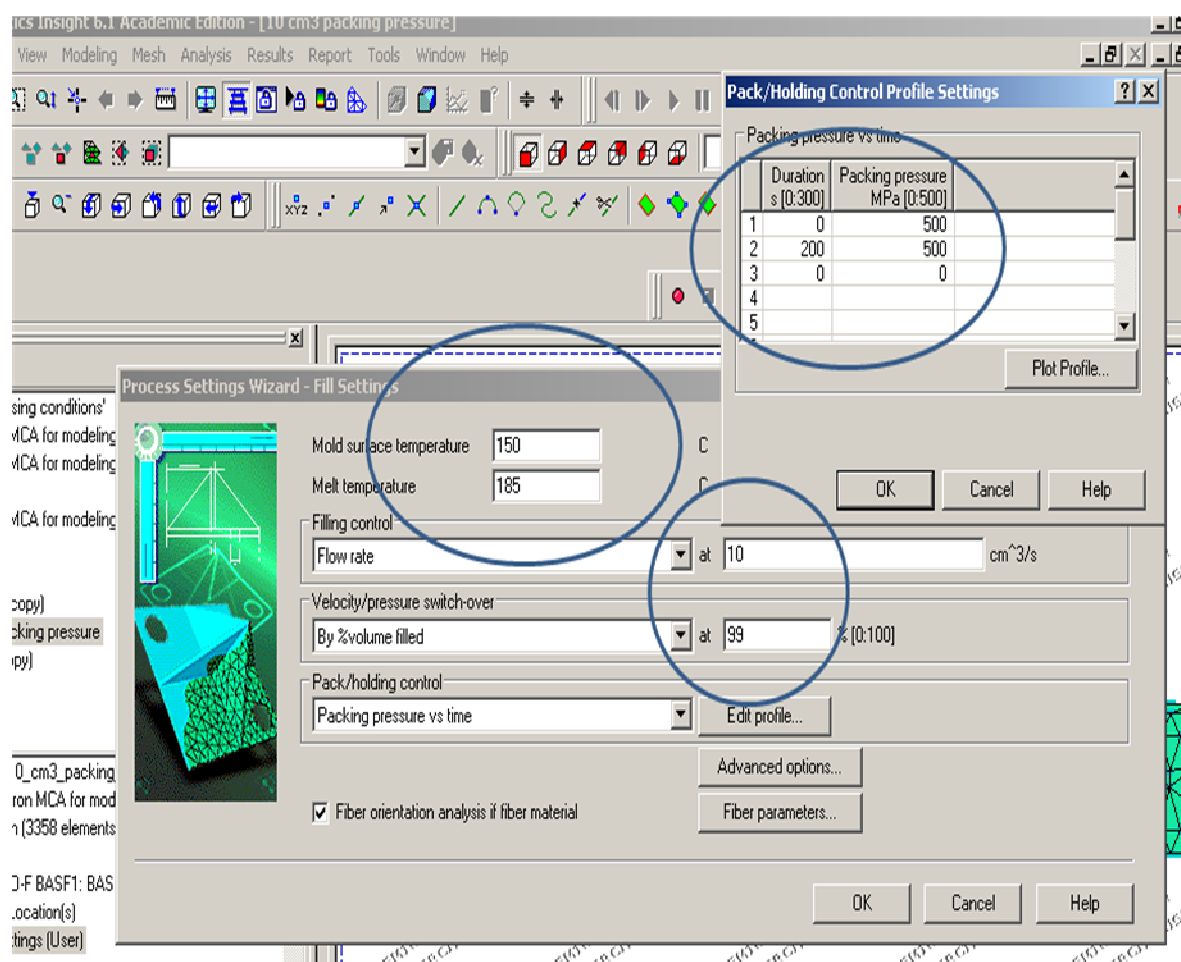


Figure 43: The print screen of the MPI software while changing packing pressures

3.2.3 Melt Temperature

It was found that higher melt temperatures caused a higher flow of feedstock into the microchannels. Figure 44 shows the effect of changing melt temperature on microchannels, bulk and complete fill of the part. Figure 45 shows the actual amount of the material flowing through the different sections of the part per unit area per unit time. The study was done for both the feedstocks, however, only the data for Catamold AO-F is reported here. Standard Mix also followed the same trend.

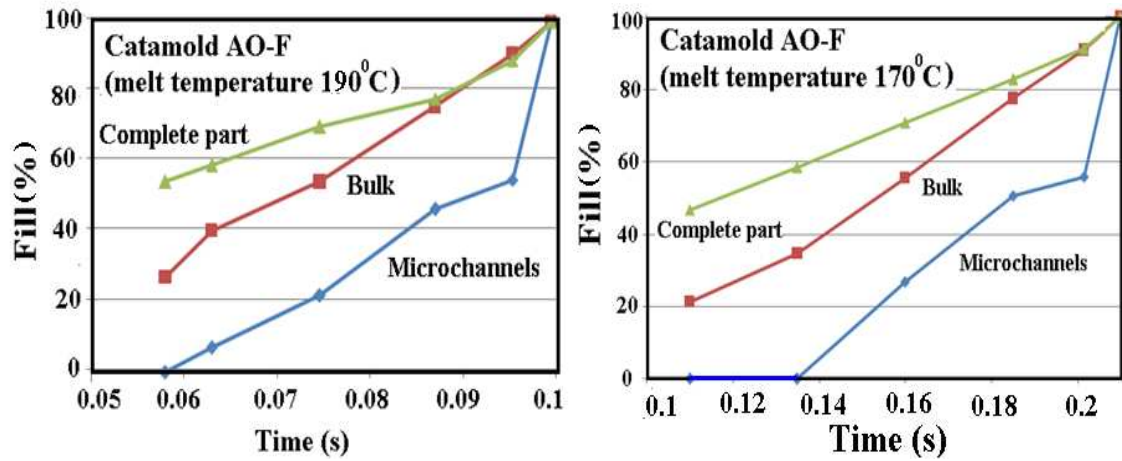


Figure 44: The effect of changing melt temperature on microchannels, bulk and complete fill of the part

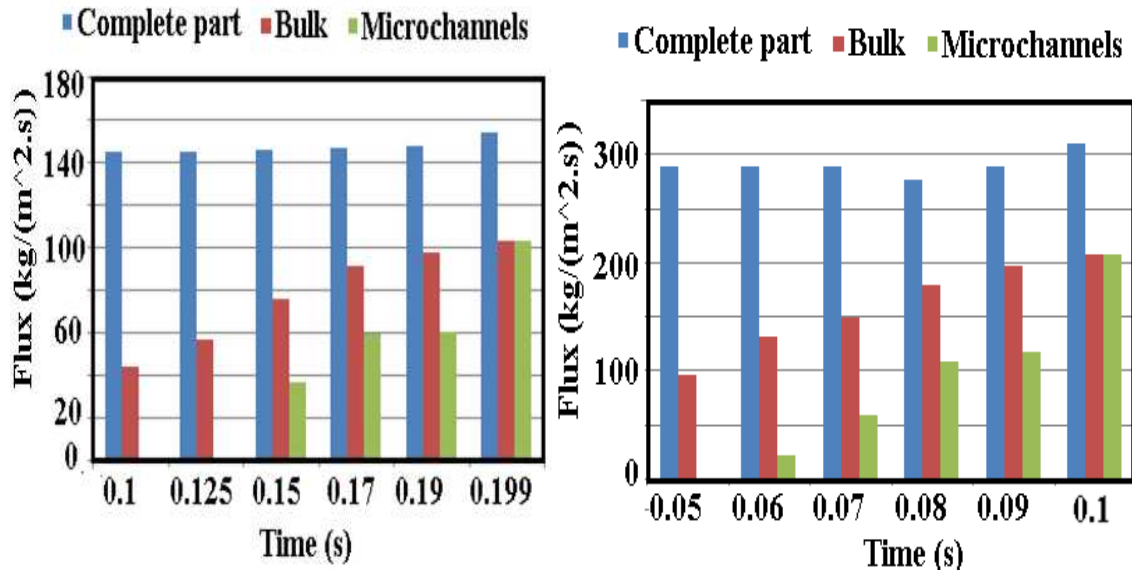


Figure 45: The actual amount of the material flowing through the different sections of the part per unit area per unit time for Catamold AO-F.

It is obvious that the amount of the material flowing through the microchannel increases by increasing the melt temperature. The same trend is shown graphically in Figure 46.

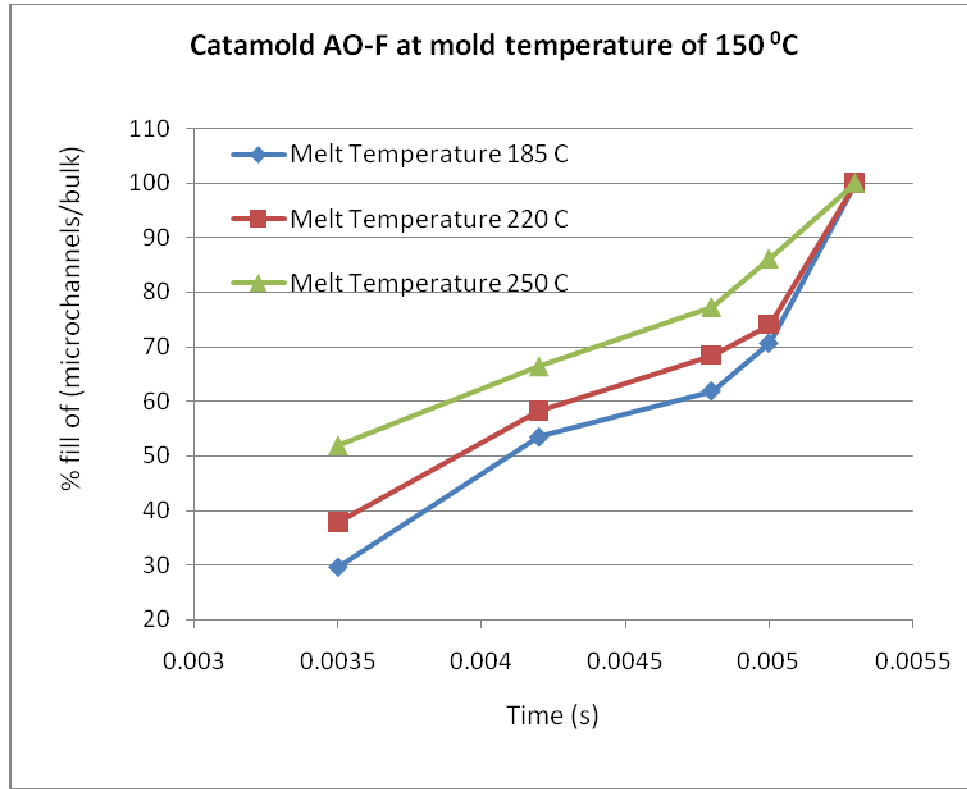


Figure 46: Effect of melt temperature on microchannels to bulk fill for Catamold AO-F

3.3 Part Geometry

3.3.1 Bulk thickness

In order to avoid defects like incomplete mold fill, some studies on part geometries were conducted. Percentage of microchannels fill to bulk fill was quantified using Moldflow Plastic Insight (MPI) for parts having different bulk thicknesses. Parts with various thicknesses of the bulk were studied using MPI. It was found that decreasing the bulk thickness, increased the amount of feedstock flow into the microchannels. A possible reason for this observation is that

decreasing the bulk thickness increases the cavity pressure and forces the feedstock to flow into the microchannels. The Catamold AO-F was observed to move faster into the microchannels compared to the Standard Mix as shown in Figure 47. Figure 48, 49 and 50 shows the same part with 0.25mm, 0.5mm and 1.5mm thick bulk from MPI for Catamold AO-F feedstock.

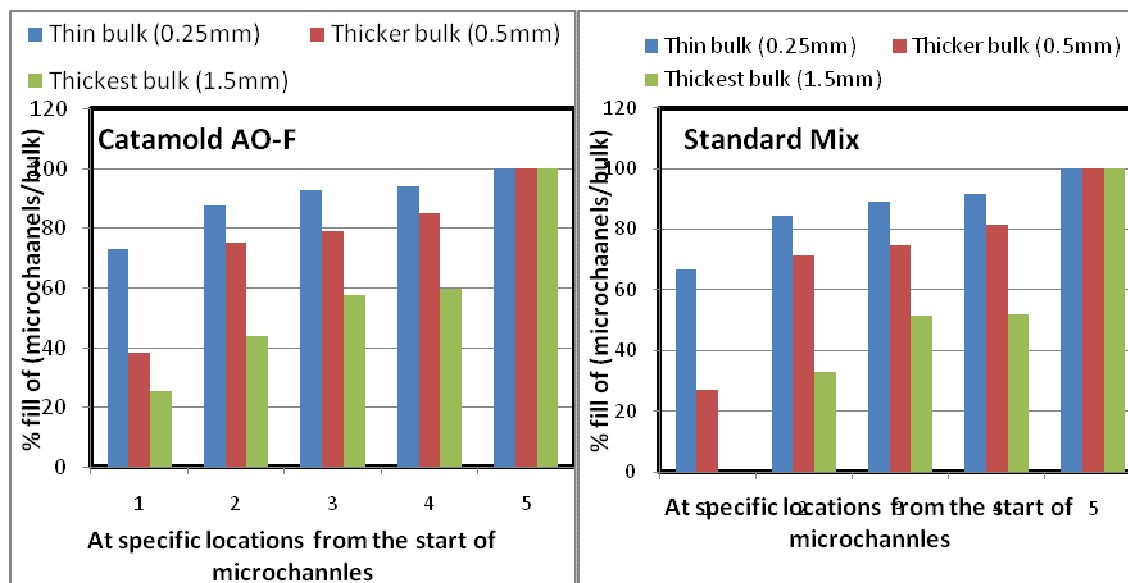


Figure 47: Comparison of bulk thicknesses for Catamold AO-F and Standard Mix

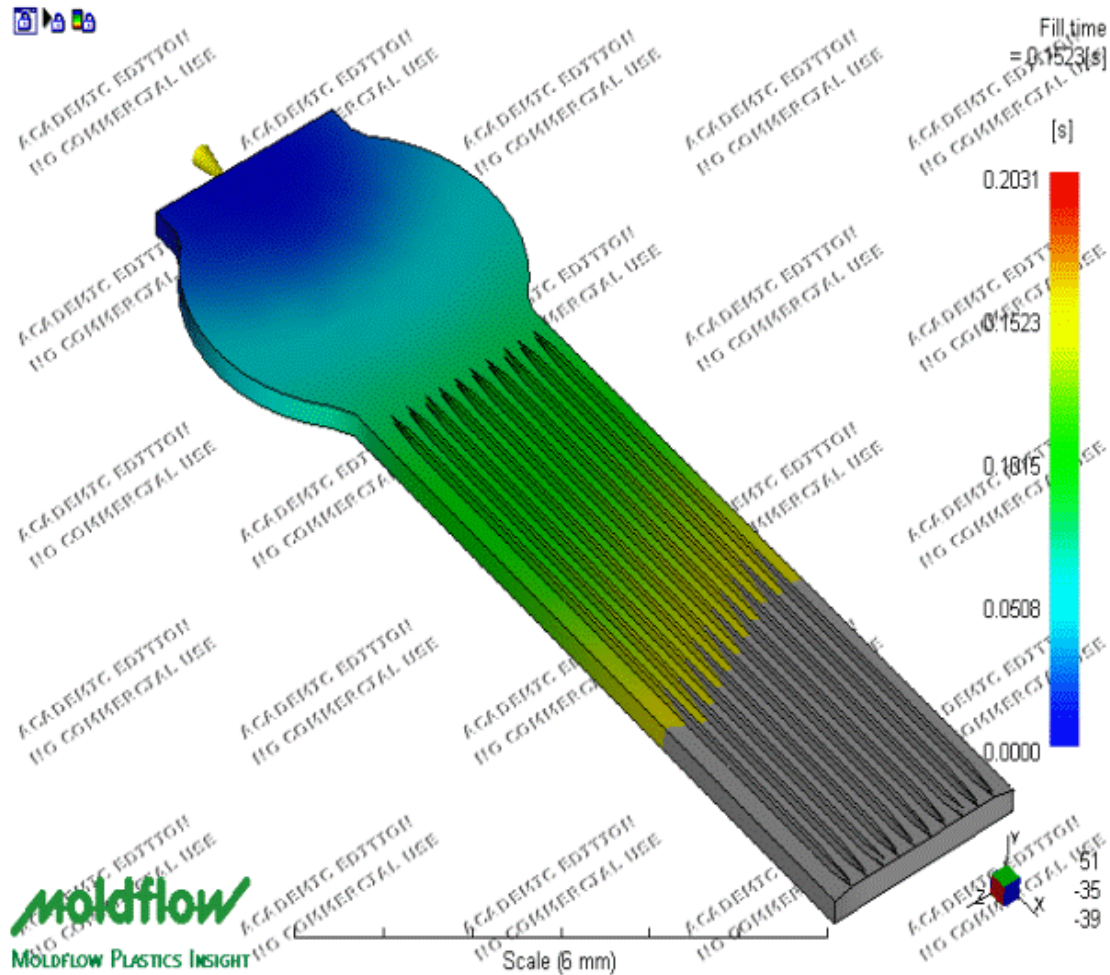


Figure 48: 0.25 mm thick bulk from MPI

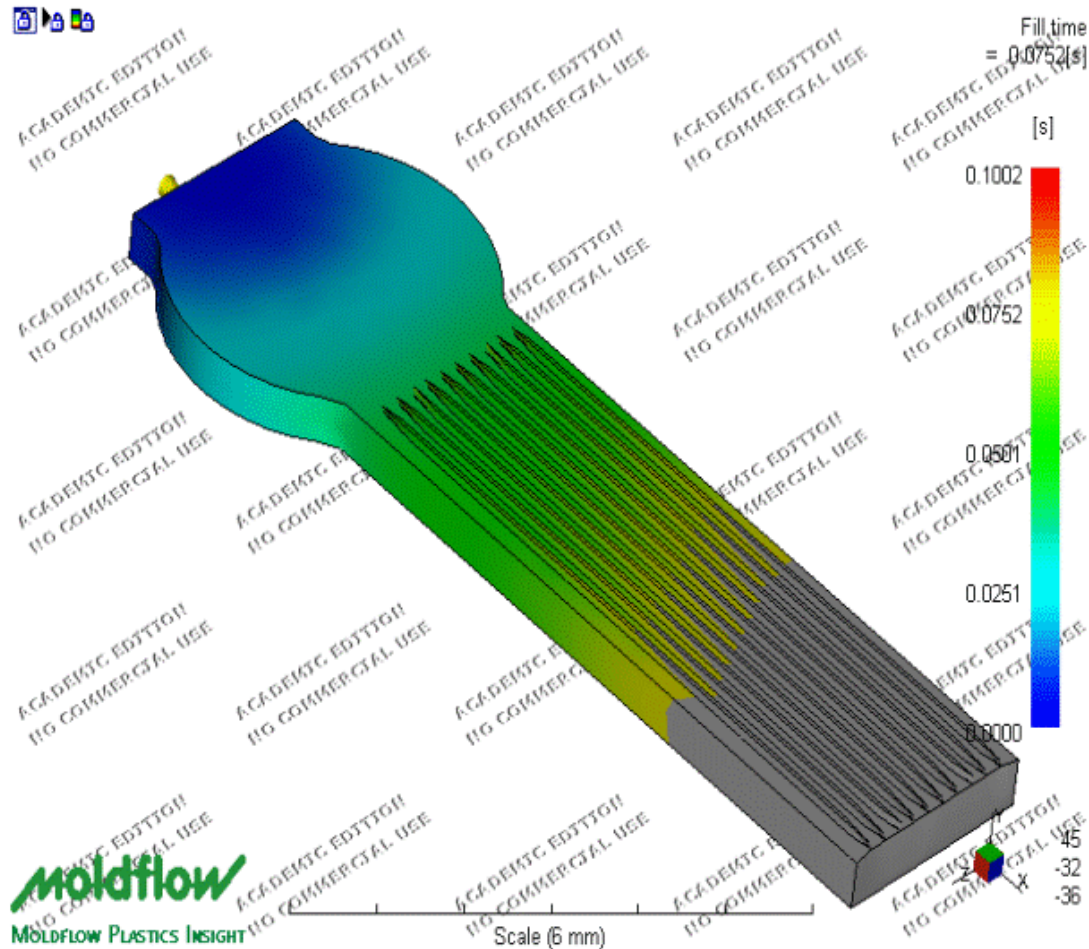


Figure 49: 0.5 mm thick bulk from MPI

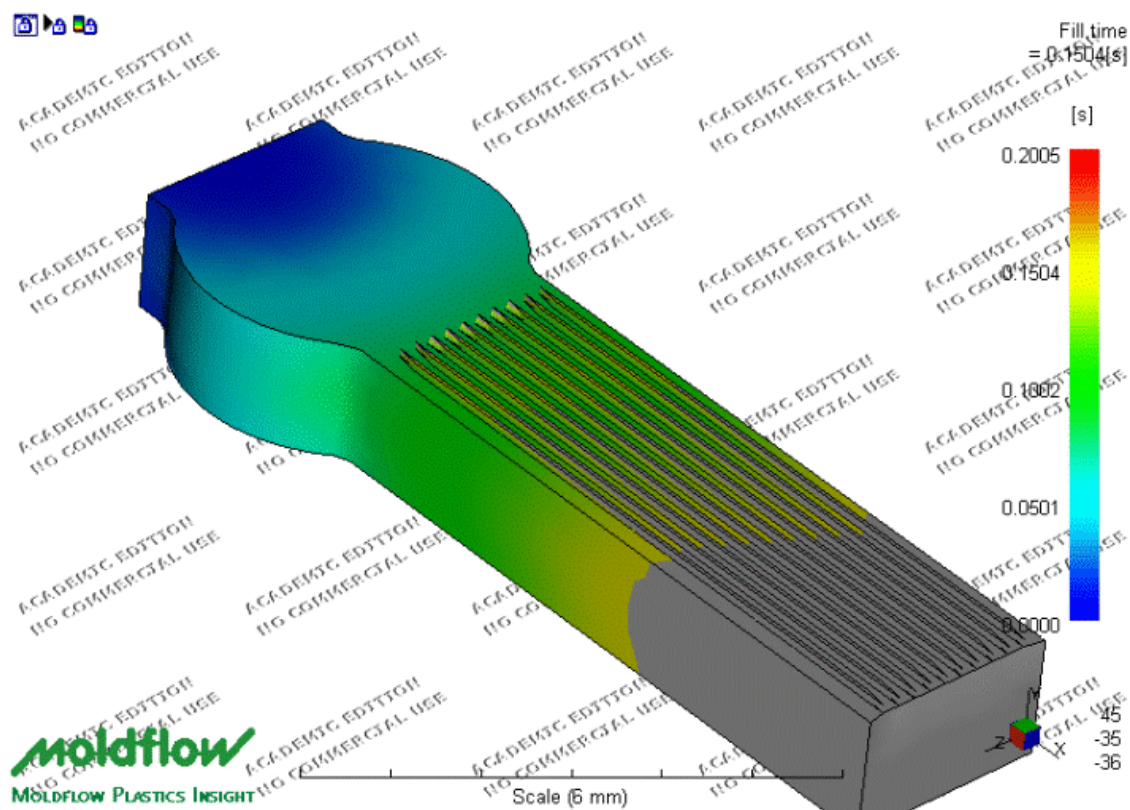


Figure 50: 1.5 mm thick bulk from MPI

3.3.2 Microchannel end

A simulation run was also conducted by cutting a triangle in the bulk of the part.

This experiment was done to see the effect of change in shapes of bulk on the flow of feedstocks in microchannels. Figure 51A shows the cut of $0.5\text{mm} \times 0.5\text{mm}$ on a 0.5mm thick bulk. Figure 51B shows the cut of $0.5\text{mm} \times 2\text{mm}$ on a 0.5mm thick bulk. Similarly, Figure 51C shows the cut of $0.25\text{mm} \times 8\text{mm}$ on a 0.5mm thick bulk. All these three change in the shape of the bulk did happen to make any difference in the flow of the feedstocks in the microchannels.

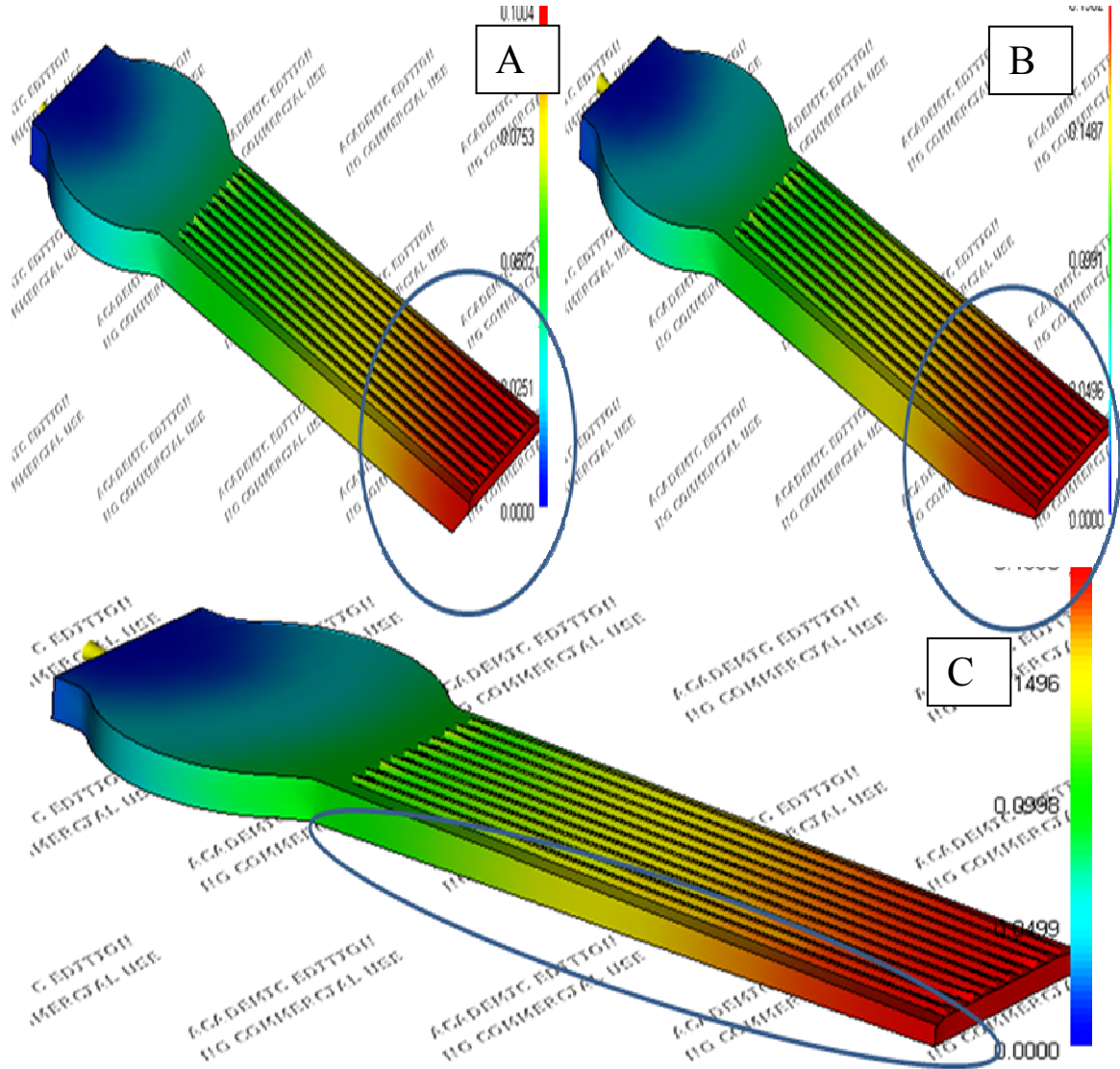


Figure 51: A - shows the cut of $0.5\text{mm} \times 0.5\text{mm}$ on a 0.5mm thick bulk; B - shows the cut of $0.5\text{mm} \times 2\text{mm}$ on a 0.5mm thick bulk; C - shows the cut of $0.25\text{mm} \times 8\text{mm}$ on a 0.5mm thick bulk.

3.3.3 Multiple gates

Figure 52 shows the effect of multiple gates on the flow of feedstocks in microchannels. However, it is observed that multiple gate entry as shown in

Figure 52 does not make any difference in the flow of feedstocks in microchannels.

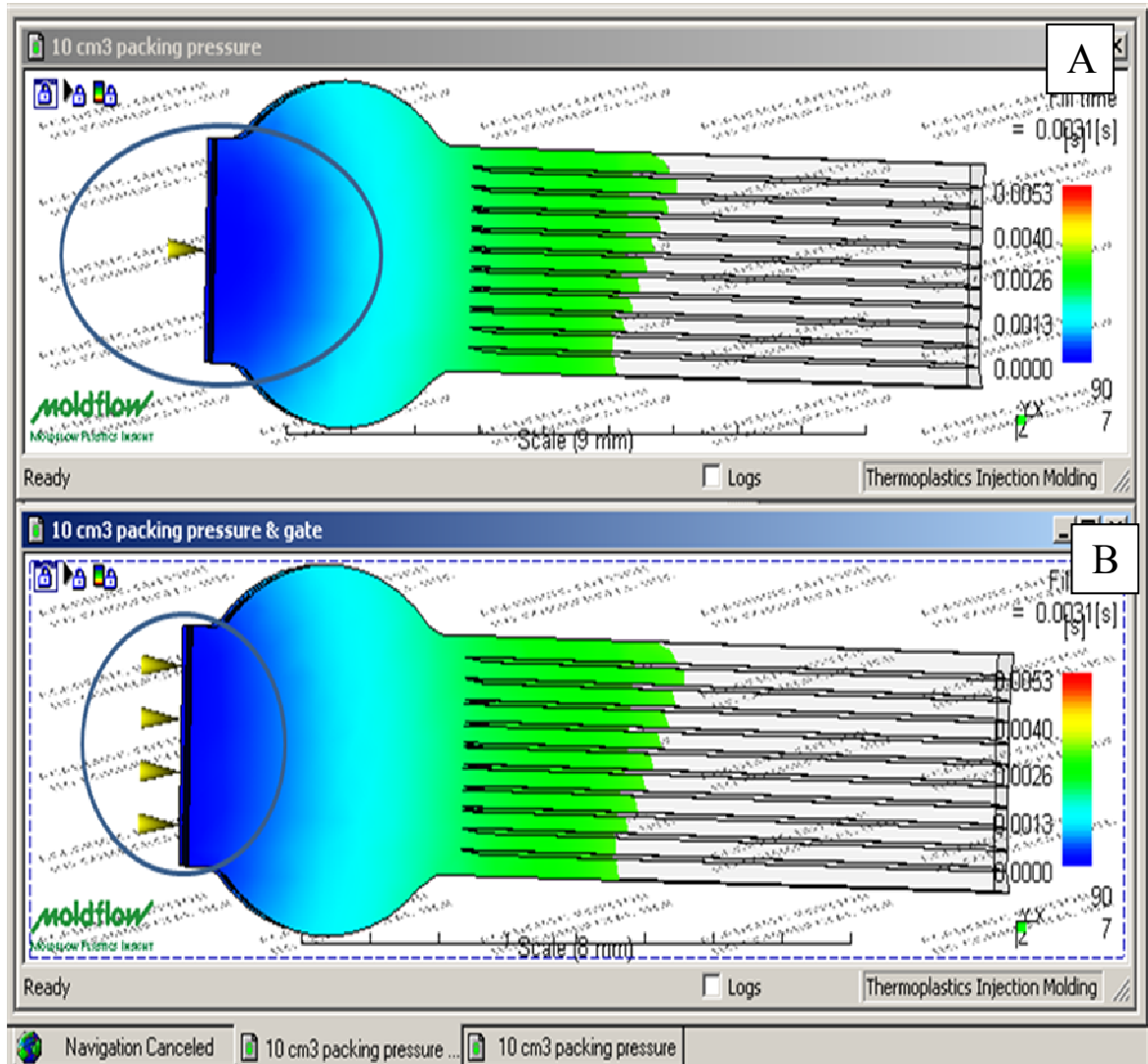


Figure 52: A – single gate entry; B – multiple gate entry

3.4 SUMMARY OF SENSITIVITY ANALYSIS

All the material parameters (viscosity, PVT, thermal conductivity, specific heat), processing parameters (melt and mold temperature) and part geometry were varied by 10% each about their experimental values to study their effect on

the filling of the microchannels. Appendix III gives the details of the variations conducted. The 6 main parameters identified after this sensitivity analysis are shown in Table 12.

The negative values in the Table 12 shows the % increase in the mold filling time of the experimental part, compared to the mold filling time when the parameters are not changed. On the other hand, the positive values denote the % decrease in the total fill time of the cavity, compared to the mold filling time when the parameters are not changed. The table gives the trend followed by both the feedstocks (Catamold AO-F and Standard Mix) studied in the research.

Table 12: Results of the sensitivity analysis

Sr. No.	Property	% Increase or Decrease in the total mold filling time of the experimental part	
		Decreasing the experimental value of the property by 10%	Increasing the experimental value of the property by 10%
1	Thermal Conductivity	0.0	20.1
2	Specific Heat	-20.3	0.0
3	A1 - WLF temperature shift factor	-40.2	20.1
4	Melt Temperature - 190°C	-19.9	20.1
5	Mold Temperature - 150°C	-80.7	0.2
6	Bulk thickness of the part - 1.5mm	15.2%	-10.8%

It is found that, increasing the experimental value of the thermal conductivity by 10% seems to have faster filling of the mold (decrease in the total fill time by 20.1%) which in turn fills the microchannels faster.

If the specific heat of the feedstocks is decreased by 10%, then the total fill time is observed to increase by 20.3%. This increase in total fill time leads to slower fill of the microchannels.

Similarly, decreasing the mold temperature further below 150°C by 10%, increases the total fill time by 80.7%. This means that the microchannels fill further slower than they were filling at 150°C. However, increasing the mold temperature by 10% above 150°C seems to have nearly no change in the total fill time of the cavity.

Similarly, the other parameters can be interpreted, where A1 (WLF temperature shift factor) and melt temperature seems to have significant effect (decrease in the flow in the cavity or increase in the total fill time) by decrease their experimental value by 10%. However, bulk thickness of the part if decreased by 10%, the flow in the microchannels increases rapidly (by 15%).

By the end of Chapter 3, the first 3 steps leading towards the goal of the study were finished. The goal, to understand the process of μ PIM (mold filling) with the help of computer simulations (Moldflow Plastic Insight) for ceramic microchannel arrays by investigating materials, processing and part designing issues was near from this point of the thesis.

CHAPTER 4: COMPARISON OF FEEDSTOCKS IN MCA

This chapter focuses on comparing the flow of two different feedstocks into the microchannels. The feedstock which basically fills the microchannels faster would be a better feedstock among the two. Let us now observe carefully the flow progress of feedstock in the microchannels in section 4.1. The thing to be noted is that, the section 4.1 shows the filling pattern of Catamold AO-F, and the Standard Mix follows the same trend as well.

4.1 PROGRESSIVE FILLING OF MICROCHANNELS

Figure 53A, 53B and 53C shows the progressive filling of the microchannels from Moldflow simulations for Catamold AO-F at a melt temperature of 190°C. Figure 53A shows that after the bulk is filled half way then the microchannels start to fill. Figure 53B and 53C maintain the same momentum as Figure 53A. The microchannels are filled at the last which causes uneven filling of feedstock in the part. This uneven filling leads to uneven cooling and stress generation in the MCA.

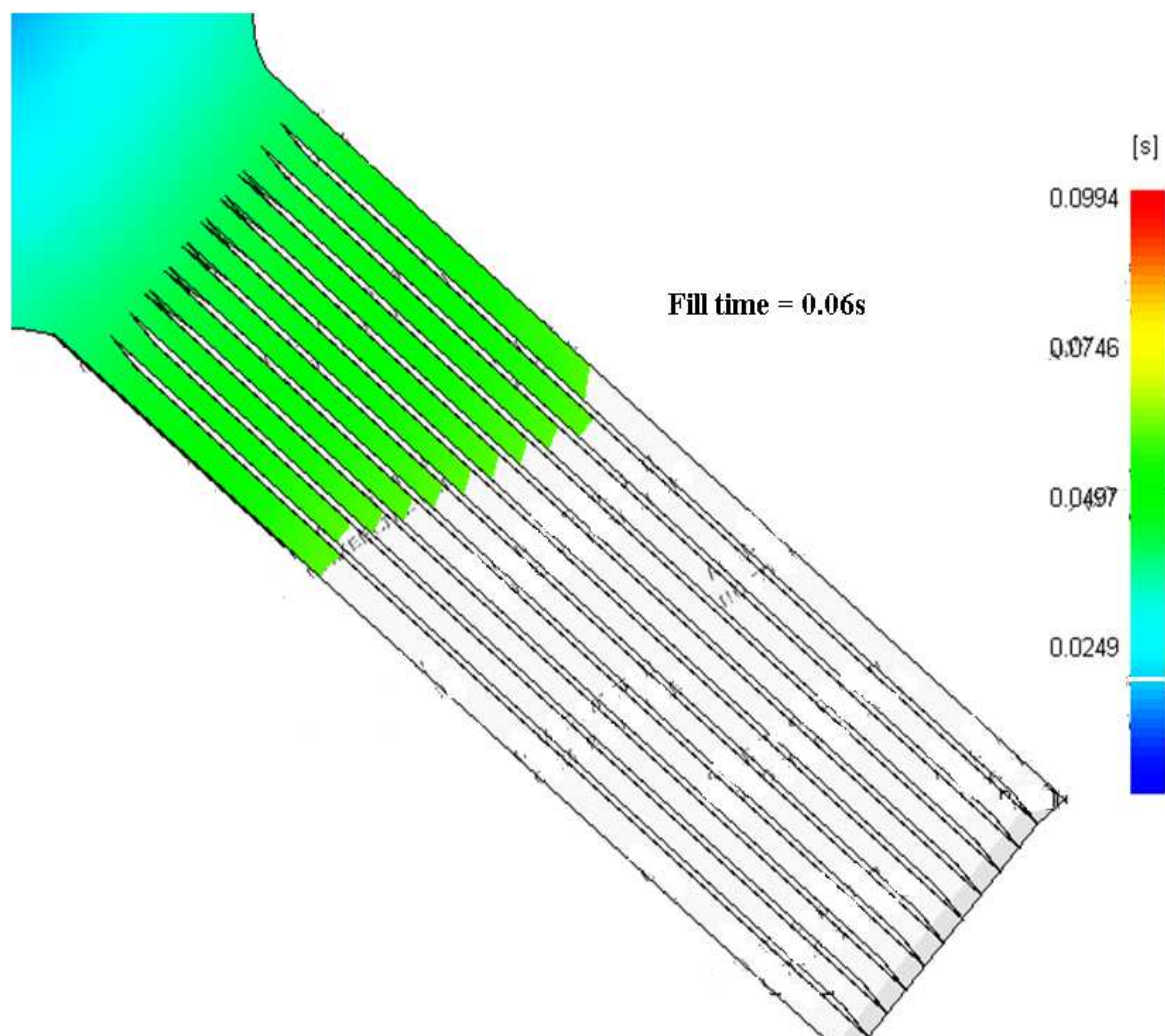


Figure 53A: Progressive filling of microchannels using Catamold AO-F at a melt temperature of 190°C from Moldflow simulations.

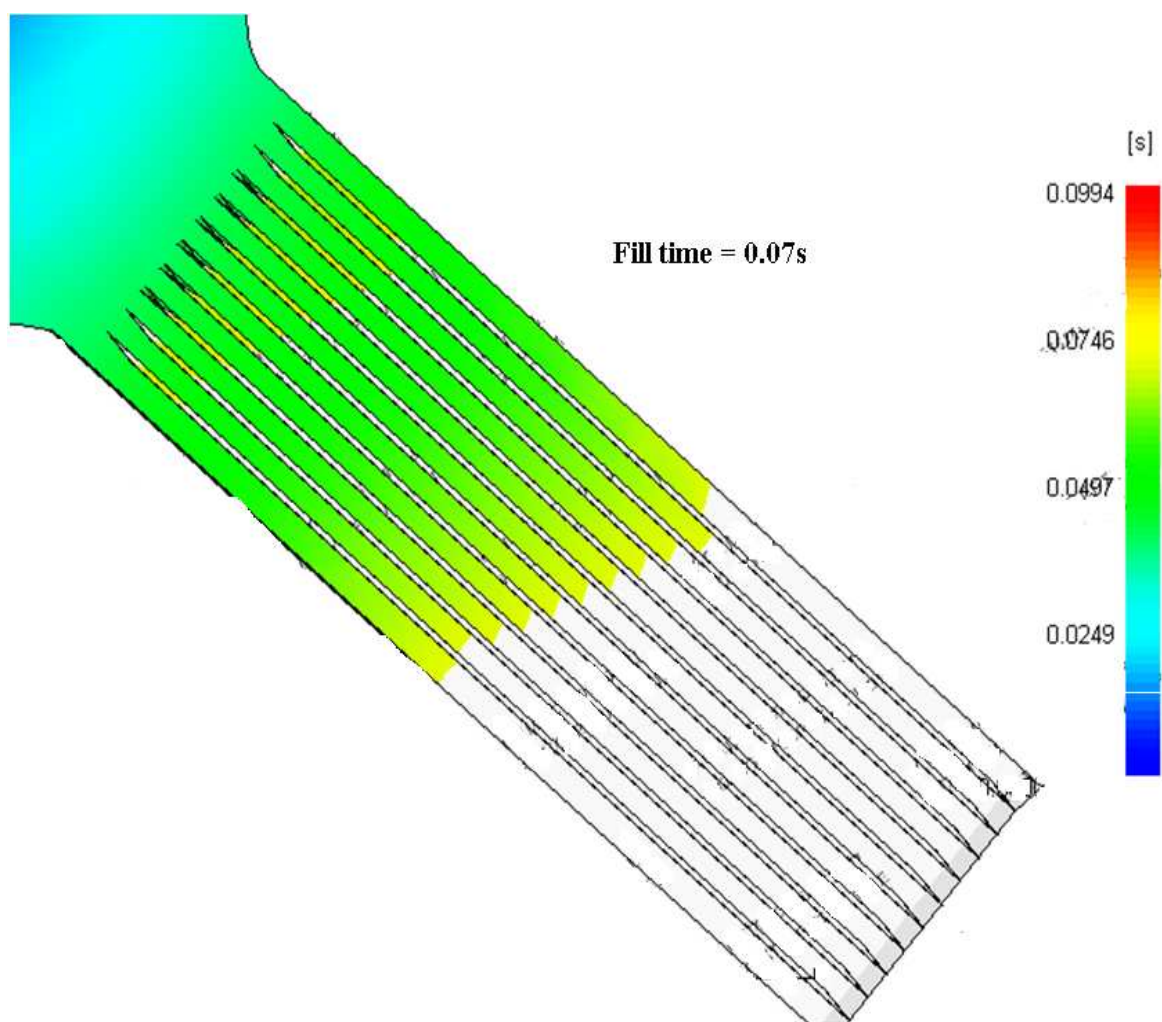


Figure 53B: Progressive filling of microchannels using Catamold AO-F at a melt temperature of 190°C from Moldflow simulations.

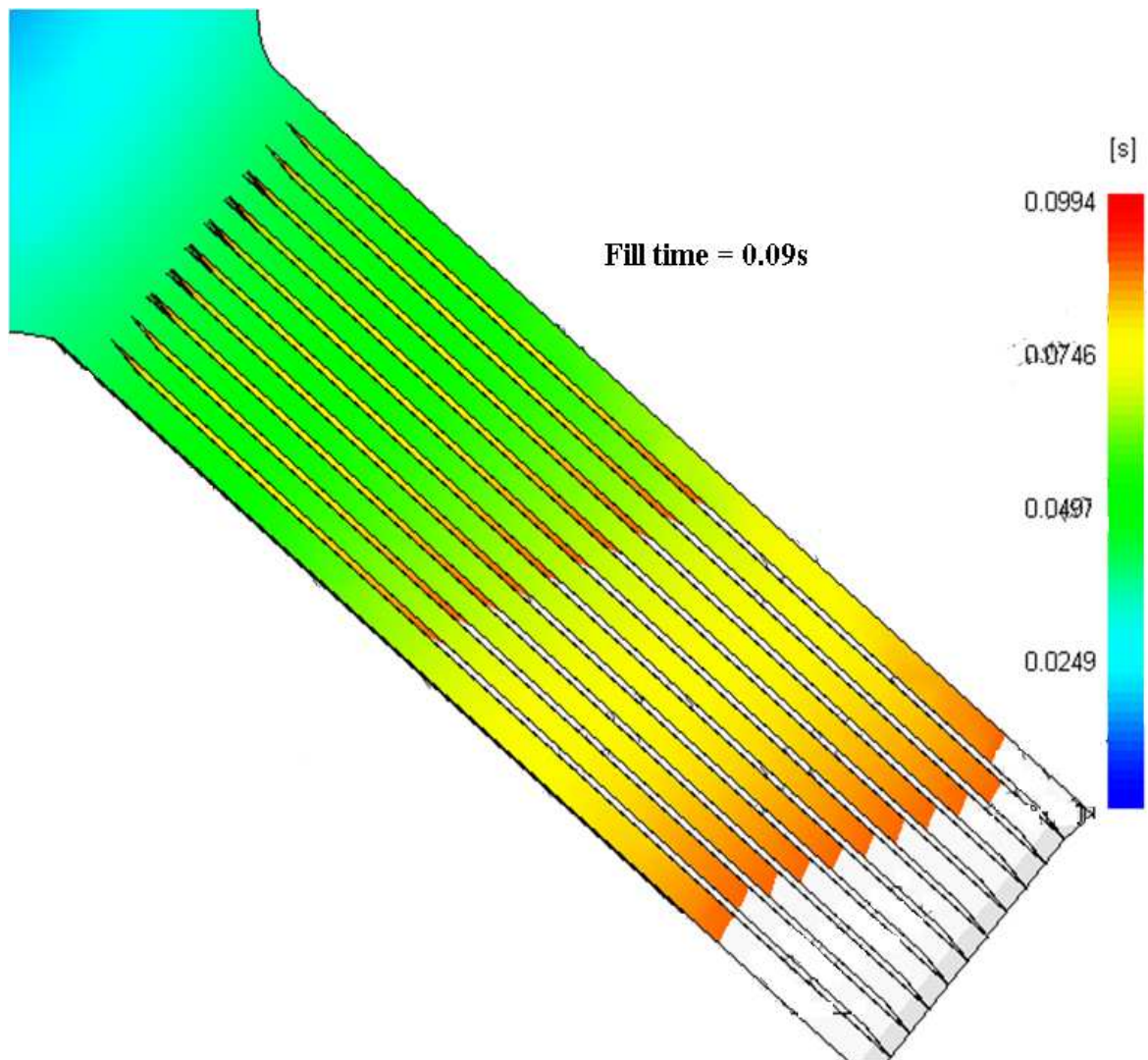


Figure 53C: Progressive filling of microchannels using Catamold AO-F at a melt temperature of 190°C from Moldflow simulations.

After having seen the flow pattern in the microchannels, now, let us compare the two feedstocks used in the study in section 4.2 and 4.3.

4.2 Comparison of feedstocks in microchannels - through simulations

To compare the two feedstocks, it was necessary to compare them using their experimental values for all the properties. Hence, all the properties shown in Appendix I and II were fed in the Moldflow Plastic Insight. Also, we could not have experimentally changed the part geometry (bulk thickness) due to the mold that we had. The only thing that we could have changes is either the melt or the mold temperature. We decided to compare the two feedstocks by keeping every other parameter based on the experimental values and just changing the melt temperature.

Analysis of MCAs using Moldflow simulations were quantified and are shown in Figure 54. It was found that at a given melt temperature, the amount of feedstock flowing in the microchannels per unit area and per unit time was greater for Catamold AO-F than the Standard Mix. However, (Figure 55) the flow in the bulk for both the feedstocks remained nearly the same.

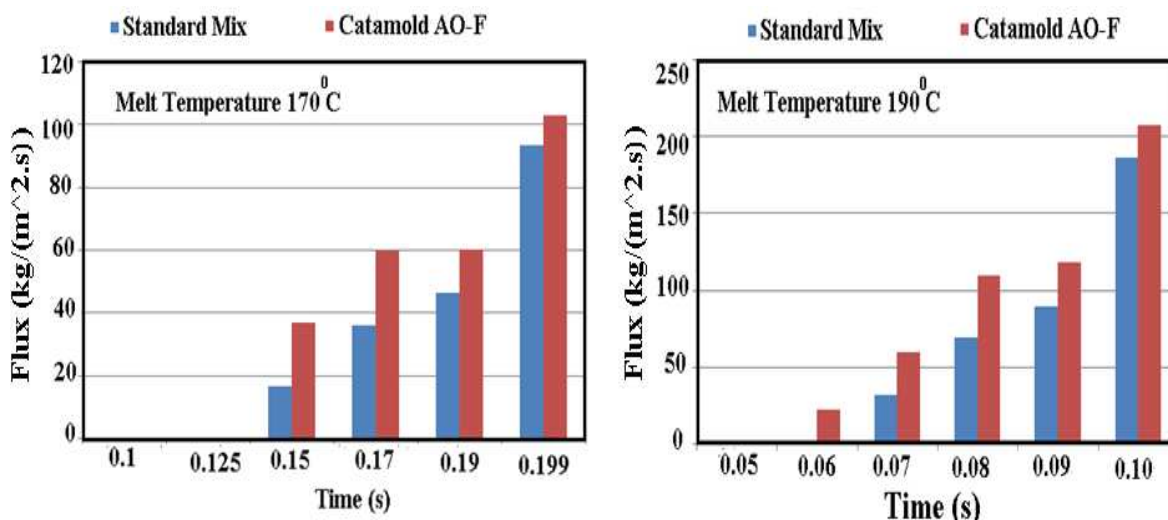


Figure 54: Comparison of Catamold AO-F and Standard Mix in microchannels and bulk at melt temperature of 170°C and 190°C.

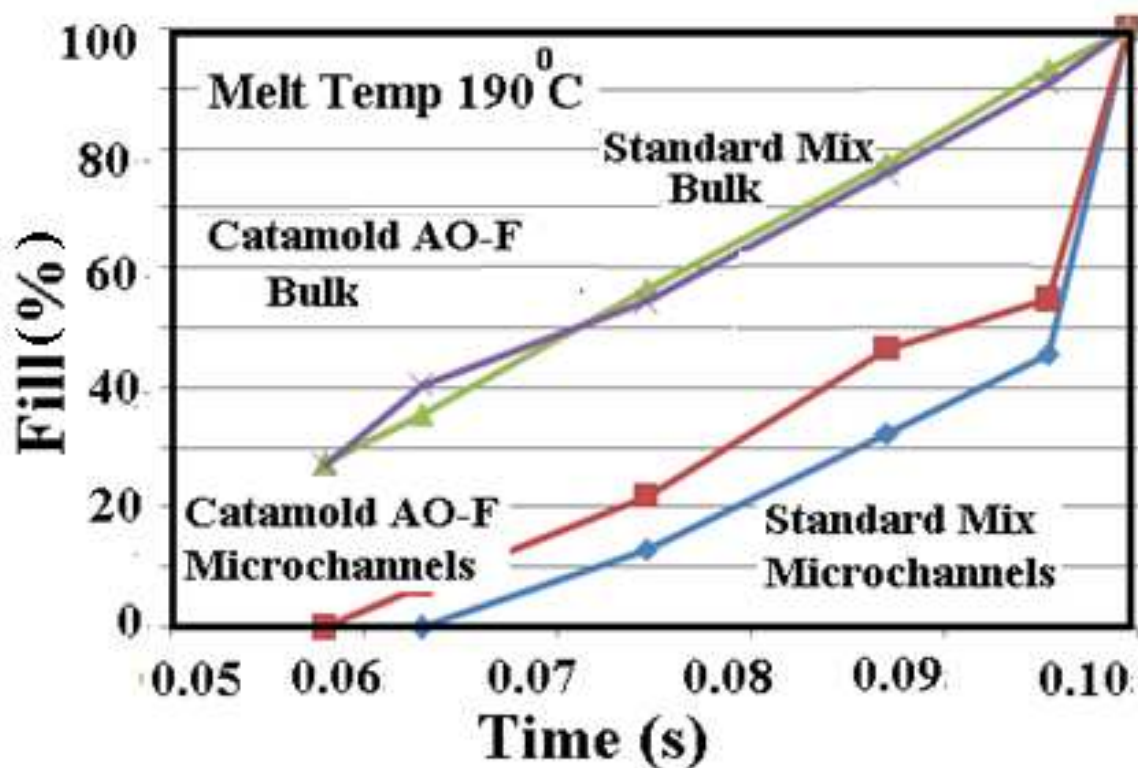


Figure 55: Comparison of Catamold AO-F and Standard Mix in microchannels and bulk at melt temperature of 190°C

4.3 Comparison of feedstocks in microchannels - through experimentations

Simulation results showed that Catamold AO-F shows better filling of microchannels compared to Standard Mix. Similar results were explored with experimentations. Figure 56 shows the cross-section of the microchannel of the molded MCA using Catamold AO-F as well as Standard Mix. The top and bottom surfaces of the microstructures molded using Catamold AO-F are fairly flat with sharp corners (Figure 56A) compared to the Standard Mix (Figure 56B). This indicates the good filling of the microchannels during injection molding for Catamold AO-F than Standard Mix.

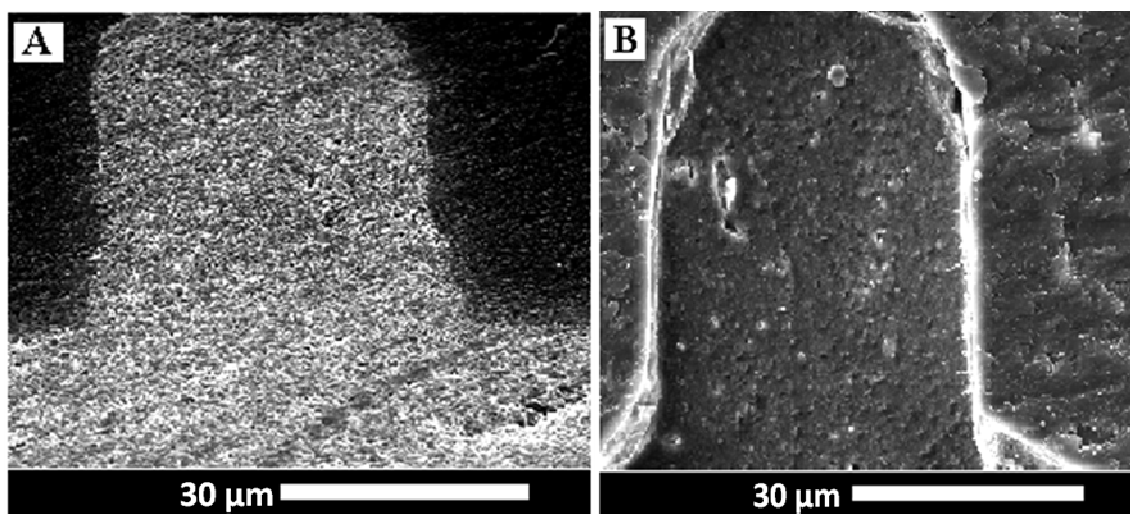


Figure 56: A and B are the cross-sections of the MCA molded using Catamold AO-F and Standard Mix respectively.

Thus the simulation results were validated using the experiments. The possible reasons for the better filling of the microchannels for Catamold AO-F might be;

- 1) Higher viscosity leading to higher pressure in the cavity. This high pressure pushes the feedstock into the microchannels leading to faster filling.
- 2) Higher thermal conductivity of the Catamold AO-F leads to faster solidification of feedstock in the microchannels. This prevents the feedstock to flow back into the bulk from the microchannels after the pressure is reduced in the cavity.

Further, the microchannels ribs were ion milled and a SEM study was done to find the particle density in the microchannels ribs (Figure 57). It was found that both the system have fairly same amount of powder (alumina) flowing into the microchannels. The waxy layer on the surface of the ribs, as seen

in Figure 57B is for due to the melting of the paraffin wax due to ion milling of the ribs.

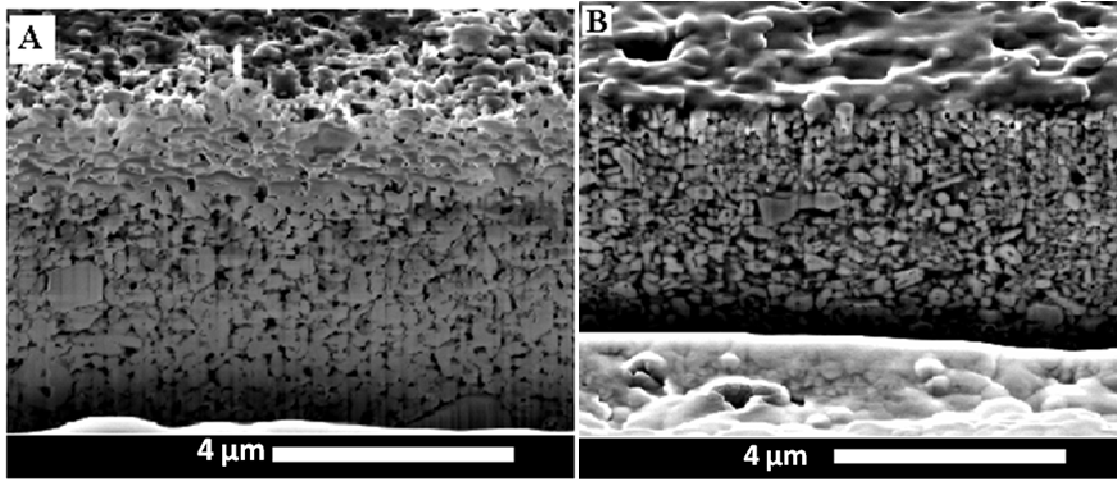


Figure 57: A and B are the cross-sections of the microchannels ribs after ion milling for Catamold AO-F and Standard Mix respectively.

By the end of Chapter 4, all the steps defined to reach the goal of understanding the process of μ PIM (mold filling) with the help of computer simulations (Moldflow Plastic Insight) for ceramic microchannel arrays by investigating materials, processing and part designing issues were reached. Chapter 5 gives few recommendations as to how effectively an MCA part can be filled in the field of μ PIM.

CHAPTER 5: CONCLUSIONS & FUTURE WORK

5.1 Conclusions

This research emphasizes the effect of the polymer system (polyacetal and wax) on the mold filling abilities of the powder-polymer suspension during the fabrication of microchannel arrays (MCAs) by μ PIM. Three aspects to avoid some of the mold filling defects in MCA's (material properties, processing parameters and part geometry,) were studied thoroughly in this research.

- The following relationships were observed with materials-related parameters:
 - Viscosity of the feedstock plays an important role to fill the microchannels. Newtonian behavior (power law index, $n \sim 1$) of the feedstocks is important for better and faster filling of microchannels.
 - Sensitivity analysis showed that the thermal conductivity if increased by 10% of the experimental value, increases the flow of feedstock in the microchannels by 20% or more.
 - Pressure-Volume-Temperature (PVT) relationships are important to predict the filling behavior using simulation software.
 - Melt and solid compressibility is higher for Standard Mix feedstock compared to Catamold AO-F.
 - When the pressure is increased, more thermal energy is required to get the chains moving, hence a higher T_g is found at higher pressures for both the feedstocks.
 - Decrease in the specific heat by 10%, decreases the flow of feedstock into the microchannels by 20% according to the sensitivity analysis.
- The following relationships were observed with processing-related parameters:

- Melt temperature and mold temperature are the most crucial processing parameters to avoid defects. Higher the melt temperature better is the feedstock flow into the microchannels. Mold temperature upto 150°C shown to have increase in the flow of feedstocks (Catamold AO-F and Standard Mix) in the microchannels. Further increase in mold temperatures does not make any significant change.
 - High injection pressure and clamp force are required to produce MCAs. As a result, there is an increased tendency to form defects such as short shots, jetting, powder-binder separation and flashing due to sub-optimal selection of process parameters or feedstock material design.
- Designing the MCA part places an important role to decrease the number of defects while molding.
 - Thinner the bulk section better is the flow of feedstock in the microchannels.
 - Any modifications in the part design which will help to decrease the number of defects, can be done using SolidWorks and later by using Moldflow Plastic Insight.

Table 13 gives few recommendations to make an effective ceramic MCA part using Catamold AO-F and Standard Mix.

Table 13: Recommendation to mold a MCA with minimum defects for both the feedstocks

Sr. No.	Properties/Parameters/Geometry	Input (Increase or Decrease from experimental values)	Output (Flow in the microchannels as a function of fill time)	Aspects
1	Thermal Conductivity	↑	↑↓	Material Properties
2	Specific Heat	↓	↓	
3	Power law index, n	↑	↑	
4	Melt Temperature - 190°C	↑	↑	Processing parameters
5	Mold Temperature - 150°C	↓	↓	
6	Bulk thickness of the part - 1.5mm	↓	↑	Part Geometry

- Comparison of the feedstocks for the mold filling time:
 - The Viscosity of the Standard Mix drops rapidly with the increase in the shear rate when compared to Catamold AO-F. This high viscosity of Catamold AO-F builds enough pressure inside the mold cavity to push the feedstock into the microchannels leading to better filling of microchannels.
 - Whereas, the specific volume of the Catamold AO-F drops rapidly with decreasing temperature and increasing pressure compared to Standard Mix. Thus the shrinkage in Catamold AO-F is lesser than Standard Mix

and hence it might give better dimensional retention and hence better parts.

- Catamold AO-F has higher thermal conductivity compared to Standard Mix. This leads to faster solidification of feedstock in the microchannels for Catamold AO-F which prevents the feedstock to flow back into the bulk from the microchannels after the pressure is reduced in the cavity.

5.2 Future work

There is a need to extend the study of MCAs after debinding and sintering steps. The conclusion of one feedstock better than the other might completely change after debinding and sintering steps. Hence, it becomes extremely important to study the MCAs after these two processing steps.

Also, further study and characterization is essential to conclude if one feedstock is better than other;

- 1) Alumina to carbon ratio in the ribs and in the bulk using x-ray photoelectron spectroscopy (XPS)
- 2) Optical profilometry to observe the dimensions of the 50 μ m MCA for the green and the sintered parts.

It will be important to predict the material properties of the PIM feedstocks in the long run. Knowing the properties of the feedstocks without actually testing it, along with simulation studies will cut down the experimental section in this field significantly. This will give faster results in less time and the chance of hitting the product to the market will be faster as well.

The current study only investigated MCA having following facts,

- 1) Feedstock has 56 vol. % alumina loading,

- 2) The average diameter of the alumina particles is 400 nm ,
- 3) Feedstocks used polyacetal and wax binders,
- 4) Only one type of geometry for MCA was studied,

The results from this study might not address the mold filling problems if any of the above parameters is changed. For example,

- 1) Use of different powder like stainless steel or titanium
- 2) Use of different binders or different binder concentration for polyacetal and wax binders
- 3) Different geometries, etc.

An entirely new set up of results and investigation is required for above mentioned few cases.

Further investigation in all the above mentioned points might further give significant contribution to the filed of μ PIM.

BIBLIOGRAPHY

1. Z.S. Rak, Powder Metallurgy and Metal Ceramics, Vol. 38, 1999, Pages: 126-132.
2. L. Liu, N.H. Loh, B.Y. Tay, S.B. Tor, Y. Murakoshi, R. Maed, Materials Characterization, Vol. 54, 2005, Pages: 230-238.
3. L.E. Khoong, Y.C. Lam, J.C. Chai, L. Jiang, J. Ma, Chemical Engineering Science, Vol. 62, 2007, Pages: 6927-6938.
4. H.K. Lin and K.S. Hwang, Acta Metallurgica Inc, Vol. 46, 1998, Pages: 4303 – 4309.
5. T. Shimizu, Y. Murakoshi, T. Sano, R. Maeda, S. Sugiyama, Microsystem Technologies, Vol. 5, 1998, Pages: 90-92.
6. C.H. Ji, N.H. Loh, K.A. Khor, S.B. Tor, Materials Science and Engineering, Vol. A311, 2001, Pages: 74-82.
7. Z.Y.Liu, N.H. Loh, S.B. Tor, K.A. Khor, Materials Characterization, Vol. 49, 2003, Pages: 313-320.
8. Songlin Li, Baiyun Huang, Yimin Li, Xuanhui Qu, Shaojun Liu, Jianglian Fan, Journal of Materials Processing Technology, Vol. 137, 2003, Pages: 70-73.
9. Gaurav Aggarwal, Seong-Jin Park and Randall M. German, Metallurgical and Materials Transactions, Vol. 38A, 2007, Pages: 606-615.
10. Z.Y. Liu, N.H. Loh, S.B. Tor, K.A. Khor, Y. Murakoshi, R. Maeda, T. Shimizu, Journal of Materials Processing Technology, Vol. 127, 2002, Pages: 165-168.
11. Min Soo Park, Jin Kon Kim, Journal of Material Sciences, Vol. 36, 2001, Pages: 5531-5536.
12. G. Fu, N.H. Loh, S.B. Tor, B.Y. Tay, Y. Murakoshi, R. Maeda, Applied Physics A, Vol. 81, 2005, Pages: 495-500.
13. R. Supati, N.H. Loh), K.A. Khor, S.B. Tor, Materials Letters, Vol. 46, 2000, Pages:109-114.

14. L.A. Dobrzanski , G. Matula, G. Herranz, A. Varez, B. Levenfeld, J.M. Torralb,
Journal of Materials Processing Technology, Vol. 175, 2006, Pages: 173-178.
15. C. Karatas, A. Kocer, H.I. Unal, S. Saritas, Journal of Materials Processing
Technology, Vol. 152, 2004, Pages: 77-83.
16. G. Fu, N.H. Loh, S.B. Tor, B.Y. Tay, Y. Murakoshi, R. Maeda, Microsyst
Technol, Vol.11, 2005, Pages: 1267-1271.
17. B.Y. Tay, L.Lui, N.H. Loh, S. B. Tor, Y. Murakoshi, R. Maeda, Materials
Characterization, Vol. 57, 2006, Pages: 80-85.
18. Adamowicz, John, "ARBURG, INC. Powder injection molding design
possibilities", *International journal of powder metallurgy*, 1997, vol. 33, pp. 17-19
19. Alcock, Jeffrey; Stephenson, David, "Powder injection moulding: Some novel
developments", *Materials world: the journal of the Institute of Materials*, 1996,
vol. 4, pp. 629-630
20. Ballard, Clifford; Zedalis, Michael, "Advances in powder injection molding",
Conference proceedings at ANTEC '98, 1998, vol. 1, pp. 358-361
21. Barriere, T.; Gelin, J.C.; Liu, B., "Experimental and numerical investigations
on properties and quality of parts produced by MIM", *Powder metallurgy*,
2001, vol. 44, pp. 228-234
22. Barriere, Th.; Liu, B.; Gelin, J.C., "Determination of the optimal process
parameters in metal injection molding from experiments and numerical
modeling", *Journal of materials processing technology*, 2003, vol. 143-144, pp.
636-644
23. Benzler, T. ; Piottter, V.; Hanemann, T.; Mueller, K.; Norajitra, P.; Ruprecht, R.;
Hausselt, J., "Innovations in molding technologies for microfabrication",
Micromachining and microfabrication process technology V : 20-22, 1999, vol. 3874,
pp. 53-60
24. Bhave, Prashant, "Metal injection molding standards review", *International
journal of powder metallurgy*, 1990, vol. 26, pp. 277-280

25. Beebhas, C. Mutsuddy; Renee G. Ford, *Ceramic injection Molding*, Chapman and Hall, London, 1995.
26. Bigg, D.M.; Barry, R.G., "Rheological analysis as a tool to predict quality in powder injection molding", *Conference proceedings at ANTEC '98*, 1998, vol. 1, pp. 997-1000
27. Bilovol, V.V.; Kowalski, L.; Duszczyk, J.; Katgerman, L., "Comparison of numerical codes for simulation of powder injection moulding", *Powder metallurgy*, 2003, vol. 46, pp. 55-60
28. Bose, Animesh, "Technology and commercial status of powder-injection molding", *JOM: the journal of the Minerals, Metals & Materials Society*, 1995, vol. 47, pp. 26-30
29. Chen, S.C.; Chen, Y.C.; Cheng, N.T.; Huang, Ming-Shyan, "Simulation of injection-compression mold-filling process", *International communications in heat and mass transfer*, 1998, vol. 25, pp. 907-917
30. Edirisinghe, M. J.; Evans, J. R. G., "Rheology of Ceramic Injection Moulding Formulations", *British ceramic, transactions and journal*, 1987, vol. 86, pp. 18-22
31. Edirisinghe, Mohan J., "Ceramic injection moulding. The effect of powder surface area", *Structural ceramics processing, microstructure and properties*, 1990, pp. 257-262
32. Edirisinghe, Mohan J., "Effect of processing additives on the properties of a ceramic-polymer formulation", *Ceramics international*, 1991, vol.17, pp. 89-96
33. Edirisinghe, Mohan J., "Injection moulding of ceramics", *Metals and materials: the journal of the Institute of Metals*, 1990, vol. 6, pp. 367-370
34. Edirisinghe, Mohan J., "Thermolysis of plastically formed ceramics: Modeling and computer simulation", *Materials and manufacturing processes*, 1997, vol. 12, pp. 109-16

35. Fox, R.T.; Moller, J.C.; Najmi, L.A.; Lee, D., "Structured approach to injection molding of powder-binder mixtures", *Powder Injection Molding Symposium*, 1992, pp. 313-325
36. Fox, Richard T.; Lee, Daeyong, "Optimization of metal injection molding. Experimental design", *International journal of powder metallurgy*, 1990, vol. 26, pp. 233-243
37. Gelin, J.C.; Barriere, T.; Dutilly, M., "Experiments and computational modeling of metal injection molding for forming small parts", *CIRP Annals - Manufacturing Technology*, 1999, vol. 48, pp. 179-182
38. German, Randall M., "Identification of the effects of key powder characteristics on powder injection molding", *Powder Injection Molding Symposium*, 1992, pp. 1-15
39. German, Randall M., "Importance of particle characteristics in powder injection molding", *Reviews in particulate materials*, 1993, vol. 1, pp. 109-190
40. German, Randall M., "Scientific status of metal powder injection molding", *International journal of powder metallurgy*, 2000, vol. 36, pp. 31-36
41. German, Randall M., "Technological barriers and opportunities in powder injection molding", *Powder Metallurgy International*, 1993, vol. 25, pp. 165-169
42. German, Randall M., *Powder Injection Molding*, Metal Powder Industries Federation, Princeton, NJ, 1990.
43. German, Randall M., *Powder Metallurgy Science*, 2nd edition, Metal Powder Industries Federation, Princeton, NJ, 1994.
44. German, Randall M.; Cornwall, Robert G., "Summary report on the worldwide market and technology for injection molding of metals and ceramics", *Advances in powder metallurgy & particulate materials: proceedings*, 1997, vol. 3, pp. 18-3-18-8

45. German, Randall M.; Cornwall, Robert G., "Worldwide market and technology for powder injection molding", *International journal of powder metallurgy*, 1997, vol. 33, p. 4
46. Haiqing, Gong, "Procedure for characterising the fountain effect in the filling of a complex mold", *Journal of materials processing technology*, 1993, vol. 38, pp. 41-50
47. Hanson, Andrew D.; Perruzza, Steven C., "Optimizing component designs for metal injection molding", *International journal of powder metallurgy*, 2000, vol. 36, pp. 37-42
48. Hens, K.F. ; Lee, D., "Process analysis of injection molding with powder products", *Advances in powder metallurgy*, 1991, vol. 2, pp. 127-140
49. Hens, K.F. ; Lee, D.; Lin, S.T.; German, R.M., "Injection molding of powders into complex shapes", *Advances in powder metallurgy*, 1990, pp. 283-298
50. Hieber, C.A.; Shen, "A Finite-Element/Finite-Difference Simulation of the Injection Molding Filling Process", *Journal of non-Newtonian fluid mechanics*, 1980, vol. 7, p. 1
51. Hieber, C.A.; Shen, S. F., "Flow analysis of the non-isothermal two-dimensional filling process in injection molding", *Israel journal of technology*, 1978, vol. 16, p. 248
52. Holme, J.D., "Powder injection moulding. Still waiting in the wings", *Materials world: the journal of the Institute of Materials*, 1993, vol. 1, pp. 552-554
53. Hwang, C.J.; Kwon, T.H., "A full 3D finite element analysis of the powder injection molding filling process including slip phenomena", *Polymer engineering and science*, 2002, vol. 42, pp. 33-50
54. Iacocca, R.G., "Critical assessment of characterization tests needed to support powder injection molding component fabrication", *Reviews in particulate materials*, 1994, vol. 2, pp. 269-314

55. Jiang, Bing-Yan ; Zhong, Jue; Huang, Bai-Yun; Qu, Xuan-Hui; Li, Yi-Min, "Element modeling of FEM on the pressure field in the powder injection mold filling process", *Journal of materials processing technology*, 2003, vol. 137, pp. 74- 77
56. Krug, S.; Evans, J.R.G., "Methods of assessing gate solidification time in ceramic injection moulding", *Ceramics international*, 1999, vol. 25, pp. 661-666
57. Krug, S.; Evans, J.R.G.; ter Maat, J.H.H., "Jetting and weld lines in ceramic injection moulding", *British ceramic transactions*, 1999, vol. 98, pp. 178-181
58. Krug, S.; Evans, J.R.G.; ter Maat, J.H.H., "Residual stresses and cracking in large ceramic injection mouldings subjected to different solidification schedules", *Journal of the European Ceramic Society*, 2000, vol. 20, pp. 2535-2541
59. Krug, S; Evans, J.R.G.; ter Maat, J.H.H., "Predicting the viscosity of ceramic injection moulding suspensions", *Journal of the European Ceramic Society*, 2001, vol. 21, pp. 2275-2283
60. Kulkarni, Kishor M., "Metal powders and feedstocks for metal injection molding", *International journal of powder metallurgy*, 2000, vol. 36, pp. 43-52
61. Kwon, T.H.; Ahn, S.Y., "Slip characterization of powder/binder mixtures and its significance in filling process analysis of powder injection molding", *Powder technology*, 1995, vol. 85, p. 45
62. Kwon, T.H.; Park, J.B., "Finite element analysis modeling of powder injection molding filling process including yield stress and slip phenomena", *Polymer engineering and science*, 1995 vol. 35, pp. 741-753
63. Lanteri, B; Burlet, H.; Poitou, A.; Campion, I, "Powder injection molding: An original simulation of paste flow", *European journal of mechanics. A, Solids*, 1996, vol. 15, pp. 465-485

64. Li, Song-Lin ; Li, Yi-Min; Qu, Xuan-Hui; Huang Bai-Yun, "Rheological properties of metal injection molding feedstock", *Transactions of Nonferrous Metals Society of China*, 2002, vol. 12, pp. 105-108
65. Lin, Tony, "Quality Improvement of an Injection-Molded Product Using Design of Experiments: A Case Study.", *Quality engineering*, 2003, vol. 16, p. 99

APPENDIX

Section I:

Raw Data: Standard Mix

All the tests were done at Datapoint Labs and following are the results for Standard mix for various tests,

C-MOLD/Moldflow *TestPak*TM Results

< 13071.21000.udb

Analysis	Property & T-CODE	Value	Units
Filling & Cooling	Cross/WLF Model (01313):		
	n	0.23220	
	τ^*	9.401E+03	Pa
	D1	1.673E+15	Pa*s
	D2	263	K
	D3	0	K/Pa
	A1	28.40	
	A2	51.60	K
	Juncture Loss Constants (01360):		
	C1		Pa^(1-C2)
	C2		
	Melt Density (01000)	2335	kg/m³
	Melt Specific Heat (01100)	1301	J/kg*K
	Melt Thermal Conductivity (01200)	1.355	W/m*K
	Transition Temperature (01500)	325	K
	Specific Heat Table (01101)	See Page 7	
	Thermal Conductivity Table (01201)	See Page 8	
Post-Filling	Two-Domain Tait PVT Model (01004):		
	b5	3.322E+02	K
	b6	1.800E-07	K/Pa
	b1m	4.015E-04	m³/kg
	b2m	2.027E-07	m³/kg*K
	b3m	2.953E+08	Pa
	b4m	4.709E-03	1/K
	b1s	3.893E-04	m³/kg
	b2s	5.312E-08	m³/kg*K
	b3s	6.574E+08	Pa
	b4s	3.868E-06	1/K
	b7	1.223E-05	m³/kg
	b8	9.116E-02	1/K
	b9	2.052E-08	1/Pa
	Shrink / Warp - Uncorrected Stress	Anisotropic Mechanical Properties (01602)	
Modulus E ₁ (flow direction)			MPa
Modulus E ₂ (transverse direction)			MPa
Poisson's ratio ν_{12}			
Poisson's ratio ν_{23}			
Shear Modulus G			MPa
Anisotropic Thermal Expansion (01702)			
CLTE α_1 (flow direction)			x 10E-6/°C
CLTE α_2 (transverse direction)			x 10E-6/°C

TestPaksTM is a trademark of DatapointLabs. C-MOLD and Moldflow are trademarks of Moldflow Corporation.

Viscosity



Method	ASTM D 3835 - 02 Determination of Properties of Polymeric Materials by Means of a Capillary Rheometer	
Instrument	Goettfert Rheograph 2003 Capillary Rheometer	
Specimen	type	pellets
	drying	none
	other preparation	none
Parameters	initial pressure	0 MPa
	barrel diameter	12 mm
	die entry angle	180 °
	die inner diameter	1 mm
	die length	20 mm
	preheating time	6 min
Data Correction	Rabinowitsch	
Precision	temperature	+/- 0.1 °C
	die inner diameter	+/- 0.0069 mm
	die length	+/- 0.025 mm
Uncertainty	per standard	

Polymer rheology characterizes the complex flow behavior of plastics. A capillary rheometer measures viscosity as a function of temperature and shear rate. The Goettfert rheometer utilizes direct measurement of melt pressures through a side mounted pressure transducer.

Data are modeled using empirical or semi-empirical equations.

Viscosity Data

140 °C		165 °C		190 °C	
Shear Rate s ⁻¹	Viscosity Pa·s	Shear Rate s ⁻¹	Viscosity Pa·s	Shear Rate s ⁻¹	Viscosity Pa·s
296	346.83	116	744.97	202	395.90
539	193.87	597	146.31	123	649.55
810	160.64	1040	101.54	1204	73.57
1729	94.98	2056	57.92	1768	59.06
3463	55.73	3441	40.64	3622	35.06
7885	33.30	7390	25.87	7986	20.57
16265	19.67	14494	16.89	15398	13.29

Viscosity Continued

Cross/WLF Model (C-MOLD, Moldflow)

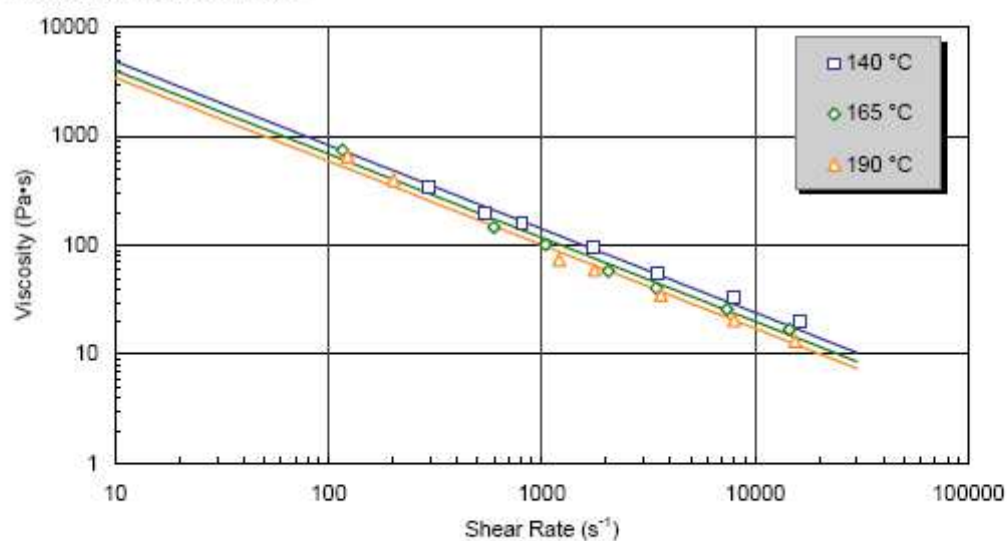
$$\eta(T, \dot{\gamma}) = \frac{\eta_0(T)}{1 + \left(\frac{\eta_0 \dot{\gamma}}{\tau^*} \right)^{1-n}}, \text{ where}$$

$$\eta_0(T) = D_1 \exp \left(- \frac{A_1 (T - D_2)}{A_2 + (T - D_2)} \right)$$

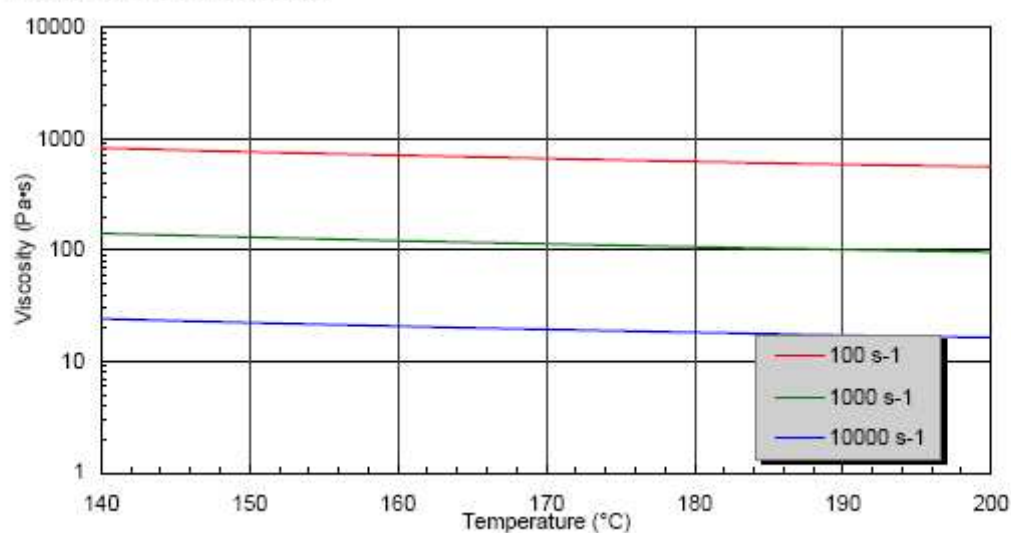
Coefficients (SI units)

n	0.23220
τ^*	9401.43
D1	1.67E+15
D2	263
A1	28.40
A2	51.6

Viscosity vs Shear Rate



Viscosity vs Temperature



Specific Heat



Method	Based on ASTM E 1269 - 05 Determining Specific Heat Capacity by Differential Scanning Calorimetry	
Instrument	Perkin Elmer DSC7	
Specimen	type	pellets
	drying	none
	other preparation	cut from pellet
Parameters	purge gas	N2
	purge gas purity	99.99 %
	purge gas rate	25 ml/min
	cooling rate	20 °C/min
	initial temperature	190 °C
	final temperature	20 °C
	equilibration times	4 min
	sample weight	11.85 mg
	sample pans	Al, volatile
Calibration Standards	temperature	In, Zn
	heat flow	In
	specific heat	sapphire

Heat capacity is a thermodynamic quantity and is a measure of the amount of heat retained by the material. The DSC can measure this property over a range of temperatures and in both solid and melt states.

Notes: Two peaks were observed. Transition analysis temperatures and specific heat data are for larger peak.

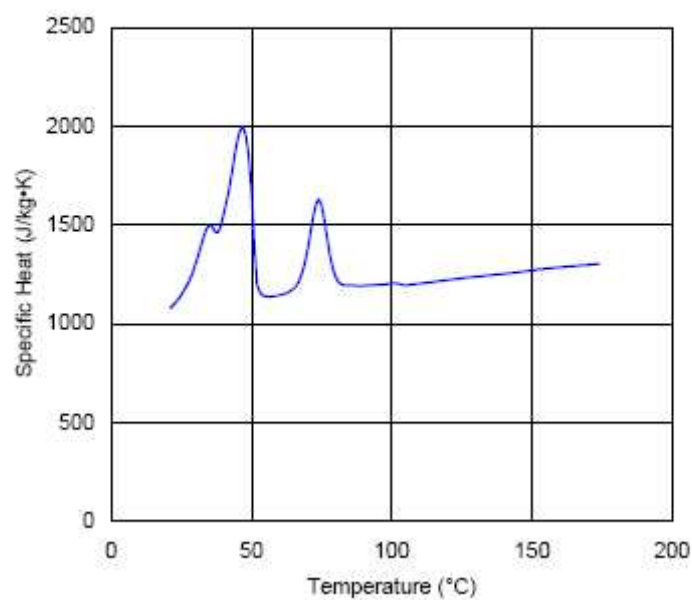
Transition Analysis

extrapolated onset	52 °C
peak	47 °C
extrapolated end	35 °C

Specific Heat Continued

Specific Heat Data

Temp °C	Cp J/kg·K
180	1298
116	1214
57	1137
47	1996
25	1146
32	1392
30	1297



Thermal Conductivity



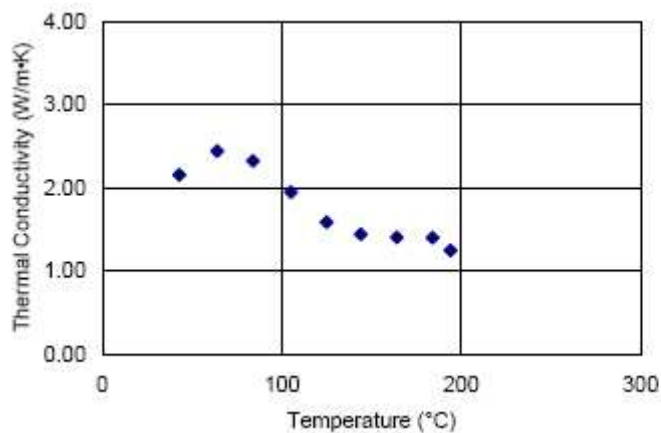
Method	ASTM D 5930 - 01 Thermal Conductivity of Plastics by Means of a Transient Line-Source Technique	
Instrument	K-System II Thermal Conductivity System	
Specimen	type	pellets
	drying	none
	other preparation	none
Parameters	calibration material	60,000 cstk PDMS
	probe constant	0.743
	probe length	50 mm
	loading temperature	170 °C
	initial temperature	190 °C
	final temperature	30 °C
	probe voltage	4 V
	acquisition time	45 s
Uncertainty	per standard	

Thermal conductivity is a measure of the rate of heat conduction of the material. It is a critical property for heat transfer calculations. The line-source method measures thermal conductivity in both melt and solid state.

NOTE: Thermal conductivity may be too high for Moldflow simulation

Thermal Conductivity Data

Temp °C	k W/m·K
194	1.253
184	1.404
164	1.408
144	1.444
125	1.590
105	1.950
84	2.326
64	2.447
43	2.159



PVT



Method	Non-standard. Pressure-specific volume-temperature measurements using high-pressure dilatometry	
Instrument	Gnomix PVT apparatus	
Specimen	type	pellets
	drying	4 hrs, 70°C/vacuum
	other preparation	cut from pellets
Parameters	solid density method	ASTM D792
	immersion liquid	water
	pVT confining fluid	mercury
	max temperature	190 °C
	measurement type	isothermal heating scan
	heating rate	approx. 3 °C/min

PVT data are equation-of-state thermodynamic properties that describe the compressibility and volumetric expansion of the material. Dilatometry measures the change in volume of a specimen subjected to different temperatures and pressures.

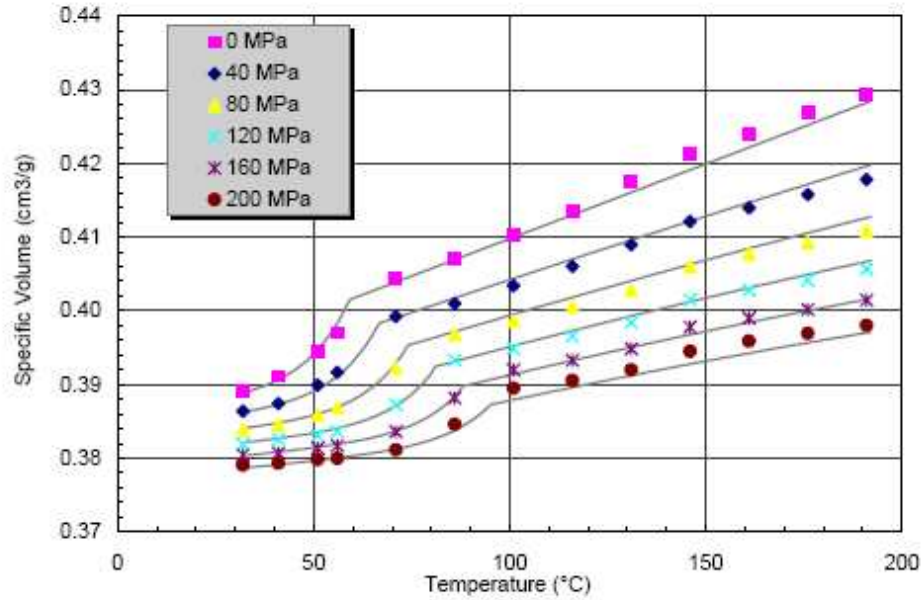
Initial Solid Density

Density 23°C	2580 kg/m ³
--------------	------------------------

Pressure-Volume-Temperature Data

Specific Volume cm ³ /g						
Temp °C	Pressure MPa					
	0	40	80	120	160	200
32	0.3891	0.3864	0.3839	0.3819	0.3805	0.3790
41	0.3911	0.3874	0.3846	0.3826	0.3807	0.3793
51	0.3946	0.3899	0.3859	0.3831	0.3814	0.3798
56	0.3970	0.3916	0.3869	0.3836	0.3817	0.3800
71	0.4043	0.3992	0.3922	0.3872	0.3836	0.3811
86	0.4070	0.4010	0.3968	0.3933	0.3882	0.3846
101	0.4102	0.4034	0.3987	0.3949	0.3920	0.3895
116	0.4136	0.4060	0.4006	0.3965	0.3933	0.3905
131	0.4174	0.4089	0.4028	0.3984	0.3948	0.3920
146	0.4213	0.4121	0.4060	0.4015	0.3978	0.3945
161	0.4239	0.4139	0.4077	0.4028	0.3990	0.3959
176	0.4268	0.4158	0.4092	0.4041	0.4002	0.3969
191	0.4294	0.4178	0.4108	0.4056	0.4014	0.3980

Modified Two-Domain Tait Model (C-MOLD, Moldflow)



Coefficients

b5	5.92E+01
b6	1.80E-01
b1m	4.015E-01
b2m	2.027E-04
b3m	2.953E+02
b4m	4.709E-03
b1s	3.893E-01
b2s	5.312E-05
b3s	6.574E+02
b4s	3.868E-06
b7	1.22E-02
b8	9.116E-02
b9	2.052E-02

Modified Two-Domain Tait Equation

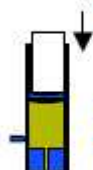
$$v(T, p) = v_0(T) \left(1 - C \ln \left(1 + \frac{p}{B(T)} \right) \right) + v_t(T, p), T_t(p) = b_5 + b_6 p$$

$$\text{for } T > T_t(p): v_0(T) = b_{1m} + b_{2m}(T - b_5), B(T) = b_{3m} \exp(-b_{4m}(T - b_5)), v_t(T, p) = 0$$

$$\text{for } T < T_t(p): v_0(T) = b_{1s} + b_{2s}(T - b_5), B(T) = b_{3s} \exp(-b_{4s}(T - b_5)), v_t(T, p) = b_7 \exp(b_8(T - b_5) - b_9 p)$$

Model Terms	Units
specific volume, v	cm³/g
pressure, P	MPa
temperature, T	°C

No-Flow Temperature



Method	non-standard	
	Moldflow specification; no-flow temperature defined by extrudate flow < 2 mm/min	
Instrument	Goettfert Capillary Rheometer	
Specimen	type	pellets
	drying	none
	other preparation	none
Parameters	equivalent load	172 kg
	barrel diameter	12 mm
	initial pressure	0 MPa
	test temperature	140 °C
	dwel time	6 min
	die inner diameter	1 mm
	die length	20 mm
	die entry angle	180 °

The no-flow temperature provides a measure of the solidification temperature of the melt. During the test, a molten specimen is cooled under constant load; the no-flow temperature is one at which flow ceases to occur.

Results

No-Flow Temperature	114 °C
---------------------	--------

Section II:

Raw Data: Catamold AO-F

All the tests were done at Datapoint Labs and following are the results for Standard mix for various tests,

C-MOLD/Moldflow *TestPak*™ Results

< DTS9254.FIT

Analysis	Property & T-CODE	Value	Units
Filling & Cooling	Cross/WLF Model (01313):		
	n	0.47658	
	τ^*	2.482E+04	Pa
	D1	1.277E+14	Pa•s
	D2	263	K
	D3	0	K/Pa
	A1	30.72	
	A2	51.60	K
	Juncture Loss Constants (01360):		
	C1		Pa^(1-C2)
	C2		
	Melt Density (01000)	2581	kg/m ³
	Melt Specific Heat (01100)	1352	J/kg•K
	Melt Thermal Conductivity (01200)	2.177	W/m•K
	Transition Temperature (01500)	416	K
	Specific Heat Table (01101)	See Page	
	Thermal Conductivity Table (01201)	See Page	
Post-Filling	Two-Domain Tait PVT Model (01004):		
	b5	4.360E+02	K
	b6	6.000E-08	K/Pa
	b1m	3.827E-04	m ³ /kg
	b2m	1.258E-07	m ³ /kg•K
	b3m	3.970E+08	Pa
	b4m	2.174E-03	1/K
	b1s	3.692E-04	m ³ /kg
	b2s	8.316E-08	m ³ /kg•K
	b3s	7.000E+08	Pa
	b4s	5.947E-03	1/K
	b7	1.347E-05	m ³ /kg
	b8	2.702E-01	1/K
	b9	1.926E-08	1/Pa
Shrink / Warp - Uncorrected Stress	Anisotropic Mechanical Properties (01602)		
	Modulus E ₁ (flow direction)		MPa
	Modulus E ₂ (transverse direction)		MPa
	Poisson's ratio ν_{12}		
	Poisson's ratio ν_{23}		
	Shear Modulus G		MPa
	Anisotropic Thermal Expansion (01702)		
	CLTE α_1 (flow direction)		x 10E-6/°C
	CLTE α_2 (transverse direction)		x 10E-6/°C

TestPaks™ is a trademark of Datapoint Labs. C-MOLD and Moldflow are trademarks of Moldflow Corporation.

Moldflow TestPak™ Results

< DTS9254.ASC

These properties are used in MPI 2.x and earlier.

MF/Flow & Cool	Thermal Data			
	Thermal Conductivity	2.177 W/m•K		
	Specific Heat	1382 J/kg•K		
	Melt Density	2581 kg/m ³		
	No-Flow Temperature	155 °C		
	Ejection Temperature	135 °C		
	Viscosity Standard Points			
	Temperature	Shear Rate	Viscosity	
	°C	1/s	Pa•s	
	180	1000	267.7	
	200	100	550.4	
	200	1000	195.9	
	200	10000	51.5	
	220	100	517.2	
	220	1000	185.2	
PVT	PVT Standard Points			
	Temperature	Pressure	Specific Volume	
	°C	MPa	m ³ /kg	
	30	0	0.0003599	
	77	0	0.0003627	
	136	0	0.0003664	
	157	0	0.0003723	
	30	160	0.0003561	
	96	160	0.0003591	
	172	160	0.0003670	
	163.1	0	0.0003831	
	172.7	160	0.0003727	
	168	0	0.0003838	
	201	0	0.0003883	
	186	160	0.0003737	
	201	160	0.0003749	
	Extensional Viscosity	a1		
		a2		
		a3		
		a4		

Viscosity



Method	ASTM D 3835 - 96 Determination of Properties of Polymeric Materials by Means of a Capillary Rheometer	
Instrument	Goettfert Rheograph 2003 Capillary Rheometer	
Specimen	type drying other preparation	pellets 2hrs 100°C / vac none
Parameters	initial pressure barrel diameter die entry angle die inner diameter die length preheating time	0 MPa 12 mm 180 ° 1 mm 20 mm 6 min
Data Correction	Rabinowitsch	
Precision	temperature die inner diameter die length	+/- 0.1 °C +/- 0.0069 mm +/- 0.025 mm
Uncertainty	per standard	

Note: Pressure unstable during 185 / 200°C testing. No degrading seen in strand.

Viscosity Data

170 °C		185 °C		200 °C	
Shear Rate s ⁻¹	Viscosity Pa·s	Shear Rate s ⁻¹	Viscosity Pa·s	Shear Rate s ⁻¹	Viscosity Pa·s
39	1343.66	45	1017.43	49	761.74
69	1065.92	72	825.71	75	622.55
129	762.73	128	625.87	130	480.48
242	588.63	5635	92.33		
579	437.74	14954	43.90		
1191	328.08				
2494	234.83				
8636	113.49				

Viscosity Continued

Cross/WLF Model (C-MOLD, Moldflow)

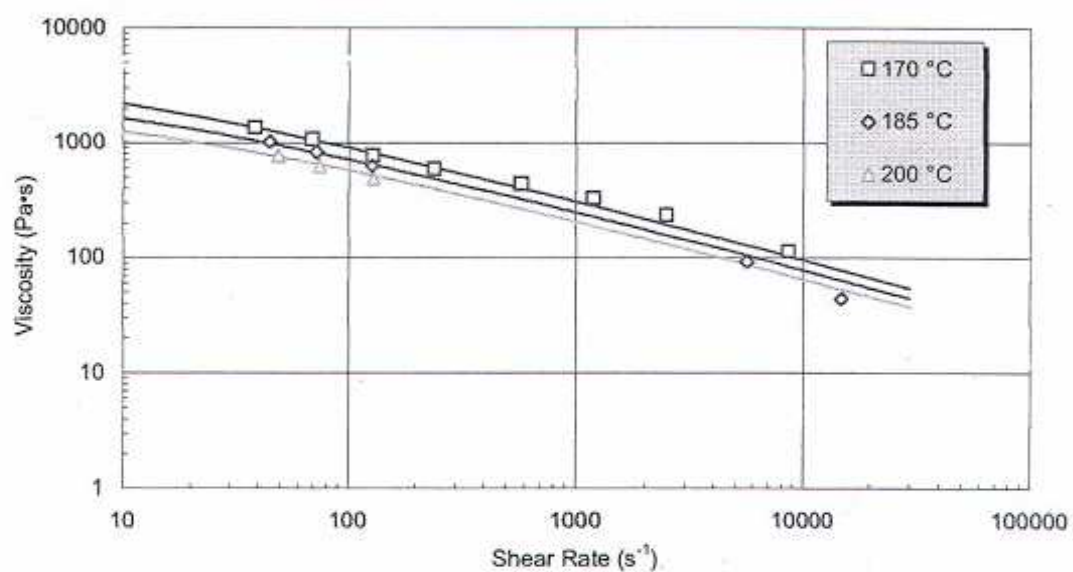
$$\eta(T, \dot{\gamma}) = \frac{\eta_0(T)}{1 + \left(\frac{\eta_0(T) \dot{\gamma}}{\tau^*} \right)^{1-n}}, \text{ where}$$

$$\eta_0(T) = D_1 \exp \left(- \frac{A_1(T - D_2)}{A_2 + (T - D_2)} \right)$$

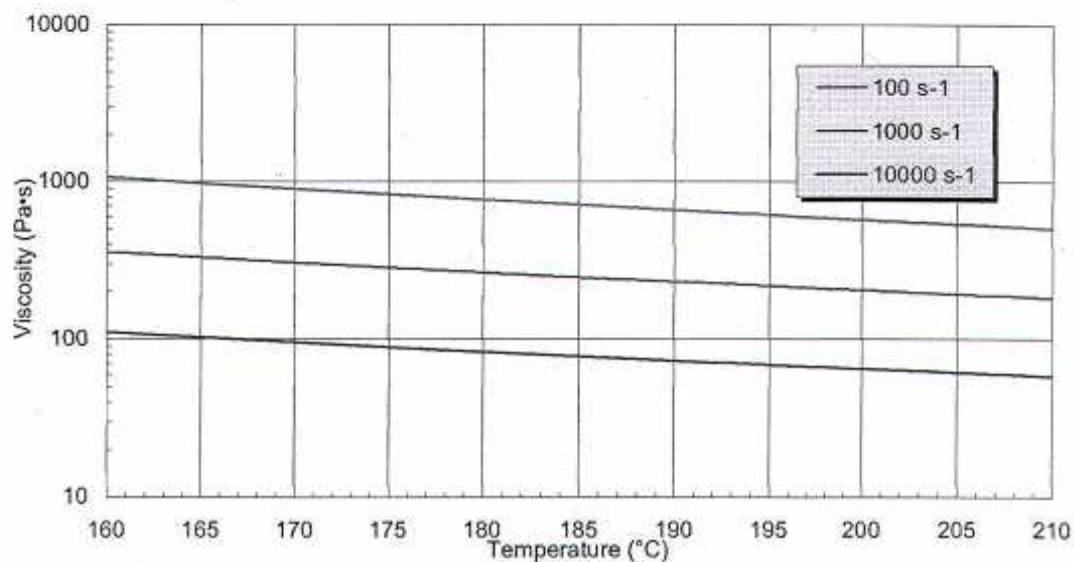
Coefficients (SI units)

n	0.47658
τ^*	24820.929
D1	1.277E+14
D2	263
A1	30.72
A2	51.6

Viscosity vs Shear Rate



Viscosity vs Temperature



Specific Heat



Method	Based on ASTM E 1269 - 01 Determining Specific Heat Capacity by Differential Scanning Calorimetry	
Instrument	Perkin Elmer DSC7	
Specimen	type	pellets
	drying	none
	other preparation	cut from pellet
Parameters	purge gas	N2
	purge gas purity	99.99 %
	purge gas rate	25 ml/min
	cooling rate	20 °C/min
	initial temperature	200 °C
	final temperature	20 °C
	equilibration times	4 min
	sample weight	7.71 mg
	sample pans	Al, volatile
Calibration Standards	temperature	In, Zn
	heat flow	In
	specific heat	sapphire

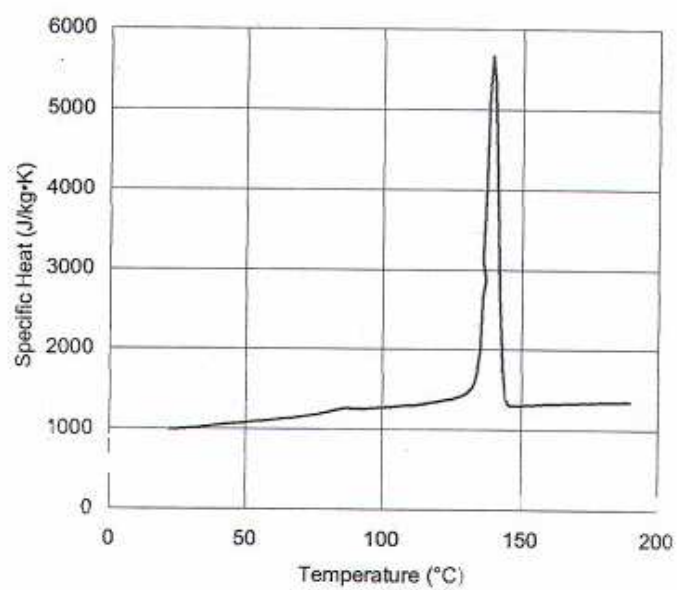
Transition Analysis

extrapolated onset	143 °C
peak	139 °C
extrapolated end	135 °C

Specific Heat Continued

Specific Heat Data

Temp °C	Cp J/kg·K
190	1358
166	1329
148	1303
139	5676
125	1389
82	1234
30	1016



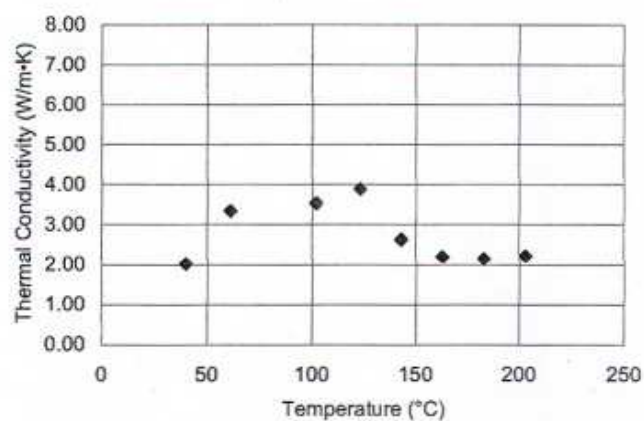
Thermal Conductivity



Method	ASTM D 5930 - 01 Thermal Conductivity of Plastics by Means of a Transient Line-Source Technique	
Instrument	K-System II Thermal Conductivity System	
Specimen	type	pellets
	drying	2hrs 100°C / vac
	other preparation	none
Parameters	calibration material	60,000 cstk PDMS
	probe constant	0.704
	probe length	50 mm
	loading temperature	170 °C
	initial temperature	200 °C
	final temperature	20 °C
	probe voltage	4 V
	acquisition time	45 s
Uncertainty	per standard	

Thermal Conductivity Data

Temp °C	k W/m•K
203	2.208
183	2.145
163	2.188
143	2.625
123	3.893
102	3.537
61	3.343
40	2.018



PVT



Method	Non-standard. Pressure-specific volume-temperature measurements using high-pressure dilatometry	
Instrument	Gnomix PVT apparatus	
Specimen	type drying other preparation	bar 2 hrs. @100°C w/vacuum cut from .5" x 2.5" bars
Parameters	solid density method immersion liquid pVT confining fluid max temperature measurement type heating rate	ASTM D792 water mercury 200 °C isothermal heating scan approx. 3 °C/min

Initial Solid Density

Density 23°C	2754 kg/m ³
--------------	------------------------

Pressure-Volume-Temperature Data

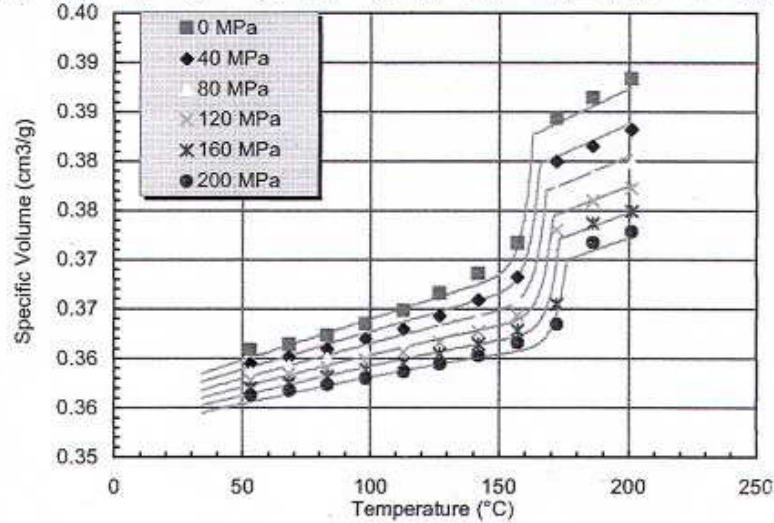
Specific Volume cm ³ /g						
Temp °C	Pressure MPa					
	0	40	80	120	160	200
53	0.3609	0.3595	0.3586	0.3578	0.3571	0.3563
68	0.3614	0.3602	0.3593	0.3584	0.3575	0.3568
83	0.3623	0.3610	0.3600	0.3591	0.3582	0.3574
98	0.3635	0.3620	0.3609	0.3599	0.3589	0.3580
113	0.3649	0.3630	0.3617	0.3606	0.3596	0.3587
127	0.3666	0.3643	0.3628	0.3616	0.3605	0.3595
142	0.3686	0.3659	0.3642	0.3627	0.3615	0.3603
157	0.3717	0.3683	0.3661	0.3644	0.3629	0.3616
172	0.3844	0.3800	0.3770	0.3731	0.3655	0.3635
186	0.3864	0.3816	0.3785	0.3760	0.3737	0.3718
201	0.3884	0.3832	0.3799	0.3773	0.3750	0.3729

Modified Two-Domain Tait Model (C-MOLD, Moldflow)

$$v(T, p) = v_0(T) \left(1 - C \ln \left(1 + \frac{p}{B(T)} \right) \right) + v_i(T, p), T_i(p) = b_5 + b_6 p$$

$$\text{for } T > T_i(p): v_0(T) = b_{1m} + b_{2m}(T - b_5), B(T) = b_{3m} \exp(-b_{4m}(T - b_5)), v_i(T, p) = 0$$

$$\text{for } T < T_i(p): v_0(T) = b_{1s} + b_{2s}(T - b_5), B(T) = b_{3s} \exp(-b_{4s}(T - b_5)), v_i(T, p) = b_7 \exp(b_8(T - b_5) - b_9 p)$$



Model Terms	Units
specific volume, v	cm³/g
pressure, P	MPa
temperature, T	°C

Coefficients

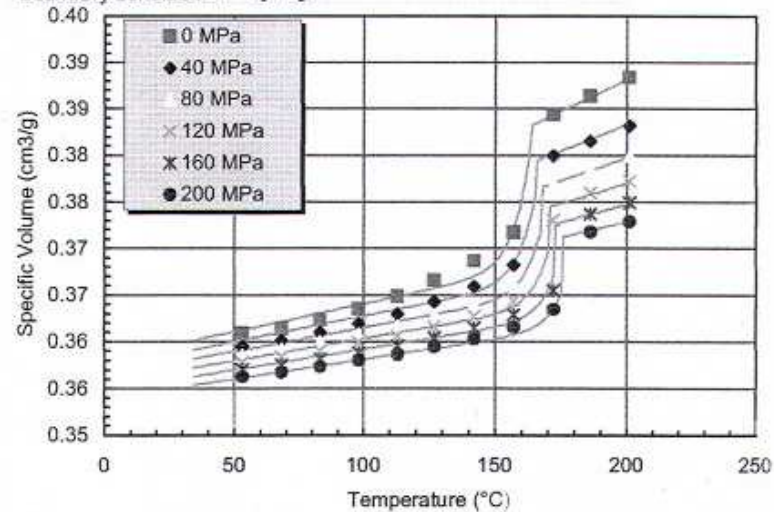
b5	1.630E+02
b6	6.000E-02
b1m	3.827E-01
b2m	1.258E-04
b3m	3.970E+02
b4m	2.174E-03
b1s	3.692E-01
b2s	8.316E-05
b3s	7.000E+02
b4s	5.947E-03
b7	1.347E-02
b8	2.702E-01
b9	1.926E-02

Moldflow PVT Model

$$\text{upper temperature region: } v = \frac{a_1}{a_4 + p} + \frac{a_2 T}{a_3 + p}$$

$$\text{lower temperature region: } v = \frac{a_1}{a_4 + p} + \frac{a_2 T}{a_3 + p} + a_5 \exp[a_6 T - a_7 p]$$

$$\text{boundary condition: } p = b_1 + b_2 T$$



Model Terms	Units
specific volume, v	m³/kg
pressure, P	Pa
temperature, T	°C

Coefficients

b1	-2.717E+09
b2	1.667E+07
a1u	1.533E+07
a2u	2.809E+01
a3u	2.046E+08
a4u	4.250E+10
a1l	6.093E+06
a2l	2.823E+01
a3l	4.721E+08
a4l	1.701E+10
a5l	5.419E-17
a6l	1.605E-01
a7l	1.540E-08

No-Flow Temperature



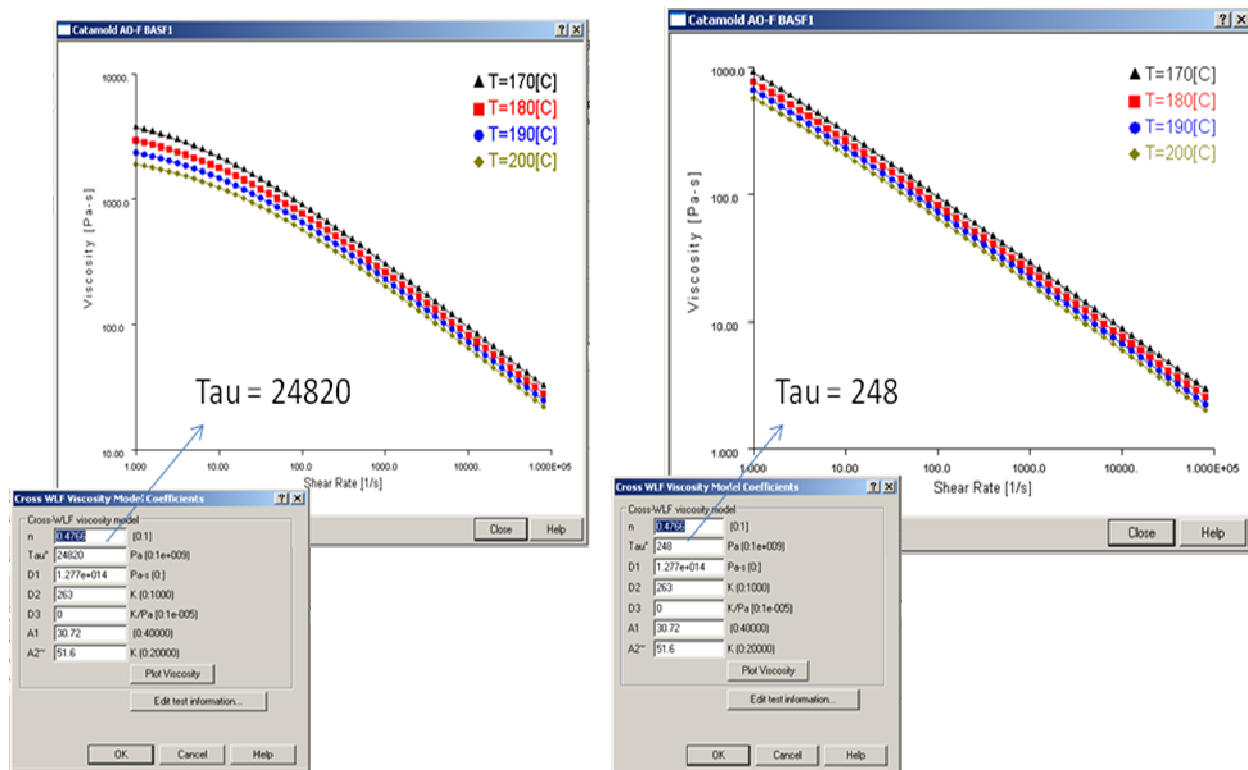
Method	non-standard	
	Moldflow specification; no-flow temperature defined by extrudate flow < 2 mm/min	
Instrument	Goettfert Capillary Rheometer	
Specimen	type	pellets
	drying	2hrs 100°C / vac
	other preparation	none
Parameters	equivalent load	172 kg
	barrel diameter	12 mm
	initial pressure	0 MPa
	test temperature	170 °C
	dwelt time	6 min
	die inner diameter	1 mm
	die length	20 mm
	die entry angle	180 °

Results

No-Flow Temperature	155 °C
----------------------------	--------

Section III: Sensitivity Analysis

All the parameters were changes systematically by 10% each about their experimental values. Following figure just gives a snapshot of how the parameters were changed.



The negative values in the following Table shows the % increase in the mold filling time of the experimental part compared to the mold filling time when the parameters are not changed. On the other hand, the positive values denote the % decrease in the total fill time of the mold compared to the mold filling time when the parameters are not changed.

Sr. No.	Property	Decrease by 10%	Increase by 10%
1	Thermal Conductivity	0.0	20.1
2	Specific Heat	-20.3	0.0
3	A1 - WLF temperature shift factor	-40.2	20.1
4	Melt Temperature - 190C	-19.9	20.1
5	Mold Temperature - 150C	-80.7	0.2
6	Melt Density	-0.2	0.0
7	b1m (PVT)	-0.4	0.2
8	b5 (PVT)	-0.2	0.4

There were many more parameters varied, but they hardly had any effect on the total fill time by changing their experimental values by 10% each.